

Of gyrators and anyons

O. Kashuba, R. Mummadavarapu, and R.-P. Riwar
*Peter Grünberg Institute, Theoretical Nanoelectronics,
Forschungszentrum Jülich, D-52425 Jülich, Germany*

In recent years there have emerged various ideas to create and control topological excitations in superconducting devices. Notably, nontrivial Chern bands were predicted to exist in conventional multiterminal Josephson junctions, but the Chern number is yet to be experimentally verified, and the pathway towards feasible quantum hardware applications is unclear. Here we show how generic multiterminal circuits can be expressed as gyrator networks with quantized gyration conductance, giving rise to anyonic excitations carrying q/p fractional fluxes (q, p integer), measurable via a fractional Aharonov-Casher phase. The magnitude of interactions between the anyons depends on the flatness of the topological bands, prompting us to investigate circuit-specific band-engineering techniques. Circular scattering in three-terminal quantum dot chains gives rise to a flat topological ground state, where disorder mitigates Chern number fluctuations and the quasiparticle continuum provides a work-around for known limitations to create nontrivial flat bands. Further band-engineering strategies are presented where the superconducting phase is scrambled either via parallelization or dissipative phase transitions. We provide concepts for error correction protocols, and quantum simulations of interacting fermionic (or generally anyonic) many-body systems—notably, introducing the possibility to mimic fractional quantum Hall physics or to implement local fermionic models that explicitly break the Wigner superselection rule. The latter indicates that a full understanding of multiterminal circuits will require grappling with a virtually unexplored class of parity-breaking quantum field theories.

I. INTRODUCTION

The quantum world offers various fascinating yet seemingly contradictory fundamental concepts that may hold the key for a revolution in information technologies. The fundamental quantization of charge and spin (or flux) is at odds with the fractional nature of anyonic excitations (in, e.g., the fractional quantum Hall effect [1–4] or spin liquids [5]) whose nontrivial exchange statistics are expected to form the basis of protected quantum gates [6]. The generation of topological flat bands in lattice materials, a central ingredient for fractional Chern insulators [7], can be achieved through quasiperiodicity [8–17], that is, incommensurate interactions that do not match the lattice constant. Inspired by these and many other emergent phenomena, there has been extensive activity to propose and study meta materials consisting of arrays of circuit elements to imitate topological phases of matter [18–28]. Superconducting circuit networks (consisting of elements like Josephson junctions and capacitors) [29–34] in particular have been proposed to imitate fractional quantum Hall physics [35, 36], lattice gauge theories [37–39], 1D [40–45] and 2D [46–52] correlated physics, and quantum gravity aspects [53–59] to name a few.

But such networks are usually limited to one or two spatial dimensions due to on-chip fabrication methods, and require a relatively large number of nodes to fully mimic their respective solid state (or general quantum field theory) counterpart—such that these concepts are in a sense limited by similar hardware challenges as universal superconducting quantum hardware [60, 61]. Recently, there emerged several related ideas [62, 63] to overcome this limitation: instead of considering the lattice quasimomenta of a given material or meta mate-

rial, the topological number (or other quantity of interest) is defined in the space spanned by the superconducting phases ϕ_z of circuit node z . In this context, the compactness of the superconducting phase ϕ [64–68] plays a pivotal role. Non-reciprocal gyrator elements have recently gained a lot of traction [69–78], and have in particular been proposed [63] to realize an effective magnetic field on an extended (non-compact) 2D lattice in ϕ -space, realizing the typical Hofstadter butterfly spectrum at incommensurate (non-integer) gyration conductance—the starting point to implement error correction codes. When compactness of ϕ is preserved, the space of superconducting phases provides a natural analogue to the Brillouin zone, and allows for the creation of topological materials in virtually *any* dimension [62]. Notably, and contrary to Majorana-based junctions in p-wave superconductors [79], a nonzero Chern number can emerge *without* involving topological materials, e.g., in superconductor-normal metal junctions forming Andreev bound states [62, 80–87], standard tunneling Josephson junctions [88–90], or proximitized quantum dots [91–93]. This idea has since been mushrooming into various directions, such as generalizations to the second Chern number [94] or tensor monopoles [95], nonhermitian topology in transport [96–99], and quasiperiodicity within transport degrees of freedom [100].

While the prospect of topological transitions without topological materials has spurred considerable progress on the experimental side in the control and measurement of multiterminal Josephson junctions [101–111], direct evidence of the predicted nonzero Chern number [62] remains to this day elusive. Moreover, the development of possible connections to qubit architectures has only very recently begun, by noting the connection between

nonzero Chern numbers in multiterminal junctions and gyration [112], and by exploring geometric effects when embedding multiterminal junctions into circuit architectures [113–115].

This work presents three central results, relevant to multiterminal circuits in particular, and to topological quantum hardware in general:

1. We demonstrate that the low-energy physics of any generic multiterminal circuit must map onto a set of fractional flux anyons, see Fig. 1.
2. We provide blueprints for quantum hardware and correction protocols to simulate highly general interacting fermionic or anyonic systems, which are of both applied and fundamental interest.
3. We present device setups and strategies to realize flat bands in ϕ -space, enabling fast Chern-number readout, and providing surprising differences to usual solid state band-engineering principles.

Item 1 in above list relies on the generic presence of geometric Berry curvature terms in quantum physics, which allows to map the dynamics of a circuit with Z nodes (terminals) onto a fictitious particle moving on a Z -dimensional torus, where nonzero Chern numbers indicate a nonzero magnetic flux protruding from a 2-dimensional subspace. Inspired by existing works on Landau levels on a 2D torus [116–118], we elucidate important gauge aspects. Based on this, we generalize to arbitrary dimensions, where the degenerate subspace of the lowest Landau level forms an algebra of q/p anyons, where q, p are integers depending on the network of first Chern numbers (behaving like gyrators [69, 112]) defined between all pairs of nodes. The first Chern number (equivalent to the gyration conductance) must be quantized, in the spirit of Dirac’s magnetic monopole argument [119].

In a next step, we show that the ground state degeneracy can be lifted by adding a Josephson junctions connecting nodes to ground or each other. When projecting onto the lowest Landau level, the original Josephson effect is mapped to a hybrid between regular and dual Josephson effects with both an Aharonov-Bohm and an Aharonov-Casher phase [67, 120–123], with a highly non-local, and intertwined sensitivity on externally applied magnetic and electric fields. While the regular Josephson effect remains integer quantized, the dual Josephson effect becomes fractional, indicating that the anyons carry integer charge and fractional flux. The latter is in a sense a consequence of the former, and can be probed by a broken periodicity in the circuit’s charge-dispersion relation [124].

Overall (item 2), both charge and flux control in combination with a tunable Josephson effect form a set of quantum gates for anyonic excitations. We supplement these quantum gates with blueprints for state read-out and preparation, by generalizing the dispersive readout scheme from circuit QED hardware [125] to the here

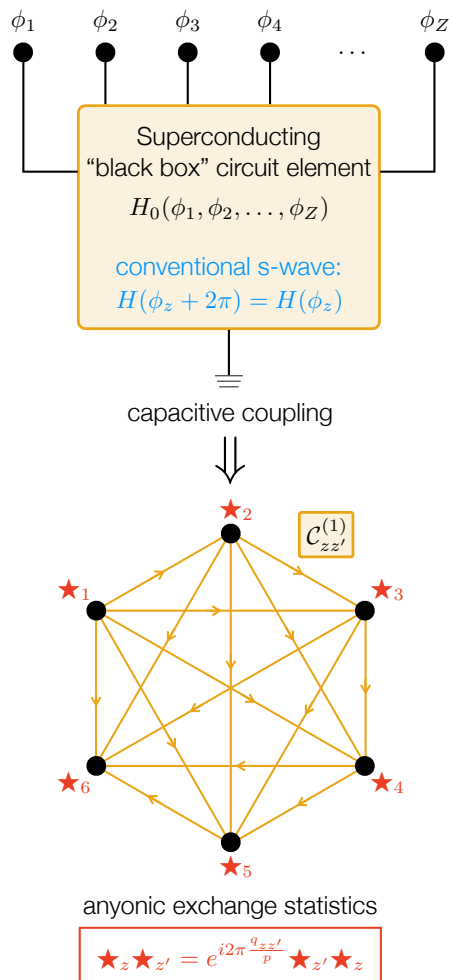


FIG. 1. Main result of our work: a general topological multiterminal junction can be reduced to a network of circuit nodes coupled by gyrators with quantized gyration conductance. Once we include capacitive interactions of the nodes, the system can be described by anyonic excitations localized on each node, with rational fractional exchange statistics depending on the gyration conductance matrix.

emerging anyons. As a consequence, networks of multiterminal junctions form a promising, highly versatile platform for quantum simulations. In particular, the Chern numbers in a given circuit network can be chosen such that all excitations have $1/2$ -fractional flux, resulting in ordinary (Majorana) fermions. This opens the door towards quantum chemistry [126, 127] or solid state [128–130] computations, or even the simulation of the Sachdev-Ye-Kitaev (SYK) model [131–133], since the implementation of non-local quartic Majorana interaction terms pose no additional conceptual hurdle.

In contrast to qubit-based universal quantum computers, the fermion exchange statistics here naturally emerges from the low-energy physics, and does not require the typical highly non-local gates to implement Jordan-Wigner chains [134, 135]—to the contrary, individual fermions are addressed through local operations,

such as gate voltages or Josephson effects. Moreover, by increasing the Chern numbers (crucially, without the need to increase the number of nodes or read-out lines in the hardware), the very same architecture can immediately swap from fermions to anyons, thus massively enlarge the class of possible simulations. The anyonic generalization is of further interest for the implementation of quantum error correction codes, like the Gottesman-Kitaev-Preskil (GKP) code [136], since it can be regarded as a regular fermion with redundancies.

Item 3 is based on the realization that Cooper pair transport across the nodes gives rise to significant many-body coupling between anyons. In order to control this interaction, we resort to the engineering of topological flat-bands. Specifically, we present physical implementations of three-terminal quantum dot models (related to models considered in Refs. [91–93]), where flat bands emerge when increasing the length of the quantum dot chains within the proximitized region of the device. Within the language of the Beenakker formalism [137], this system realizes a perfectly circular scattering region, which has recently been predicted to give rise to flat, but *topologically trivial* Andreev bands [138]. Here we show that even though the Andreev bound states are trivial, the many-body ground state of the device is nonetheless topological, due to contributions from the quasiparticle continuum. This provides an interesting loophole to recently developed no-go theorems within the solid state community [139–144] which put stringent constraints on the existence of topological flat bands in models with only few energy bands. An important caveat of this effect is that the individual single-particle Chern numbers of the continuum states fluctuate heavily, rendering the total Chern number of the device highly susceptible to quasiparticle excitations [145]. We show, however, that disorder is helpful, as it massively reduces Chern number fluctuations without having a detrimental effect on the flattening. In the flat band limit, the Chern number is probed via standard ac spectroscopy of the effective cyclotron frequency, allowing for fast correction protocols against Chern-number fluctuations.

Two further band engineering methods are discussed. A recently developed idea for on-demand engineering of arbitrary shapes of current-phase relationships by parallel shunts [146] is adapted to the generation of flat bands in multiterminal junctions by averaging the bands within ϕ -space. Another technique consists of exploiting dissipative quantum phase transitions (first predicted by Schmid and Bulgadaev [147, 148]) to suppress Josephson effects. We here argue that suppression is achieved by capacitive coupling to an Ohmic bath. We note that even though the existence of the Schmid-Bulgadaev phase transition was theoretically widely confirmed for the Caldeira-Leggett model [149–155], its experimental verification has recently been subject to some controversy [156–167]. In a recent work by some of us [168], we pointed out that while not all dissipative interactions map exactly onto Caldeira-Leggett, a pure capacitive

coupling does, such that we do not expect our finding in the here presented work to be affected by ongoing debates on the subject.

Our work also triggers a number of spin-off conceptual features of fundamental interest. First of all, the here studied circuits allow for the implementation of systems that explicitly break fermion parity superselection rule [169] (and its anyonic generalization). While this finding is conceptually very much in line with well-known issues associated to Wigner superselection in qubit-based systems [170] (where fermion parity is likewise not naturally conserved), the aforementioned *locality* of gate operations nonetheless provides some surprising twists. In particular, our setup allows for protocols that break the no-communication theorem (valid in the here considered non-relativistic limit), and thus connects to a large body of work [171–176] dedicated to the foundations of quantum mechanics, specifically to how fundamental principles like local realism (and relatedly, Wigner superselection for fermionic systems [177–180]) can be motivated on an axiomatic level. This finding hints in addition at the challenging, yet fascinating prospect that a full understanding of the behaviour of multiterminal circuits requires the study of fermion parity-breaking quantum field theories, which have to the best of our knowledge not been systematically addressed. A second fundamental aspect follows from the observation that the anyonic exchange is here mediated by a minimal gauge field in the following sense. Contrary to the ordinary vector version of Chern-Simons theory [181] (relevant to describe anyonic exchange in the fractional quantum Hall effect), the gyrator network here generates a *reduced* theory which is scalar and compact. In the outlook, we provide some ideas for establishing even deeper connections between non-reciprocal interactions in quantum circuits and the fractional quantum Hall effect.

This paper is organized as follows. Section II demonstrates the general mapping from multiterminal circuits to anyons. Section III illustrates possible quantum hardware applications, whereas Sec. IV discusses concrete experimental blueprints for engineering topological flat bands in circuits. Finally, Sec. V contains an extended outlook on a number of important ramifications and open questions resulting from our work.

II. FROM CHERN NUMBERS TO ANYONS

A. Low-energy description of multiterminal junctions

The starting point of our considerations is a generic description of a black box circuit element connecting a total number of Z nodes to ground, each with its superconducting phase ϕ_z ($z = \{1, \dots, Z\}$). Under a concise set of assumptions on the properties of the black box element, we will show that it generically reduces to a network of pairwise connections each described by a (first) Chern

number. While we here (for the sake of generality) consider a generic multiterminal setup where we impose no upper bound on the number of nodes Z , we will show in a moment that any arbitrarily large network can always be decomposed into elementary three-terminal building blocks. In a second part of the work, we discuss in more detail how these constituents are physically implemented, cf. Sec. IV.

The internal degrees of freedom of the black box element are described by a Hamiltonian as a function of the superconducting phases, $H_0(\{\phi_z\})$. The only further restrictions we place on this system are that it has a nondegenerate ground state with a finite gap to the first excited state, and that the Hamiltonian shall be 2π -periodic in all phases ϕ_z , indicating that we consider conventional s-wave superconducting contacts. While we have multiterminal Josephson junctions as concrete physical realizations in mind, we note that in the first part of this work, we will not have to invoke a concrete physical picture to understand the fundamental behaviour of the circuit, as long as the Hamiltonian meets the above conditions.

When including capacitive coupling of the nodes to ground and between each other, we have to keep track of the number of charges on each node, and account for resulting charging energy. This yields the circuit Hamiltonian

$$H = 2e^2 \sum_{zz'} n_z (C^{-1})_{zz'} n_{z'} + H_0(\{\phi_z\}) \quad (1)$$

where now phases are operators, as well as the canonically conjugated charges that satisfy the ordinary cQED commutation relations [64, 182, 183], $[n_z, \phi_{z'}] = i\delta_{zz'}$. The capacitance matrix C encapsulates all the relevant capacitive couplings between different nodes and ground.

Expressing the black box Hamiltonian in terms of its eigenstates $H_0 = \sum_k \epsilon_k |k\rangle\langle k|$ (the ϕ_z -dependence of energy ϵ_k and state $|k\rangle$ is no longer explicitly denoted), and denoting the nondegenerate ground state as $k = 0$, we perform a geometric version of a Born-Oppenheimer approximation, which was first developed in the context of atomic physics [184] (and whose importance was recently appreciated for Josephson junctions [114, 115]), where projecting onto $|0\rangle$ yields the low-energy description,

$$H \approx 2e^2 \sum_{zz'} (n_z + A_z)(C^{-1})_{zz'} (n_{z'} + A_{z'}) + \epsilon_0, \quad (2)$$

with the Berry connections $A_z = i\langle 0|\partial_{\phi_z}|0\rangle$. Defining in addition to the canonical charge n_z on node z the kinetic charge $N_z = n_z + A_z$, the commutator of the latter (between nodes z and z') is gauge-invariant,

$$[N_z, N_{z'}] = \partial_{\phi_{z'}} A_z - \partial_{\phi_z} A_{z'} = \mathcal{B}_{zz'}, \quad (3)$$

and given by the Berry curvature $\mathcal{B}_{zz'}$. Note that the kinetic charge is the physical charge on the island determining, e.g., the electric field between circuit nodes.

B. Gyration conductance quantization

As recently noted [112, 114], geometric effects in the multiterminal Josephson effect are deeply related to quantum circuit versions of gyrator elements [63, 69], see Fig. 2. Indeed, in the circuit QED language, the latter can be described by a Lagrangian term of the form [63],

$$L_G = - \sum_z \dot{\phi}_z A_z \quad (4)$$

where A_z is a function of the phases ϕ_z only, and can be identified as the above introduced vector potential. Adding charge energy terms, $L = \frac{1}{8e^2} \sum_{zz'} \dot{\phi}_z C_{zz'} \dot{\phi}_{z'} + L_G - \epsilon_0$, and following standard quantization rules, we arrive at Eq. (2).

Crucially, though, depending on whether or not we impose compactness of the superconducting phases ϕ_z , there are marked differences in the description of nonreciprocal circuit elements described by Eq. (4). These differences are deeply related to gauge properties on compact spaces, which form the basis of our endeavour. To begin, note that if we assume ϕ_z compact (more precisely, closed—default assumption throughout this work), the first Chern number, defined as

$$C_{zz'}^{(1)} = \frac{1}{2\pi} \int_0^{2\pi} d\phi_z \int_0^{2\pi} d\phi_{z'} \mathcal{B}_{zz'}, \quad (5)$$

is integer quantized. As indicated in the introduction, nontrivial geometric (Berry curvature) effects, including a resulting nonzero Chern number, are known to emerge for *conventional* multiterminal Josephson junction devices [62, 88–93].

In general, all Berry curvatures $\mathcal{B}_{zz'}$, and the potential energy ϵ_0 depend on ϕ_z . Specifically for the Berry curvature, it is convenient to define $\mathcal{B}_{zz'} = C_{zz'}^{(1)}/2\pi + \delta\mathcal{B}_{zz'}$ where the integral of $\delta\mathcal{B}_{zz'}$ over $\phi_z, \phi_{z'}$ is zero per definition. In a first step, it is convenient to consider topological flat bands, that is, assuming ϵ_0 constant and $\delta\mathcal{B}_{zz'} = 0$, as this problem can be solved exactly. We stress however that on the one hand, the flat band assumption is more than just a mathematical trick: as we show in a second part below, topological flat bands are realizable with various band-engineering methods. On the other hand, deviations from flat bands are by no means a nuisance: as we argue momentarily, Josephson effects actually play a pivotal role in understanding and probing many of the nontrivial properties at play. Ultimately, band flattening is only insofar important as our theory relies on the projection onto the lowest band of the Hamiltonian H_0 . This projection is most accurate if the band width of the ground state of H_0 (the difference between minimum and maximum value of ϵ_0 as a function of all ϕ_z) is smaller than the energy gap to the first excitation ($m = 1$).

A constant ϵ_0 can simply be discarded. For the Berry curvature on the other hand, the constant part refers to

the nonzero Chern number, which will be crucial. We choose the following gauge for the vector potentials

$$A_z = \sum_{z'} g_{zz'} \phi_{z'}, \quad (6)$$

where the matrix g can take arbitrary real values, with the only condition that none of the matrix elements depend on ϕ_z . Apart from that, there is still quite some freedom to choose the matrix g . The only other necessary condition on g is obtained via Eq. (3), such that it is easy to show that g is directly related to the gauge-invariant Berry curvatures

$$\mathcal{B}_{zz'} = (g - g^T)_{zz'} = \frac{1}{2\pi} \mathcal{C}_{zz'}^{(1)}, \quad (7)$$

and as a result, to the quantized Chern numbers.

The attentive reader may object that the gauge choice for the Berry connections in Eq. (6) seems to fundamentally break 2π -periodicity and, thus, compactness in ϕ_z , such that it appears impossible to meaningfully represent the system on a torus. This problem can however be mended by invoking a curvature $\tilde{\mathcal{B}}_{zz'}$ distinct from the Berry curvature by subtracting $\mathcal{C}_{zz'}^{(1)}$ Dirac-delta-like ‘‘horns’’ [118],

$$\tilde{\mathcal{B}}_{zz'} = \mathcal{B}_{zz'} - \frac{1}{2\pi} \sum_i \mathcal{K}_{zz'}^{(i)} \delta(\phi_z - \phi_z^{(i)}) \delta(\phi_{z'} - \phi_{z'}^{(i)}), \quad (8)$$

at arbitrary positions $\phi_z^{(i)}$ of the integer heights $\mathcal{K}_{zz'}^{(i)}$, such that $\sum_i \mathcal{K}_{zz'}^{(i)} = \mathcal{C}_{zz'}^{(1)}$. This curvature satisfies by construction the Gauss-Bonnet theorem (note that the boundary term is absent due to the manifold being closed)

$$\frac{1}{2\pi} \int_0^{2\pi} d\phi_z \int_0^{2\pi} d\phi_{z'} \tilde{\mathcal{B}}_{zz'} = \chi_T = 0 \quad (9)$$

where the Euler characteristic χ_T of the torus is zero. It further allows for a gauge choice of A_z , such that its curl yields $\tilde{\mathcal{B}}$ instead of \mathcal{B} . This vector potential is locally given by Eq. (6) but globally contains jumps to satisfy 2π periodicity in the superconducting phases. This construction is helpful for explicit numeric calculations by, e.g., discretizing ϕ_z -space (in the Appendix A, we explicitly consider a 2-dimensional system for illustration). At any rate, note that for quantum coherent trajectories on the torus, the above introduced horns do not change the dynamics, simply because the phase picked up when circumventing them is $e^{i2\pi} = 1$. Therefore, while $\tilde{\mathcal{B}}$ is necessary for a consistent construction of the low-energy H in ϕ -space, we can nonetheless work with \mathcal{B} in other basis representations, as long as we take care that the construction of the pertinent operator algebra respects phase compactness.

Overall, the system here maps to a particle moving in a constant magnetic field on a Z -dimensional torus. In this picture, it becomes obvious that the well-known Dirac

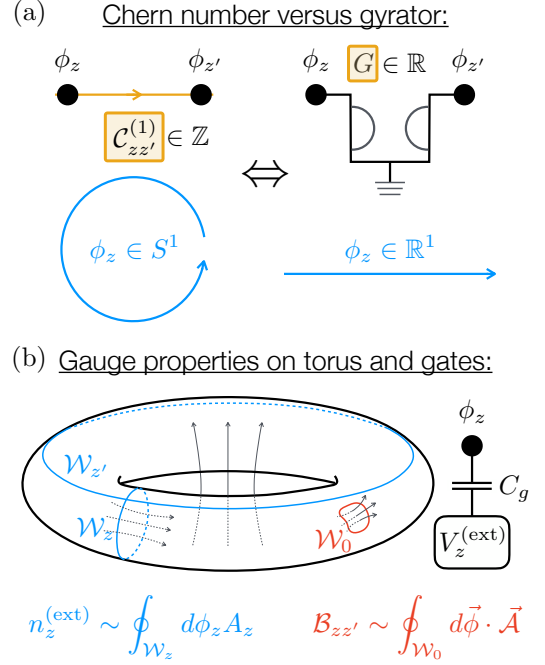


FIG. 2. Important aspects regarding phase compactness. (a) A nonzero Chern number between two nodes (left) essentially maps onto a gyrator (right, denoted by Tellegen’s symbol), however, with the difference that the Chern number (equivalent to the gyration conductance) must be integer quantized when defined on compact superconducting phases. Conceptually, the circuit element is a three-terminal devices (one terminal to ground), where in the left symbol, we omit the explicit representation of the ground for simplicity. (b) Upon including capacitive coupling, the dynamics of a circuit with Z nodes reduces to a fictitious particle moving in a magnetic field on a Z -dimensional torus (here shown for two dimensions). Contrary to the ordinary Landau level problem in extended space, the gauge invariance on the torus comes with a number of complications. For instance, in addition to the trivial W_0 loops there are two types of nontrivial loops W_z and $W_{z'}$, which can not be controlled by the value of the magnetic field only. The phase accumulated across these extra loops is defined by gate-voltage induced offset charges.

quantization condition for magnetic monopoles [119] is perfectly equivalent to the integer quantization of the Chern numbers. We further note that since each Chern number is defined in a 2D subspace, the magnetic field can always be decomposed into components connecting two nodes z and z' . It is in this sense, that we can always think of the generic $(Z+1)$ -terminal junction (connecting ground with Z active nodes) as a network of fundamental three-terminal junctions (connecting from ground to two out of the Z nodes), as announced above.

The above discussion is in significant contrast to many existing works on gyrators [63, 69, 77, 78, 185] where the gyration conductance matrix $g - g^T$, can take on any real value (which may have different physical realizations than the Josephson junctions considered here). Crucially,

for the enticing proposition to realize Hofstadter butterfly physics on emergent lattices in ϕ -space [63] the non-integer nature of the effective magnetic field is very much a *prerequisite*: if $g - g^T$ were quantized as in Eq. (7) above, the circuit behaviour in Ref. [63] would be trivial and equivalent to the gyrators being absent altogether. Relatedly, Ref. [63] could only provide a consistent quantum mechanical treatment when assuming extended ϕ 's (by adding additional linear inductive shunts). To the best of our knowledge, there is still no full understanding as to when and under what conditions the values of $g - g^T$ are subject to constraints. We believe though, that it may well be plausible that nonquantized values are possible when the nonreciprocity occurs within a finite frequency window [69] or requires periodic driving [78]. However, under the axioms present in this work, where [consistent with the derivation of Eq. (2)] the physics emerge via a projection onto a single, nondegenerate ground state of a Hamiltonian H_0 periodic in ϕ , phase compactness is guaranteed, and monopole quantization cannot be broken. Consequently, in our work, the gyration conductance $g - g^T$ must be quantized. It is nonetheless interesting to note that if gyration quantization (in conjunction with the compact base space) would be present or could be engineered in any of the other recently studied platforms, our proposal below could be straightforwardly realized in an even larger class of device designs.

As we elaborate in what follows, the compact manifold has an even more decisive role, as nontrivial gauge-considerations allow us to demonstrate that integer-valued $g - g^T$ are far from having a trivial effect in the above setups—to the contrary, they give rise anyonic excitations carrying fractional flux, providing the opportunity to explore a plethora of nontrivial emergent phenomena in conventional multiterminal circuits. To distinguish our work from Ref. [63]: we work in the opposite regime where the charging energies are large with respect to the Josephson energies, such that our wave functions are not per se localized in ϕ -space.

C. Landau levels on closed manifolds and anyonic exchange statistics

The Hamiltonian in Eq. (2) with flat bands [i.e., $\epsilon_0 = \text{const.}$, and the vector potentials as in Eq. (6)] is quadratic. If ϕ_z were extended, this Hamiltonian would be readily solved through a standard Bogoliubov transformation and yield (infinitely degenerate) Landau levels in a Z -dimensional system. Let us briefly recapitulate the diagonalization for extended ϕ_z , before we delve into the compact case. In this case of the extended ϕ_z , the kinetic charges N_z can be expressed as linear combinations terms of bosonic ladder operators $a_j^{(\dagger)}$ switching the Landau level number, resulting in the diagonal form, $H = \sum_j \omega_j a_j^\dagger a_j$ (the index j indicates that in more than 2 dimensions, Landau levels have in general many cy-

clotron eigenfrequencies). At the same time, the Landau-level degeneracy can be captured by zero modes (a set of operators commuting with N_z , and thus with H), which can be regarded as a kinetic flux,

$$\Phi_z = \phi_z - \sum_{z'} \left(\frac{1}{g - g^T} \right)_{zz'} N_{z'} . \quad (10)$$

This construction of course necessitates that $\det(g - g^T) \neq 0$, in order for $g - g^T$ to be invertible. Furthermore, since $g - g^T$ is skew-symmetric (essentially by definition), the inverse can only exist if Z is even. Both even Z and $\det(g - g^T) \neq 0$ will be the default assumption in the remainder of this work. We will in a moment relate invertibility to the existence of higher Chern numbers.

Phase compactness has an important impact on the Fock space of our system: the Landau levels have a finite degeneracy. To see this, we note that while the construction of the bosonic N_z is still valid on a torus [186], we have to construct a set of kinetic phase operators that satisfy 2π -periodicity, which is accomplished with exponentiation, $e^{i\Phi_z}$. These operators still satisfy $[e^{i\Phi_z}, N_z] = 0$, and provide the algebra

$$e^{im\Phi_z} e^{im'\Phi_{z'}} = e^{i2\pi m m' q_{zz'}/p} e^{im'\Phi_{z'}} e^{im\Phi_z} , \quad (11)$$

where $m^{(\prime)} \in \mathbb{Z}$. We therefore find that for compact ϕ_z , the excitations within a given Landau level give rise to an *abelian anyonic exchange statistics*, with the exchange phase matrix

$$\frac{q_{zz'}}{p} = \frac{1}{2\pi} \left(\frac{1}{g - g^T} \right)_{zz'} . \quad (12)$$

As the second equality indicates, the exchange phase is always a rational number with q being an integer-valued matrix, and p an integer scalar. As a matter of fact, p is equal to the $Z/2$ Chern number (we remind that Z is even, and ϵ is the Levi-Civita symbol),

$$p = \mathcal{C}^{(Z/2)} = \sum_{z_1, \dots, z_{Z/2}} \frac{\epsilon^{z_1, \dots, z_{Z/2}} \mathcal{C}_{z_1 z_2}^{(1)} \dots \mathcal{C}_{z_{Z/2-1} z_{Z/2}}^{(1)}}{2^{Z/2} (Z/2)!} , \quad (13)$$

whereas the matrix q is given as a “transposed” $Z/2 - 1$ Chern number

$$q_{zz'} = \bar{\mathcal{C}}_{zz'}^{(Z/2-1)} = \sum_{z_3, \dots, z_{Z/2}} \frac{\epsilon^{z', z, z_3, \dots, z_{Z/2}} \mathcal{C}_{z_3 z_4}^{(1)} \dots \mathcal{C}_{z_{Z/2-1} z_{Z/2}}^{(1)}}{2^{Z/2-1} (Z/2 - 1)!} . \quad (14)$$

Translating this to the language of skew-symmetric matrices, p is the Pfaffian of the matrix $\mathcal{C}^{(1)} = 2\pi(g - g^T)$. The matrix q plays the same role for inversion of skew-symmetric matrices, as the adjoint one for general matrices. The ordinary adjoint matrix consists of minors which are determinants of the smaller matrices $A^{\hat{z}\hat{z}'}$ obtained by removing one row z and one column z' from matrix A [187]. In our case, the determinants are substituted by Pfaffians, where the two columns and rows z and

z' are removed symmetrically from the original matrix. Consequently, the inverse matrix is matrix q divided over the Pfaffian of the original skew-symmetric matrix. The Pfaffian can be calculated by the recursive formula [188]

$$\text{Pf } \mathcal{C} = \sum_{zz'=1}^{2n} (-1)^{z+z'+1+\theta(z-z')} c_{zz'} \text{Pf } \mathcal{C}^{\hat{z}\hat{z}'}, \quad (15)$$

from which one can immediately see, that p and any element of q are also integer. To provide specific examples, for two nodes ($Z = 2$) we simply have (in matrix representation)

$$\frac{q}{p} = \frac{1}{\mathcal{C}^{(1)}} \begin{pmatrix} 0 & -1 \\ 1 & 0 \end{pmatrix}, \quad (16)$$

where there is only one first Chern number, hence the omission of node indices. In contrast, for four nodes ($Z = 4$), we find

$$\frac{q}{p} = \frac{1}{\mathcal{C}^{(2)}} \begin{pmatrix} 0 & -\mathcal{C}_{34}^{(1)} & \mathcal{C}_{24}^{(1)} & -\mathcal{C}_{23}^{(1)} \\ \mathcal{C}_{34}^{(1)} & 0 & -\mathcal{C}_{14}^{(1)} & \mathcal{C}_{13}^{(1)} \\ -\mathcal{C}_{24}^{(1)} & \mathcal{C}_{14}^{(1)} & 0 & -\mathcal{C}_{12}^{(1)} \\ \mathcal{C}_{23}^{(1)} & -\mathcal{C}_{13}^{(1)} & \mathcal{C}_{12}^{(1)} & 0 \end{pmatrix}, \quad (17)$$

where the second Chern number emerges in the denominator, $\mathcal{C}^{(2)} = \mathcal{C}_{12}^{(1)}\mathcal{C}_{34}^{(1)} - \mathcal{C}_{13}^{(1)}\mathcal{C}_{24}^{(1)} + \mathcal{C}_{14}^{(1)}\mathcal{C}_{23}^{(1)}$. This calculation can be continued in analogy for higher Z .

We draw from the above the following conclusions. The requirement $q, p \in \mathbb{Z}$ follows simply from the first Chern numbers $\mathcal{C}_{zz'}^{(1)}$ being all integer. The existence of the inverse of $g - g^T$ requires $\mathcal{C}^{(Z/2)}$ (the highest possible Chern number for a device with Z nodes) to be nonzero. Note though, that this by no means implies that $\det(g - g^T) = 0$ gives rise to any problematic behaviour whatsoever; in that case one simply has to carefully separate zero and nonzero eigenvalues of $g - g^T$ and construct the kinetic flux operators accordingly. We merely omit discussing this special case for simplicity [see also the comment after Eq. (10)].

Overall, the above result illustrates that in spite of the system being in principle fully described by the first Chern numbers connecting two nodes, the resulting (nonzero) second and higher Chern numbers appear very prominently in the anyonic exchange statistics of multi-node devices. As a matter of fact, the all Chern numbers also appear in the energy spectrum. Specifically for $Z = 2, 4$, we calculate the Landau level frequencies for the case of dominant capacitive coupling ground (for simplicity we assume the capacitance matrix to be $C_{zz'} = C_g \delta_{zz'}$, such that the model only includes a capacitance to ground). For $Z = 2$, we obtain a single cyclotron mode, $H = \omega a^\dagger a$, with frequency

$$\omega = \frac{2e^2}{\pi C_g} \mathcal{C}^{(1)}, \quad (18)$$

whereas for $Z = 4$, there are two modes, $H = \omega_+ a_+^\dagger a_+ + \omega_- a_-^\dagger a_-$, with frequencies

$$\omega_\pm = \frac{2e^2}{\sqrt{8}\pi C_g} \sqrt{|q|^2 \pm \sqrt{|q|^4 - 4[\mathcal{C}^{(2)}]^2}} \quad (19)$$

where we defined the norm for q , $|q|^2 = \sum_z \sum_{z' > z} |q_{zz'}|^2$. As a consequence, both second and first Chern number can be directly tracked in an experiment measuring the circuits resonance frequencies (such as, e.g., a standard dispersive readout). This means that for the here considered topological flat bands, a measurement of the Chern number does not necessarily require a long time-averaged transport measurement (as proposed for non-flat bands [62]), but is achieved via fast ac spectroscopy techniques, readily available and maturely developed within superconducting circuit architecture.

Let us return to the anyonic subspace within a Landau level. Given that the anyonic exchange phase is rational, we can infer that an appropriate group representation of the operators $e^{i\Phi z}$ must be cyclic and discrete, since $e^{ip\Phi z}$ is guaranteed to commute with everything, and thus must return an ordinary c-number (consistent with one of the fundamental properties of a parafermion). For generic cases, we refer to the pertinent literature for recipes to construct group representations for operators satisfying Eq. (11). The way to the solution of this problem paved by finite groups theory starts from finding the factor group. One can build the regular representation and exploit Cauchy–Frobenius lemma [189–191] to identify the group structure (for pedagogical purposes we recommend to start from the short description of the regular representation in Ref. [192]). One can decompose the group in such a way into point groups, the irreducible representations of which are known. At any rate, for the special cases we consider in the remainder of this work it is easy to find explicit representations, where each Landau level is exactly p -fold degenerate.

D. Charge quantization and flux fractionalization

After the above formal discussion, we now move on to a more physical interpretation of the anyonic excitations. As indicated in the introduction, the emergence of anyonic excitations always comes hand in hand with the fractionalization of some physical quantity. We will show in the following, that the here emerging anyons carry fractional *flux*, and that both flux fractionalization and exchange statistics can be probed by addressing circuit nodes via a Josephson effect.

Let us motivate this exercise with a somewhat naive, first comparison to the fractional quantum Hall effect (a more solid relationship will follow momentarily). For instance, for the 2-node device [Eq. (16)] we simply have one pair of $1/p$ anyons, which are obviously reminiscent of Laughlin quasiparticles, however, with the difference that here p is not restricted to odd integers, but can

assume both even and odd values. With the 4-node device, Eq. (17), we can construct even more general rational numbers. While for the full exchange matrix q/p there are of course restrictions as to the possible combinations of numbers [since p is not independent of q , due to $|p| = \sqrt{\det(q)}$], for a single phase between two nodes $q_{zz'}/p$ we expect no significant number-theoretic limitations. Specifically, with $\mathcal{C}_{13}^{(1)} = 0$ and $\mathcal{C}_{14}^{(1)} = -\mathcal{C}_{23}^{(1)} = 1$, we get the exchange phase for nodes 1 and 2 as

$$\frac{q_{12}}{p} = \frac{\mathcal{C}_{34}^{(1)}}{\mathcal{C}_{12}^{(1)}\mathcal{C}_{34}^{(1)} + 1}, \quad (20)$$

which thus mimics the Jain sequence [193, 194] with $\mathcal{C}_{12}^{(1)}$ playing the role of the effective filling factor and $\mathcal{C}_{34}^{(1)}$ the number of fluxes attached to the electrons—again with the distinction that here, neither $\mathcal{C}_{12}^{(1)}$ nor $\mathcal{C}_{34}^{(1)}$ have any even/odd restriction.

The above comparison is, of course, superficial up until now. The excitations of the fractional quantum Hall effect carry a fractional charge, and the nontrivial exchange statistics have a concrete physical meaning for the motion of excitations in 2 spatial dimensions—all of which are properties we did not explore so far. We now move on to a more in depth analysis of the anyonic exchange statistics for the concrete circuit system, where we show that in our case, the anyonic excitations carry fractional flux, and that large networks indeed map to anyonic particles that are free to move on a discrete lattice, allowing to probe (and even exploit) the nontrivial exchange statistics in various ways. As it turns out, these findings are intimately linked to the Josephson effect, and the specific gauge properties of quantum systems on the torus.

To prepare the ground, let us therefore add a generic Josephson effect to the Hamiltonian, which can have various origins. For instance, we can (as previously foreshadowed) reintroduce the neglected ϕ_z -dependence in both ϵ_0 and \mathcal{B}_0 in the black box element, which in both cases (due to 2π -periodicity in ϕ_z) is expressed in terms of a generic Fourier series of harmonics, e.g., for $\epsilon_0 = \sum_{m_1, m_2, \dots} \epsilon_{m_1, m_2, \dots} e^{im_1\phi_1} e^{im_2\phi_2} \dots$ with $m_z \in \mathbb{Z}$ (and similarly for \mathcal{B}_0). Or we can directly connect the nodes z with additional Josephson junctions, e.g., a tunnel contact between ground and a given node z , $\sim \cos(\phi_z)$, between two nodes $\sim \cos(\phi_z - \phi_{z'})$ or any more generic (e.g., multiterminal) junction adding yet another contribution to ϵ_0 (or a topologically trivial contribution to the Berry curvatures $\mathcal{B}_{zz'}$ [195]).

In either case, it is easy to analyse the impact of such a Josephson effect in the low-energy regime where the Josephson energy (i.e., the amplitudes of any Josephson harmonics) is weak compared to the cyclotron frequency. Here, we can project onto the lowest Landau level with the operator P_0 (such that $a_j P_0 = P_0 a_j = 0$ for all cyclotron modes j , while the anyon subspace stays untouched). For the first harmonic, we get

$$P_0 e^{i\phi_z} P_0 = \alpha e^{i\Phi_z}, \quad (21)$$

where the scalar prefactor is real, smaller than 1, and equal to $\alpha = \text{tr}[e^{\sum_{z'} (\frac{1}{g-gT})_{zz'} N_{z'}} P_0]$. It simply arises from projecting out the Landau level excitations, which renormalizes the amplitude of the Josephson effect. The same principle generalizes for arbitrary higher harmonics in the Josephson effect,

$$P_0 e^{\sum_z m_z \phi_z} P_0 \sim e^{\sum_z m_z \Phi_z}. \quad (22)$$

Note that we also get the same qualitative result for higher harmonics in the Berry curvature, which provide extra terms of the form $P_0 N_{z'} e^{\sum_z m_z \phi_z} P_0 \sim e^{\sum_z m_z \Phi_z}$ [when expanding the kinetic energy in Eq. (2)]. The only difference here is that the renormalization prefactor changes due to the extra N_z operator.

Consequently, at low energies, any Cooper pair leakage (either through residual deviations from flat bands, or by design when adding an extra Josephson junction) lifts the degeneracy of the Landau level. To give an example, let us add a regular tunneling junction (only first harmonic) between ground and node z , $-E_J \cos(\phi_z)$. Projected to the lowest Landau level, this yields the Hamiltonian $H = -\tilde{E}_J \cos(\Phi_z)$, revealing a fine structure of the degenerate subspace. The Josephson energy is renormalized, $E_J \rightarrow \alpha E_J \equiv \tilde{E}_J$ in accordance with Eq. (21). For example, for $Z = 2$ the prefactor is simply $\alpha = e^{-\pi/(2p)}$ (i.e., the higher the value of the first Chern number $\mathcal{C}^{(1)}$, the weaker the renormalization). A Josephson effect between two nodes $\sim \cos(\phi_z - \phi_{z'})$ is treated on the exact same footing, yielding at low energies a tunneling of anyons between sites z and z' , $\sim \cos(\Phi_z - \Phi_{z'})$, thus allowing anyons to move on the circuit lattice. Such couplings will be fully exploited in Sec. III for simulations of generic fermionic and anyonic systems.

Importantly, the resulting energy splitting is affected by both Aharonov-Bohm *and* Aharonov-Casher effects [67, 120, 124, 196–198]. The former is straightforwardly included as a classical flux offset, $\phi_z \rightarrow \phi_z + \phi_z^{(\text{ext})}$, which arises from a coupling to an external magnetic field [199]. The latter on the other hand emerges when including offset charges to each node z , $n_z \rightarrow n_z + n_z^{(\text{ext})}$ by applying the gate voltage V_{gz} to node n , such that $n_z^{(\text{ext})} = C_{gz} V_{gz} / (2e)$, where C_{gz} is the capacitance between node z and the gate attached to it. The duality of these two effects can be better understood if we perceive the flux as a magnetic dipole [196]. Then we cannot distinguish whether the charge is moving around the flux, or vice versa. We can detect only a mutual movement or charge and flux with respect to each other (as illustrated in Fig. 3(a)). It is well known that for circuits with compact phases (such as the charge qubit [124]), the energy spectrum is sensitive to charge offsets—giving rise to the so-called charge dispersion effect (which was, e.g., recently used to track quasiparticle poisoning [200, 201] or to probe higher Josephson harmonics [202]). In quantum mechanical terms, the system picks up a phase proportional to the offset charge $n_z^{(\text{ext})}$ as it travels along the periodic ϕ_z and completes one cycle. For a two-dimensional

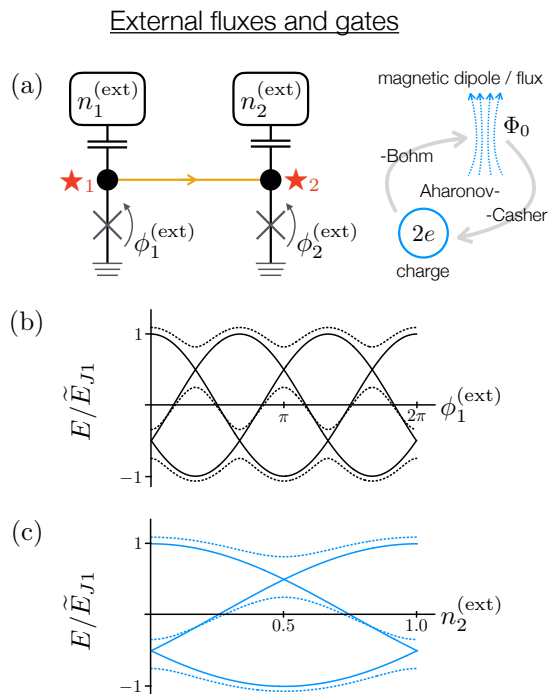


FIG. 3. Gapping the degeneracy of the lowest Landau level by means of Josephson couplings reveals the intricate gauge properties on the torus, and the resulting nonlocal interplay between charge and flux. (a) Minimal example of a circuit with two nodes, connected by a Chern number, each additionally coupled to ground via a Josephson junction. Coupling to an external magnetic field is represented by flux shifts for each Josephson junction, $\phi_{1,2}^{(ext)}$, and interaction to a static electric field is accounted for by a capacitive coupling to a gate voltage, resulting in the offset charges $n_{1,2}^{(ext)}$. The external fields result in a finite flux and charge dispersion, which can be interpreted as a superposition of an Aharonov-Bohm, respectively, Aharonov-Casher effect. Panels (b) and (c) show the different periodicity with respect to applied flux at node 1 and applied offset charge at node 2, here for $p = C^{(1)} = 3$. The broken periodicity with respect to the offset charge indicates that the anyons carry a fractional flux (but integer charge). The solid lines show the case when only one site is shunted by a Josephson junction (i.e. $\tilde{E}_{J2} = 0$), while the dashed lines mark the case when $\tilde{E}_{J2} = \frac{1}{2}\tilde{E}_{J1}$.

subspace ($\phi_z, \phi_{z'}$), this means that the system is not fully determined by the Berry curvature $\mathcal{B}_{zz'}$ alone, since it only determines the geometric phases of paths that do not probe the torus topology (i.e., paths that can be shrunk to single points). The torus however offers two more distinct types of paths (see Fig. 2) whose phases need to be fixed by $n_z^{(ext)}$. Ultimately, by adding the respective flux and charge offsets to N_z and Φ_z respectively, we can show that when projecting to the lowest Landau level, the Josephson effect reveals both types of

shifts as

$$H = -\tilde{E}_J \cos \left(\underbrace{\Phi_z + \phi_z^{(ext)} - 2\pi \sum_{z'} \frac{q_{zz'}}{p} n_{z'}^{(ext)}}_{\Phi_z^{(ext)}} \right), \quad (23)$$

where we defined the total phase shift $\Phi_z^{(ext)}$ as the sum of flux and charge offsets. Since the eigenvalues of $e^{i\Phi_z}$ are discrete and bounded, neither flux nor charge offsets can be gauged away (unless they take on precise quantized values). Instead, in the low-energy projection, the circuit's eigenspectrum is explicitly sensitive to both the Aharonov-Bohm phase (regular Josephson effect) and the Aharonov-Casher phase (effectively a dual Josephson effect), with the latter being *fractional*, as it directly reflects the anyonic exchange statistics. We conclude that the excitations carry a *superposition* of integer charge and fractional flux. Note that here, the anyonic exchange phase and the value of the fractional flux have a one-to-one correspondance. This is in contrast to, e.g., the fractional quantum Hall effect: even though anyonic exchange phase and fractional charge are in general related, they do not exactly assume the same values [181]. Overall, the duality between charge and phase manifests itself in Eq. (23) as a highly nonlocal interdependency between applying a flux offset between ground and node z and adding an gate (inducing an offset charge) at another node z' defined by the connectivity of the gyrator network. The nonlocality of charge and flux gate operations stems from the elimination of the propagation of electro-magnetic waves (valid under the assumption that the speed of light is much faster than any of the other time scales, typical for circuit QED considerations [199]). The non-locality of the theory (in the non-relativistic regime) will reemerge as an important ingredient further below.

To conclude with a concrete example, let us illustrate both the fractionalization and interdependency of charge and phase explicitly for $Z = 2$. The exchange statistics in Eq. (16) are here represented, e.g., by the constructions

$$e^{i\Phi_1} = Z_p \quad e^{i\Phi_2} = X_p \quad (24)$$

where Z_p, X_p form the unitary operator basis for a *qudit* with p degenerate states $\{|d\rangle\}$ ($d = 1, 2, \dots, p$), such that $Z_p|d\rangle = e^{i2\pi d/p}|d\rangle$ and $X_p|d\rangle = |d-1 \bmod p\rangle$. We now add a Josephson effect according to Eq. (23) to each of the two nodes (with the same Josephson energy \tilde{E}_J). Using the representation in Eq. (24), we get a Hamiltonian which is easy to diagonalize. The resulting energy spectrum is shown in Fig. 3(b,c). It confirms flux-fractionalization with the same periodicity as the offset charge depends on the value of p , and demonstrates that changing the offset charge at node 1 and the offset flux at node 2 have the same effect (and are thus linearly dependent).

A final comment regarding our use of the term flux fractionalization. This term has surfaced in other recent

works dealing with superconducting rings and p-wave vortices [203–206] or in Kagome structures [207]. But this usage of the term refers generically to flux quantization in superconducting rings or vortices, which follows from the usual considerations of the superconducting condensate as a macroscopic coherent wave function, where the flux quantum depends on the effective charge of the condensate. Thus, in our language, this notion of fractional flux quantum would involve a change of the fundamental unit of *charge* carried by the condensate. We on the other hand observe the converse: fractionalization of the flux of a given excitation, which is visible when applying an electric (instead of magnetic) field.

III. APPLICATIONS

The above presented findings are (as we will elaborate in detail at various points below) already of significant fundamental interest. But as an initial exercise, we strive to investigate in more depth, how multiterminal circuits can be used as a serious contender for quantum information hardware, including possible methods for quantum error correction. Within this section, we assume for simplicity that H_0 provides a flat topological ground state (again, we refer the reader to Sec. IV for band-engineering methods), where Josephson junctions are added as extra circuit elements in a controlled manner at given nodes. In an actual experiment, it is also perceivable that deviations from flat bands in H_0 itself might be designed in such a way that they provide the desired effects for the read/write implementations. The only important prerequisite is that the Josephson effects be tunable.

A. Establishing qudit gates, read-out, and initialization

We expect the degenerate subspace of the lowest Landau level to be predestined to store and manipulate quantum information. In particular, the impact of flux and charge offsets as shown in Eq. (23) can be used to implement gates. Consider for instance the two-terminal qudit (i.e., $Z = 2$) as defined in Eq. (24). Shifting $\Phi_z^{(\text{ext})}$ (which is achieved either by a shift of $\phi_1^{(\text{ext})}$, or equivalently, by using a charge-type gate, $n_2^{(\text{ext})}$) by value $-2\pi m/p$ ($m \in \mathbb{Z}$) is equivalent to applying gate X_p^m to the qudit state. A similar shift in $\Phi_2^{(\text{ext})}$ yields a Z_p -type gate.

Moreover, by switching on a tunable Josephson effect to node 1 (2) and performing a projective measurement of the eigenfrequency, we can initialize it in the eigenbasis of Z_p (X_p). This measurement can be accomplished, e.g., by a dispersive read-out in very close analogy to transmon devices [208]. The idea is simply to add a (e.g., LC) resonator with resonance frequency ω_R , described by the Hamiltonian $\omega_R b^\dagger b$ and couple it to one of the nodes, ei-

ther inductively or capacitively [209], see Fig. 4(a). In either case, the impact of a resonator coupling to node z can be described by a resonator shift in the offset phase defined in Eq. (23),

$$\Phi_z^{(\text{ext})} \rightarrow \Phi_z^{(\text{ext})} + g(b + b^\dagger). \quad (25)$$

Let us compute the impact of such a coupling explicitly for $Z = 2$ and a Josephson coupling to node 1. The uncoupled qudit Hamiltonian (for $g = 0$ and setting external charge and flux offsets to zero) is $H = -\tilde{E}_J(Z_p + Z_p^{-1})/2$, resulting in the qudit eigenfrequencies $\omega_d = -\tilde{E}_J \cos(2\pi d/p)$. Next, we include the coupling to the resonator mode as described above ($g \neq 0$), and perform a perturbative treatment up to second order in g . This yields a Lamb shift of the qudit frequency by $\omega_d \rightarrow \omega_d - 2g^2 \tilde{E}_J^2 \sin^2(2\pi d/p)/\omega_R$, as well as a Stark shift in the resonator frequency by

$$\omega_R \rightarrow \omega_R + \frac{g^2}{2} \tilde{E}_J (Z_p + Z_p^{-1}) \quad (26)$$

such that the eigenstate of Z_p is readily measured via probing the resonator frequency. Of course, the very same mechanism that provides qudit initialization also allows for projective readout at the end of the algorithm. Initialization, respectively, readout in the X_p basis works in complete analogy, except that we have to switch on a Josephson coupling to node 2.

B. Blueprints for quantum error correction codes

The above text outlines a complete description of a qudit with its gate operations, initialization and readout. In order to protect the qudit against errors, we first list the most common sources of perturbations:

- (i) Excitations to higher Landau levels due to finite frequency noise sources.
- (ii) Parasitic Cooper pair leakage across the H_0 device due to ϕ_z -dependent fluctuations of $\epsilon_0, \mathcal{B}_0$.
- (iii) Adiabatic offset charge and flux noise on each node z due to random fluctuations of $\phi_z^{(\text{ext})}$ and $n_z^{(\text{ext})}$.
- (iv) Chern number fluctuations due to quasiparticle poisoning [62] or charge noise [88, 89] [210].

Source (i) is unproblematic as it does not affect the qudit subspace. Source (ii) generates error gates of the form Z_p, X_p . Since the amplitude of such leakage Josephson effects can be fluctuating in time (see also further below), these perturbations should be considered as stochastic. There may be higher harmonics of the considered leakage, but those will likely be suppressed (see later). As previously discussed, gates Z_p, X_p are equivalent to offset flux shifts in $\phi_{1,2}^{(\text{ext})}$ by discrete values $\pm 2\pi/p$. Hence, both sources (ii) and (iii) are of the same type, except that the

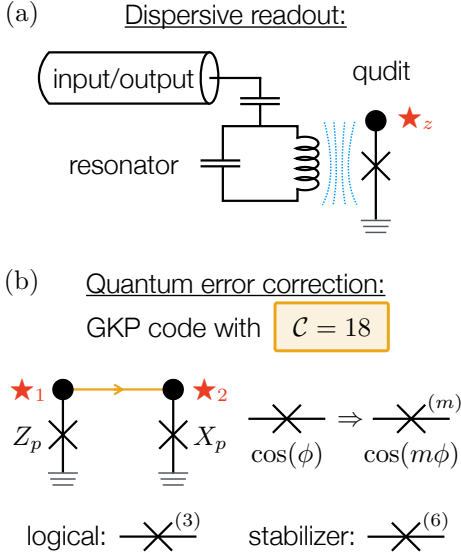


FIG. 4. Working towards quantum hardware applications. (a) Schematic representation of dispersive readout, adapted to the anyonic qudit state at a given node z . The projective readout in the eigenbasis of the operator $e^{i\phi_z}$ occurs via (e.g., inductive) coupling between Josephson junction and a resonator connected to a transmission line. (b) Realization of a GKP code, where the redundancy is achieved by increasing the value of the Chern number (here, $C^{(1)} = 18$). Logical qubit and stabilizer codes are implemented by multistable Josephson junctions, where the dominant charge transfer process corresponds to the simultaneous co-tunneling of m Cooper pairs.

latter describes continuous, instead of discrete shifts. Finally, perturbation (iv) is immediately detectable by a readout of the circuit resonance frequency, as changes in the Chern number directly affect the cyclotron frequency, see Eq. (18) [or Eq. (19) for four terminal devices]. In devices based on Andreev bound states [62] the ground state Chern number is recoverable by means of microwave irradiation evacuating quasiparticle excitations [211–213] which can (in principle) be fed to the qudit by the same transmission lines that perform initialization and readout. We further note that recent experimental data indicate quasiparticle processes in Andreev bound state devices on the order of seconds [214] and gate charge fluctuations in charge qubits (responsible for changes in the Chern number in tunnel junction multiterminal devices [88, 89]) on the order of minutes [110].

With (i) irrelevant, and (iv) detectable and likely slow, we now present ideas for the correction of the perturbations of type (ii) and (iii). As a matter of fact, the group representation of the qudit in terms of Eq. (24) allows for an exact mapping to the Gottesman-Kitaev-Preskill (GKP) code [136]. One of the simplest codes that corrects against (ii) and (iii) is created for $p = 18$, and having the logical qubit basis defined by Z_p^3, X_p^3 and

the commuting stabilizers by Z_p^6, X_p^6 . While the corresponding gates are straightforward to realize (e.g., the gate Z_p^m is implemented by a shift of $\phi_1^{(\text{ext})}$ by $-2\pi m/p$), the initialization and readout is more challenging, as [according to Eqs. (21) and (26)] it involves generating multistable Josephson junctions of the form $\cos(3\phi_z)$, respectively, $\cos(6\phi_z)$, see also Fig. 4(b). As already indicated above, parallel arrangements of Josephson junctions and inductors are known [215, 216] to generate $\cos(m\phi)$ (for $m \in \mathbb{Z}$), as recently demonstrated experimentally for $\cos(2\phi)$ [217]. On-demand engineering of arbitrary energy-phase relationships has recently been strongly generalized in Ref. [146].

While the generation of arbitrary $\cos(m\phi)$ is therefore within reach given recent experimental and theoretical progress on superconducting hardware, it is nonetheless a bottleneck requirement for the proper implementation of the GKP code. We therefore point out an example of a $Z = 4$ device, which allows for lowering that particular hurdle. Consider a network with Chern number matrix

$$C^{(1)} = 2\pi(g - g^T) = \begin{pmatrix} 0 & -1 & 0 & -3 \\ 1 & 0 & 3 & 0 \\ 0 & -3 & 0 & 9 \\ 3 & 0 & -9 & 0 \end{pmatrix}, \quad (27)$$

which has the second Chern number $C^{(2)} = \text{Pf}C^{(1)} = 18$, as well as the maximal denominator $p = 18$. The group representation of the Josephson effects to each of the four nodes can here be cast into the form,

$$\begin{aligned} e^{i\Phi_1} &= Z_p, & e^{i\Phi_2} &= X_p, \\ e^{i\Phi_3} &= Z_p^3, & e^{i\Phi_4} &= X_p^3. \end{aligned} \quad (28)$$

Consequently, applying $\cos(\phi_z)$ and $\cos(2\phi_z)$ Josephson junctions at nodes $z = 3$ and $z = 4$ allows for the implementation of the logical qubit (Z_p^3, X_p^3) and stabilizers (Z_p^6, X_p^6), respectively. Hence, this particular $Z = 4$ circuit requires only Josephson junction elements that have already been experimentally tested.

Some concluding remarks on this idea. With most currently existing proposals for multiterminal junctions reaching only low Chern numbers [88, 89, 91–93] it may seem like a tall order to realize $p = 18$ or similar. However, first of all, we note that multiterminal junctions with higher channel number per contact have been predicted to create ground states with large Chern numbers [62]. Moreover, as we show below, there are certain band-engineering techniques where high Chern numbers appear naturally, essentially as a convenient byproduct. It has to be further noted that physically, the above GKP code is here always implemented by two circuit nodes ϕ_1 and ϕ_2 , that is, creating a device with higher p only requires engineering a higher Chern number, but does *not* necessitate increasing the number of circuit nodes, such that we expect there be a trade-off in terms of hardware complexity. In particular, independent of p there are only as many read-out and gate ports and resonators

needed as there are nodes. As a further potential advantage, with a tunable Chern number (which is the case for most of the currently proposed multiterminal device plans [62, 88, 89, 91–93]) the size of the qudit space can be flexibly tuned in situ to a desired value.

C. Simulations of many-body fermionic systems

One particularly promising application for quantum hardware is the simulation of fermionic quantum many-body systems, described as

$$H = \sum_{z_1 z_2} h_{z_1 z_2}^{(2)} c_{z_1}^\dagger c_{z_2} + \sum_{z_1 z_2 z_3 z_4} h_{z_1 z_2 z_3 z_4}^{(4)} c_{z_1}^\dagger c_{z_2} c_{z_3}^\dagger c_{z_4}, \quad (29)$$

where the fermion operators $\{c_z, c_z^\dagger\} = \delta_{zz'}$ are cast into an appropriate basis. Such Hamiltonians are of great interest for quantum chemistry computations [126, 127], but also various solid state problems [128–130]. Generalizations from regular fermions to Majoranas further provide interesting connections to the SYK model [131, 133, 218] and host so-called fracton excitations [219, 220].

Qubit-based quantum computational chemistry has been widely studied, and is considered one of the prime applications of near-term quantum hardware [126, 127]. While a Fock space representation allows for a straightforward state initialization [221], there usually remains the well-known problem of fermions statistics. The anticommutation already causes problems for classical computation methods such as the famous sign problem in quantum Monte Carlo methods [222]. Specifically for digital quantum hardware simulations [134], anticommutation properties require strongly non-local quantum gates, due to the Jordan-Wigner mapping from fermion operators to the qubit (Pauli) operators [135], which in turn necessitates quantum algorithms of prohibitively large depth (upon sequential application of universal gates) for currently (or near future) available NISQ devices [223]. As a consequence, the nonlocality of Jordan-Wigner chains has led to the development of more efficient (but still nonlocal) encodings of anticommutation properties [224, 225] or to sophisticated techniques for increasing the simultaneity of qubit gates [226–230].

In contrast, the here presented platform provides an alternative pathway towards simulating fermionic Hamiltonians [Eq. (29)], which permits the use of *local* gates and, thus, replaces large scale parallelization of gate operations. This is possible because excitations with anyonic exchange statistics emerge directly and physically from the nonzero Chern number and do not require a complicated synthesis from another (e.g., qubit) basis. We note that recently, proximitized quantum dots have been proposed as a platform for universal fermionic quantum computation [231]. In contrast to that work, we here can with the same platform simulate an entire range of anyonic excitations. The generalization to anyons is of further importance, since the Chern number can be increased to create redundancy (and thus error protection)

in a very similar fashion as described in the GKP code above—again, without requiring a larger number of circuit nodes. Finally, since the fermions are effective, emergent excitations from an underlying nonreciprocal (geometric) circuit interaction, it turns out that they are not bound to ordinary restrictions, such the Wigner supers-election rule (more on that later).

To start, take again a generic circuit with Z nodes (recall that Z is even), and set each first Chern number equally to the value 2, i.e., $C_{zz'}^{(1)} = 2$ (for $z' > z$). In accordance with Eq. (12) and the subsequent discussion, we here find an exchange statistics of $p = 2^{Z/2}$ and (again with $z' > z$) $q_{zz'} = (-1)^{z+z'} 2^{Z/2-1}$ [where $(-1)^{z+z'}$ simply provides an alternating sign depending on the z and z' indices, due to the Levi-Civita tensor in Eq. (14)]. We thus observe the following. The lowest Landau level has $p = 2^{Z/2}$ -fold degeneracy. Moreover, all exchange ratios simplify to $q_{zz'}/p = \pm 1/2$, such that the anyons $e^{i\Phi_z}$ anticommute, and for the same reason $e^{i2\Phi_z}$ must be a c-number (which, upon appropriate choice of the offset phase contributions, can be set to 1). The system thus generates a set of Z real Majorana fermions (Fig. 5), i.e.,

$$e^{i\Phi_z} \equiv \gamma_z \quad (30)$$

with $\{\gamma_z, \gamma_{z'}\} = 2\delta_{zz'}$. Since Z is even, we can always represent these Z Majoranas in terms of $Z/2$ ordinary complex fermions, and thus open the road towards implementations of the Hamiltonian in Eq. (29). To this end, we introduce the well-known mapping between the Majorana basis and the actual fermion basis, by choosing the representation

$$\begin{aligned} \gamma_z &= c_z + c_z^\dagger, \\ \gamma_{z+Z/2} &= i(c_z - c_z^\dagger), \end{aligned} \quad (31)$$

where the z index range is cut in half, $z = 1, \dots, Z/2$, when referring to fermions instead of Majoranas. This mapping is not unique. Any $SO(Z)$ transformation applied to γ_z still results in the same the fermionic algebra.

We are now left with adapting initialization/readout, state preparation, gate operations, and error protection strategies from the previous section to the specific fermion problem present here. The fermionic Hamiltonian in Eq. (29) is written in Majorana language as

$$H = \sum_{z_1 z_2} \tilde{h}_{z_1 z_2}^{(2)} \gamma_{z_1} \gamma_{z_2} + \sum_{z_1 z_2 z_3 z_4} \tilde{h}_{z_1 z_2 z_3 z_4}^{(4)} \gamma_{z_1} \gamma_{z_2} \gamma_{z_3} \gamma_{z_4}. \quad (32)$$

In fact, Eq. (32) is more general than Eq. (29), as it also allows the inclusion of pairing terms, $\sim c_z^\dagger c_{z'}$. As already foreshadowed, the Majorana Hamiltonian with quartic interactions ($\sim \tilde{h}^{(4)}$) was recently studied in connection with so-called fracton excitations [219, 220]. If the quartic term dominates and its elements take random values, it falls into the area of the applicability of the SYK model [131, 133, 218]. With the here proposed hardware, both Eqs. (29) and (32) can be implemented on the very same footing.

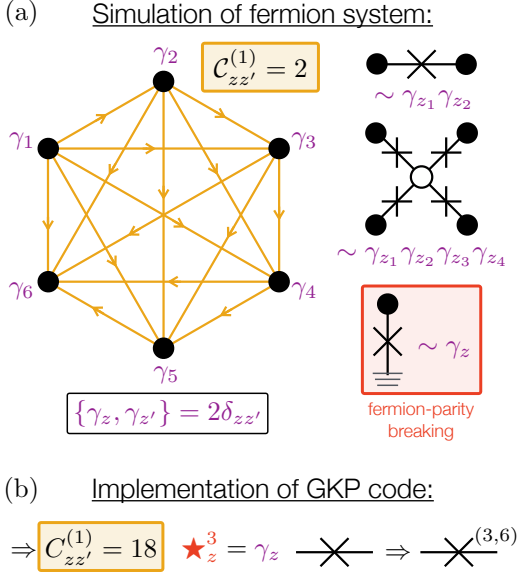


FIG. 5. Blueprint for simulations of fermionic systems with multiterminal circuit hardware. (a) Choosing all Chern numbers identically equal 2 reduces the anyons to regular (Majorana) fermions. Quadratic and quartic interaction terms are realized with regular two-terminal, respectively 4-terminal Josephson effects. Note that with Josephson couplings to ground (which do not conserve the total Cooper pair charge on the nodes) the circuit architecture allows for the generation of terms in the Hamiltonian which break the fermion-parity superselection rule (see Sec. III D for a dedicated discussion of this issue). (b) The fermion simulator can be stabilized with the GKP code, where higher Chern numbers conveniently provide a redundancy, where a $1/18$ -flux parafermion allows to encode copies of the Majorana fermion. Logical (Majorana) gates and stabilizers are implemented in analogy to Fig. 4.

Initialization and readout, as well as state preparation work in close analogy to the above GKP example. The only difference is that we here do not necessarily want to be able to only initialize in the Majorana basis (γ_z), but also in the fermion basis. This is done as follows. By coupling nodes z and $z + Z/2$ by a regular tunneling Josephson junction, we arrive at a coupling term $\sim -i\gamma_z\gamma_{z+Z/2} = 2c_z^\dagger c_z - 1$, which has eigenvalues ± 1 . Just like in the previous sections, the amplitude of this term is tunable with external flux or charge offsets, and the eigenvalues are amenable to the very same dispersive readout as demonstrated in Eq. (26), again with a resonator coupling to the phase (flux or charge offset) of the Josephson effect. With appropriate tuning of the parameters, and sequential projective measurement, we can postselect the state corresponding to the fermion vacuum $|\text{vac}\rangle$ (which has eigenvalues -1 for all $1 \geq z \geq Z/2$). Once this vacuum state is prepared, it can be filled with fermions via the same flux or charge offset gates as for the GKP code. In particular, a flux offset π between ground and node z is equivalent to applying the unitary

gate operator γ_z to the vacuum state. Since the vacuum state is empty, $c_z^\dagger|\text{vac}\rangle = \gamma_z|\text{vac}\rangle$ (or $i\gamma_{z+Z/2}|\text{vac}\rangle$), such that this corresponds to filling state at site z with an electron. In order to create superpositions between different sites z and z' , as well as simulating the quadratic parts of the Hamiltonians, Eqs. (29) or (32), we again switch on a tunnel junction coupling, but this time between two arbitrary nodes, which maps [in accordance with Eq. (22)] to the gate $\sim \gamma_z\gamma_{z'}$. The final gate we need to discuss is the one to implement the quartic interaction term [$\sim \tilde{h}^{(4)}$ in Eq. (32) or equivalently, $\sim h^{(4)}$ in Eq. (29)]. Such a term can obviously not be generated by a simple tunnel junction coupling. Nonetheless, its generation needs only minimal requirements beyond sequential Cooper pair tunneling. Specifically, thanks to the Majorana property $\gamma_z^2 = 1$ in conjunction with Eq. (22), it immediately follows that any charge conserving four-terminal junction with higher harmonics (connecting nodes z_1, z_2, z_3, z_4) yields a sum of bilinear terms $\sim \gamma_z\gamma_{z'}$ ($z, z' = z_1, z_2, z_3, z_4$) and a single quartic term $\sim \gamma_{z_1}\gamma_{z_2}\gamma_{z_3}\gamma_{z_4}$. To give an example, consider a central charge island coupled via regular SIS junctions to four nodes $z_{1,2,3,4}$, see Fig. 5(a). Denoting the central charge island with phase ϕ_0 , the Hamiltonian for this particular four-terminal junction is found according to the standard circuit QED recipe [182, 183],

$$H_4 = E_C(n_0 + n_{g0})^2 - E_J \sum_{j=1}^4 \cos(\phi_0 - \phi_{z_j}). \quad (33)$$

In the above equation, we treat the phases ϕ_{z_1, \dots, z_4} as classical, and only consider quantization of the central island, $[n_0, \phi_0] = i$. Assuming $E_C > E_J$ and tuning the offset charge close to the charge-degeneracy point, $n_{g0} = -1/2 + \delta n_{g0}$, we can approximate by reducing the Hilbert space to the two charge states $n_0 = 0, 1$, which can be represented as Pauli matrices $\sigma_x = |1\rangle\langle 0| + \text{h.c.}$, $\sigma_y = -i|1\rangle\langle 0| + \text{h.c.}$, and $\sigma_z = |1\rangle\langle 1| - |0\rangle\langle 0|$. We approximate $(n_0 - 1/2 + \delta n_{g0})^2 \approx \delta n_{g0}\sigma_z + \text{const.}$, and $e^{\pm i\phi_0} \approx (\sigma_x \pm i\sigma_y)/2$, such that the ground state energy of H_4 is

$$-\sqrt{E_C^2 \delta n_{g0}^2 + E_J |e^{i\phi_{z_1}} + e^{i\phi_{z_2}} + e^{i\phi_{z_3}} + e^{i\phi_{z_4}}|^2}, \quad (34)$$

plus an irrelevant constant offset. The ground state energy depends only on the phase differences $\phi_z - \phi_{z'}$ (indicating Cooper-pair charge conservation on the four nodes $z_{1, \dots, 4}$). Via Taylor expansion in E_J , and subsequent projection onto the lowest Landau level, one can easily see that this circuit element provides the sought after bilinear and quadratic terms. If the bilinear terms between two nodes z and z' are undesired, they can be removed by shunting the corresponding nodes with the previously discussed ordinary tunnel junction and appropriate flux or gate tuning.

With the above recipe, the multiterminal device can act as NISQ platform for the simulation of interacting fermionic and Majorana systems as outlined in Eqs. (29)

and (32). The experimental availability of multiterminal junctions and the high degree of tunability (with either applied fluxes or gates) provides the opportunity to solve a wide class of problem instances within the same device. And as demonstrated above, contrary to qubit based hardware, the here developed platform with anyonic excitations allows for the implementation of interacting Hamiltonians with local gates and readout. Nonlocality is already engrained within the hardware due to the Chern network (which remains static for most purposes). The only other nonlocal component is due to the implementation of interaction terms. The interaction depth can be increased as follows. While quartic interactions require (as just shown) four-terminal junctions with finite higher harmonics, a hypothetical three-body interaction (a sextic term) would require a 6-terminal junction, and so on.

Importantly, note that one can conveniently combine the fermion simulator blueprint with the above introduced error correction scheme. To illustrate this, let us increase all the Chern numbers from 2 to 18. The resulting q matrix and p number retain their general shape, except that now the emerging excitation no longer represent Majorana fermions, but $1/18$ parafermions (again one on each node z), η_z , such that $\eta_z\eta_{z'} = e^{\pm i\pi/9}\eta_{z'}\eta_z$ and $\eta_z^{18} = 1$. On the one hand, such a hardware could implement a highly exotic parafermion system, where interaction terms could be generated in the same way as above. But we can use the exact same hardware to still simulate regular (Majorana) fermions with a *redundancy*, which can be paired with the exact same logical qubit construction as for the GKP code, see also Fig. 5(b). Here $\gamma_z \equiv \eta_z^3$ gives yet again a subspace of regular, anticommuting Majorana fermions. The stabilizer code which can detect errors is likewise now constructed with operators η_z^6 . As already stated, the redundancy requires gates that contain $\cos(3\phi)$ and $\cos(6\phi)$ Josephson effects instead of regular $\cos(\phi)$ tunnel junctions. This in turn renders also the engineering of the aforementioned quartic interaction effect more challenging. For instance, in the previously introduced four terminal device to implement quartic interactions, Eq. (33), all regular SIS Josephson effects, $\sim \cos(\phi_0 - \phi_{z_j})$, need to be replaced by $\sim \cos(3[\phi_0 - \phi_{z_j}])$.

That notwithstanding, the here considered device setup allows for a quantum hardware implementation with the following two advantages. First, the setup is expected to benefit from reduced hardware cost when including quantum error correction, insofar as the redundancy does not scale with the number of circuit nodes but the Chern number. Second, the emergence of anyonic excitations associated to each circuit node allows for the simulation of fermionic (or more general) exchange statistics with local read-out, and time-dependent gates whose degree of non-locality scales with the number of particles involved in an interaction event. Especially the latter might provide a promising alternative to qubit-based simulation of fermionic systems, allowing to avoid

the necessity of implementing large scale parallelization of gates for single fermion operators [226–230].

D. Fermion parity

We close this section with an interjection of more fundamental nature, based on a simple, but surprising observation. Notice that the quadratic ($\sim h^{(2)}, \tilde{h}^{(2)}$) and quartic ($\sim h^{(4)}, \tilde{h}^{(4)}$) terms in the above fermion simulation, Eqs. (29) and (32), rely on Josephson contacts between two, respectively, four nodes. We can however, as already pointed out above, connect a single node via a Josephson effect to ground, see also Fig. 5(a). Crucially, a contact to ground provides a *linear* term in the Hamiltonian, $\sim \sum_z h_z^{(1)}\gamma_z$ (with $h_z^{(1)}$ real). While such terms are perfectly Hermitian, they clearly break the fermion parity superselection rule [169] (also referred to as Wigner superselection). On a physical level, we can connect the breaking of the Wigner superselection rule to charge conservation on the circuit. The two and four node Josephson contacts conserve the total Cooper-pair charge on the nodes $\sum_z n_z$. The contact to ground does not, which is a legitimate feature since the ground can be seen as an infinite Cooper-pair reservoir.

Let us diffuse right away any concerns that our theory might violate fundamental laws of nature. The backbone of the Hamiltonian in Eq. (2) are the set of ground states of H_0 for all ϕ_z , $|0(\{\phi_z\})\rangle$. If H_0 is formulated as a regular, fermion-parity-conserving theory (which must be true on some level for any field theory based on electronic degrees of freedom), then $|0(\{\phi_z\})\rangle$ preserves fermion-parity superselection for the regular electrons, independent of the values of the set $\{\phi_z\}$. The low-energy theory in Eq. (2) then merely provides many-body wave-function solutions that are coherent superpositions of the states $|0(\{\phi_z\})\rangle$ with ϕ_z -dependent amplitudes. Hence any low-energy pair of states $|\psi\rangle$ and, e.g., $c_z^\dagger|\psi\rangle$ [see Eq. (31)] both have the same fermion-parity in terms of the original electronic degrees of freedom. The fermion-parity breaking property only appears in the new set of anyonic excitations satisfying Eq. (11), which emerge through the Landau level physics on the closed torus manifold.

The here observed fermion-parity breaking is therefore conceptually very similar to implementations of fermionic operators in terms of universal qubit hardware. However, we again have to insist that the latter requires highly non-local gates (such as Jordan-Wigner chains [134, 135]) in order to recreate the anticommuting property. Our theory on the other hand is (to the best of our knowledge) the first to implement a fermion-parity breaking theory with local gates. And it is exactly this difference between local and nonlocal fermionic gates, which is of quite some conceptual interest.

To appreciate this point, we refer to a prominent emerging fundamental research area, which strives to derive the axioms of quantum mechanics not from physical principles, but from a quantum information point of

view [171–176]. Within this research thrust, there has been quite some debate as to whether Wigner superselection in fermionic systems requires physical, relativistic arguments, or whether it can be justified in a non-relativistic setting, by fundamental quantum-information theoretic axioms, such as local realism (in the quantum mechanical sense) [177–180].

Importantly, our theory provides a counter-example of a theory that breaks Wigner superselection, and thus allows for the formulation of protocols which demonstrably break the no-communication theorem. This breaking of local realism does not break relativistic principles, since our theory relies on integrating out the photon degrees of freedom (which propagate at the speed of light). Nonetheless, if one were to impose no-signalling without explicitly invoking relativistic arguments [179], one would have erroneously excluded the possibility that a theory like the one presented here exists in the first place.

In the Appendix B, we present a circuit realization of a simple but elegant protocol presented in Ref. [179], which demonstrates how breaking Wigner superselection allows for changing the outcome of a measurement in one subsystem (Alice), by only performing local gates in another, spatially separated subsystem (Bob). This protocol requires only two actual fermionic modes (one for Alice, one for Bob), such that it can be run on a circuit with 4 Majorana nodes, and involves the above introduced machinery of quantum gates and measurements via Josephson junctions and read-out lines.

Overall, this protocol kills two birds with one stone: it provides a smoking gun experimental signature for the presence of anticommuting (fermionic) excitations, as well as a breaking of the no-communication theorem. Moreover, we note that precision in the gate operations is not required, and similarly, the suppression of errors is not critical for a successful probing of the sought-after effect. To the contrary, this experiment is highly sensitive to any ever so slight breaking of fermion parity.

One final remark. The discussion up until now has either been geared towards concrete quantum applications for the simulation regular (parity-conserving) fermionic quantum field theories, or to specifically designed cases of small systems where the breaking of Wigner superselection can be probed. However, it has to be noted that for a large circuit without specific band-engineering, the parity-breaking case is the *default scenario*. That is, circuits without targeted suppression of Josephson leakage generically map onto Hamiltonians of the form

$$H = \sum_{z_1} \tilde{h}_{z_1}^{(1)} \gamma_{z_1} + \sum_{z_1 z_2} \tilde{h}_{z_1 z_2}^{(2)} \gamma_{z_1} \gamma_{z_2} + \sum_{z_1 z_2 z_3} \tilde{h}_{z_1 z_2 z_3}^{(3)} \gamma_{z_1} \gamma_{z_2} \gamma_{z_3} + \dots, \quad (35)$$

or more general anyonic forms (depending on the Chern number network). And it is a perfectly legitimate goal to simply explore the behaviour of such circuits, without having a concrete application or sought-after effect

in mind. But to the best of our knowledge, there exists no literature attempting to analyze even the basic properties of Hamiltonians of the above type, let alone investigate possible quantum phase transitions or other collective phenomena, since the parity-breaking terms were obviously not expected to exist in nature. Our work thus very organically unravels the existence of an entirely unexplored class of quantum field theories—calling for a dedicated future research effort to explore or extend quantum field theoretic methods to tackle parity-breaking fermionic systems (and anyonic generalizations thereof), as we further outline in the outlook at the end.

IV. IMPLEMENTATIONS

The above described emergent anyonic excitations have been derived under the assumption of topological flat bands. Deviations from flat bands emerge in two flavours, which can both be appreciated on the general level of the Hamiltonian given in Eq. (1). If the band width of ϵ_0 is of the same order as the charging energies [first term in Eq. (1)], then the projection onto the lowest Landau level is no longer a very accurate approximation. Although, note that the cyclotron frequency scales linearly with the Chern number, see Eq. (18), such that higher Chern number (higher effective magnetic field) protects to some degree against occupation of higher Landau levels. As a second possibility, the band width could be comparable to the energy gap in H_0 , such that we need to include higher bands ($m > 0$). Importantly, none of the above deviations fundamentally destroy the anyon excitation picture. The first mechanism simply leads to a Hamiltonian where anyon interactions can become strong (which, as layed out in Sec. (III C) can actually be a desired effect). As for the inclusion of higher bands of H_0 , it can be noted that also those bands may have a Chern number, such that their presence essentially just introduces a second type of anyon, again with potentially strong interactions, even between different bands. Overall, especially for applications towards quantum simulation architectures (which rely on a high control of Josephson effects between nodes as gate operations), it may nonetheless be desirable to flatten the bands for high precision. In this remaining section, we show how band engineering in the space of superconducting phases ϕ_z is accomplished.

While band engineering is a highly active emergent field in the context of solid state physics (where the energy bands are defined in k - instead of ϕ -space), the circuit equivalent has only very recently gained traction in some special cases [138, 146, 232, 233]. Here we provide some additional results and concepts, based either on fine tuning of system parameters (inspired by Ref. [138]), parallel shunts of circuit elements (similar in spirit to Ref. [146]), or dissipative phase transitions (as an application of a capacitive version of the Schmid-Bulgadaev phase transition [147, 148, 168, 234]).

As pointed out in Sec. II, any generic multiterminal junction can be reduced to a matrix of first Chern numbers between two nodes, see Eq. (7) and Fig. 1. We therefore focus in this section on three-terminal junctions (with one contact to ground, resulting in two active nodes ϕ_1 and ϕ_2) as the minimal required building block which hosts a nonzero first Chern number defined in ϕ_1, ϕ_2 . Constructing a more general network with a higher number of nodes ϕ_z ($z = 1, \dots, Z$) can be achieved by connecting any number of minimal three-terminal building blocks between two nodes ϕ_z and $\phi_{z'}$.

A. Andreev bound states versus continuum

As already summarized in the introduction, depending on the concrete physical realization, there is a number of ways to describe the physics of the multiterminal junctions [62, 88, 89, 91–93]. A quite generic, yet simple approach relies on expressing the transport properties of a given multiterminal junction with a Cooper pairs scattering matrix S . Including Andreev reflection at the superconducting contacts, the system can be solved by means of ordinary wave function ansatz, whose boundary conditions at the junction and contacts are stitched together [235]. The superconducting gap Δ defines the central energy scale. There exist solutions with subgap energies $|E| < \Delta$ which are so-called Andreev bound states (ABS), that is, quasiparticle states that are localized at the junction. For short ballistic junctions, these states have a discrete spectrum. Solutions above the gap, $|E| > \Delta$, are extended quasiparticle states that form a continuum. The ABS part of the spectrum is conveniently computed via the Beenakker determinant equation [137]. In alignment with the Bogoliubov-de-Gennes formulation of superconducting devices, each positive energy solution E has a particle-hole symmetric negative energy solution $-E$, where the many-body ground state has all negative energy states occupied.

The ABS energy spectrum typically has a strong dependence on the superconducting phases, and thus provides a finite supercurrent. However, it has recently been remarked [138] that special choices of *chiral* scattering matrix for three-terminal junctions of the form

$$S = \begin{pmatrix} 0 & 0 & 1 \\ 1 & 0 & 0 \\ 0 & 1 & 0 \end{pmatrix} \quad (36)$$

gives rise to *flat* ABS energy bands. This matrix describes a scattering region with zero reflection (the diagonal of S is zero), and perfect chiral transmission, such that an incoming electron from terminal 1 (2, 3) is transmitted to terminal 2 (3, 1) with 100% probability. Importantly, Ref. [138] showed that this perfectly flat ABS energy band contributes zero Chern number, which led the authors to identify this particular chiral junction as topologically trivial.

Indeed (as we comment on in more detail below), this finding seems consistent with recent formal results derived within solid state theory, which put significant constraints on the possible existence of topological flat bands. In particular, the subgap part of the energy spectrum of the above three-terminal junction essentially boils down to a two-band model [236] for which it has been shown [143] that there cannot be topological flat bands. But as we show now, Andreev physics offers a surprising loop-hole, in the form of the continuous quasiparticle states. In alignment with the Bogoliubov-de-Gennes formulation, the many-body ground state Chern number must be given by the sum of all negative energy contributions [62], and it has already been noted [82] that in certain cases the (negative energy) continuum might provide a finite Chern number contribution to that ground state.

This motivates us to revisit result of Ref. [138] under proper inclusion of the quasiparticle continuum. By means of very general topological arguments, we can show that even though the flat ABS state is indeed trivial, the total ground state, including continuum is not. In the next subsection, we illustrate these findings with a concrete example of a quantum dot chain model, which recreates the chiral scattering properties, and which allows to explicitly include the continuum contributions via simple numerical diagonalization of a discrete version of the Bogoliubov-de-Gennes equation.

Our general topological argument relies on representing three-terminal scattering matrices in terms of the generators of the SU(3) group, $S = e^{i \sum_s \theta_s \lambda_s / \sqrt{3}}$, where $s = 1, \dots, 8$, θ_s are real scalars, and λ_s are the Gell-Mann matrices [237]. The details of this argument can be found in the Appendix C. Here follows a summary. The space of all available unitary scattering matrices (without any further symmetries) is represented on an 8-dimensional real space (one dimension per Gell-Mann matrix). Within this space, there are two particular points of interest. First, we observe that the chiral scattering matrix corresponds to the point $\theta_2 = -\theta_5 = \theta_7 = 2\pi/3$ and $\theta_{1,3,4,6,8} = 0$. The other point of interest is the trivial starting point where all $\theta_s = 0$. This corresponds to the case of a fully reflective, trivial scattering matrix $S = 1$, where all 3 superconducting contacts are disconnected, and as a result, the many-body ground state is guaranteed to be topologically trivial. In order to understand the topology of the ground state for the chiral scattering matrix, it suffices to analyse a parametric path (parametrized with the variable θ) from the trivial point ($\theta = 0$) to the chiral point ($\theta = 2\pi/3$) in the 8-dimensional space, and track the evolution of the Chern number of the bound states, as well as all topological phase transitions (energy gap closings either at $E = 0$ or $E = \pm\Delta$), see Fig. 6.

It turns out that we are guaranteed to cross at least two topological phase transitions. First there is a transition (T , between phases ① and ②, see Fig. 6(a) whereby the bound state exchanges a Chern number with the contin-

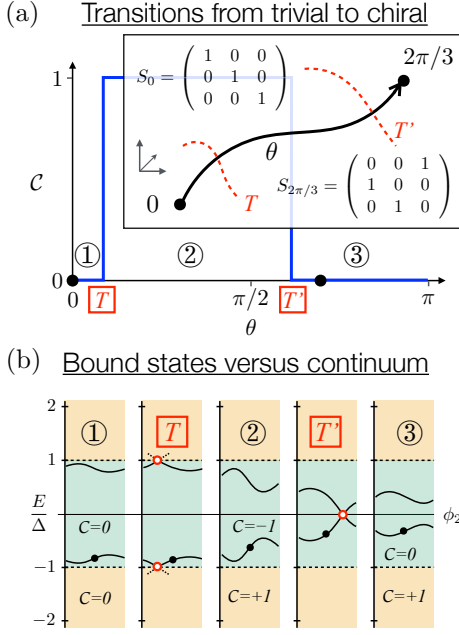


FIG. 6. Relationship between bound state and continuum contribution to the Chern number for three-terminal junctions. (a) We consider a parametrization (θ) of a three-terminal scattering matrix in the space of the $SU(3)$ generators, where the trajectory starts from a completely reflecting junction ($\theta = 0$) and ends at the perfectly circular scattering ($\theta = 2\pi/3$, details in the Appendix C). This trajectory traverses two phase transitions T, T' with band gap closings. (b) Sketch of the different topological phases (①, ②, ③) separated by said band gap closings (T, T'). A first closing (T) occurs at $|E| = \Delta$, where the bound state part of the spectrum (green) and continuum (yellow) exchange a Chern number, but the many-body ground state (sum of all negative energies) remains trivial. A second transition (T') at $E = 0$ exchanges a Chern number between positive- and negative-energy bound states. The bound state thus returns to a trivial zero Chern number and becomes flat at the chiral point, but the many-body ground state has nonzero Chern number thanks to the the continuum.

uum (see Fig. 6(b), second column). Note that in order to see the first transition, one has to choose a more accurate parametrisation as one given above, since Andreev levels touch the continuum for $\theta \rightarrow 0$ (see Appendix C). While the ABS now has a nonzero Chern number (phase ②), the many-body ground state is still trivial, since the ABS and continuum Chern number mutually cancel. There is however a next phase transition (T' , between phases ② and ③) where the bound states at positive and negative energies cross such that they cancel their respective Chern numbers. The ABS state now has zero Chern number (phase ③, in accordance with the finding of Ref. [138]), but there remains a finite Chern number in the continuum, rendering the many-body ground state topologically nontrivial.

To summarize, the above finding can be put in contrast

to the recent surge of band engineering efforts in the solid state context, where a number of theorems put significant constraints on the possibilities of topological flat bands in lattice models in the form of no-go theorems [139–144]. The presence of the continuum states allows circumventing such restrictions: while the flat two-band model for the bound state spectrum with chiral scattering must be topologically trivial [143], the continuum contribution still allows for a topological many-body ground state.

B. Chiral scattering and flat bands with quantum dot chains

Let us now discuss how the previously introduced chiral scattering matrix is physically realized. While chiral transport properties have already been investigated with a quantum hall edge element [238], we here strive for a conceptually simpler realization. For this purpose, we propose a triple quantum dot chain as shown in Fig. 7, which is a variation of earlier proposed proximitized quantum dot models [91–93] with longer chains. The model in the absence of superconducting pairing is written as

$$H_{\text{dot}} = -t \sum_{\sigma} \sum_{z=1}^3 \left(\sum_{j=1}^J d_{z,j,\sigma}^{\dagger} d_{z,j-1,\sigma} + e^{i\frac{\phi_0}{3}} d_{z,1,\sigma}^{\dagger} d_{z-1,1,\sigma} + \text{h.c.} \right), \quad (37)$$

where $j = 1, \dots, J$ is the site index for a single chain, z enumerates the three chains (which will in a moment be connected to superconducting terminals) [239], and σ denotes the spin of an electron on dot z, j . The operators $d_{z,j,\sigma}^{(\dagger)}$ are regular fermion annihilation (creation) operators. The parameter ϕ_0 indicates the presence of a finite flux enclosed by the central triangle. For infinitely long chains $J \rightarrow \infty$, the transport across the central junction is described by a scattering amplitude for incoming and outgoing plane waves to and from the three chains. In particular, for $\phi_0 = \pi/2$ it can be shown that the resulting scattering matrix is indeed perfectly chiral, and thus of the form as in Eq. (36) (see Appendix D).

We next add a local s-wave pairing, $H_{\text{dot}} \rightarrow H_{\text{dot}} + \Delta \sum_z \sum_{j=2}^J \left(e^{i\phi_z} d_{z,j,\uparrow}^{\dagger} d_{z,j,\downarrow}^{\dagger} + \text{h.c.} \right)$, where we set the third terminal to ground, $\phi_3 = 0$. For the infinite chain ($J \rightarrow \infty$), this problem maps exactly to the discussion in the previous subsection. Realistically however, the chain length J will be finite, such that the continuum turns into a quasicontinuum with a small level spacing scaling as $\sim 1/J$. For finite J , this model is solved numerically exactly via a lattice version of Bogoliubov-de Gennes through direct diagonalization, allowing us to extract the energy spectrum as well as Berry curvature of each band (the latter via a convenient projector formula [240]) as a function of ϕ_1 and ϕ_2 , see left 3D plots in Fig. 6(c). A particularly helpful quantity is the inverse flatness index

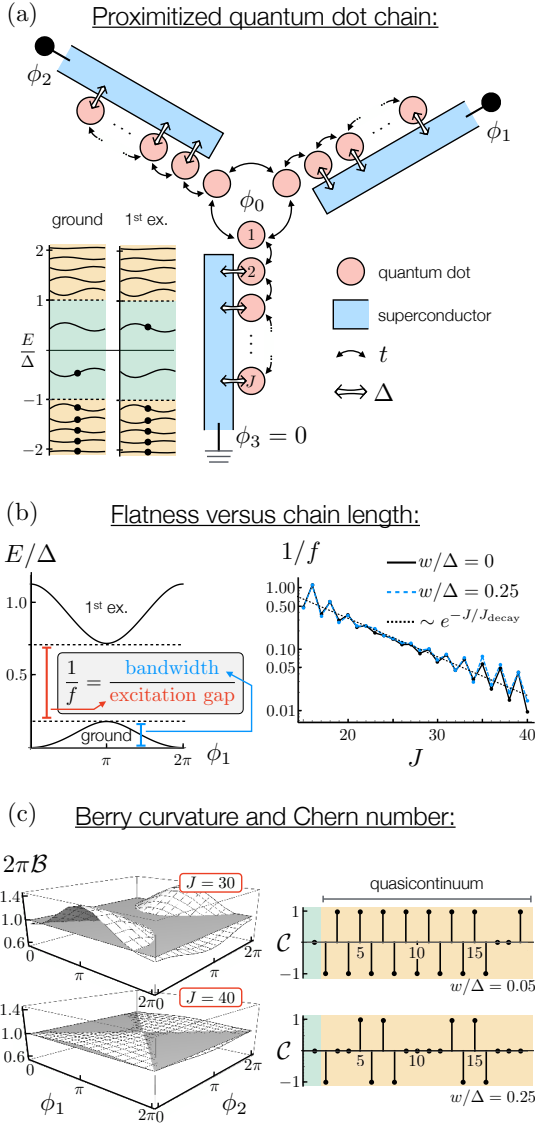


FIG. 7. Realizing a flat topological ground state with proximitized quantum dot chains. (a) Sketch of the three-terminal quantum dot chain model. Electrons tunnel between dots with amplitude t (small arrows). The proximity effect (double arrows) generates an effective order parameter $\Delta e^{i\phi_z}$. The central triangle is penetrated by a magnetic flux, giving rise to a phase ϕ_0 , equal to the magnetic flux in units of the magnetic flux quantum (scaled by 2 for Cooper pairs). The panel on the left illustrates the band structure in the topological configuration ③ from Fig. 6(b) in ground and first excited states. (b) The left panel shows the energy spectrum of the ground and first excited states of the device, as a function of superconducting phase ϕ_1 , for $t = \Delta/10$, $\phi_0 = \pi/2$, $\phi_2 = 0$, and chain length $J = 20$. We define the inverse flatness $1/f$ as the ratio between the band width of the ground state and the excitation gap to the first excited state. The right panel illustrates that the inverse flatness increases exponentially with the chain length. Disorder ($w \neq 0$) has no detrimental impact on the flatness. (c) Left: the flatness of the Berry curvature increases with the chain size. Right: the Chern number of each separate level of continuum and ABS, indicating strong fluctuations of the single level Chern numbers in the continuum. These fluctuations decrease with stronger disorder w .

$1/f$ for the energy, which we define as the ratio of the bandwidth of the many-body ground state [which corresponds to ϵ_0 in Eq. (2)] with respect to the excitation gap to the lowest (parity-conserving) excited state [see right plot in Fig. 6(b)]. Indeed, we can show that as we increase J , the index tends to zero, indicating flat energy bands. The plots on the left in Fig. 6(c) also show that the Berry curvature of the many-body ground approaches the flat value ($\sim 1/2\pi$) to a very high precision, which—in passing—also confirms that the ground state has a finite Chern number, in accordance with the above qualitative discussion about the continuum contribution to the ground state topology.

The aforementioned finite level spacing of the quasi-continuum (due to finite J) allows us to further analyse each single-particle quasicontinuum band contribution to the Chern number individually, see plots on the right in Fig. 6(c). The quasicontinuous states exhibit a strongly alternating Chern number. Their sum of the explicitly calculated Chern numbers for each level will result in total $\mathcal{C} = +1$, consistent with the discussion in the previous subsection, and with the left panel of Fig. 6(c). As mentioned in the introduction, the ground state Chern number has as of now not yet been experimentally observed. The here presented result of strongly alternating Chern numbers in the continuum limit might provide a possible explanation. Namely, as first proposed in Ref. [62], the Chern number can be detected as a quantized transconductance response, when averaging over the dc current. However, if the individual Chern numbers in the continuum are strongly fluctuating, then any inelastic scattering process of a single non-equilibrium quasiparticle in the continuum can completely blur the Chern effect, and thus jeopardize a dc measurement of the Chern number. However, since the ground state of the considered device is a flat topological band, the Chern number is also directly visible in the cyclotron frequency of the lowest Landau level [when including capacitive coupling of the nodes $z = 1, 2$], see Eq. (18)]. Consequently, the Chern number is here accessible to fast read-out with ac methods. This finding also aligns with the error correction discussion presented in Sec. III B: a fast ac read-out of the circuits frequency can quickly detect a quasiparticle poisoning event. Applying an ac tone to the same transmission line at different frequency in response to such an event can, e.g., evacuate the quasiparticle [211–213].

For the quasiparticle evacuation via ac driving to work, we however need an energy window within the quasicontinuum, where the Chern number is zero. For this purpose, we introduce disorder in the quantum dot chain, with disorder strength w . Within the numerical diagonalization of above quantum dot model, disorder is included as a local detuning of the quantum dot levels, i.e., by adding a term $+\sum_{z,j,\sigma} w_{z,j} d_{z,j,\sigma}^\dagger d_{z,j,\sigma}$ to the Hamiltonian. The individual onsite energies $w_{z,j}$ are random numbers (completely uncorrelated for different j and z), which average to zero. For simplicity, we take their random distribution to be uniform from the value $-w/2$ to

$w/2$, such that the standard deviation scales with $\sim w$. Indeed, we can show that already for very moderate disorder, the alternation of the Chern number within the quasicontinuum is significantly thinned out, see Fig. 6(c) (where we chose the values $w/\Delta = 0.05, 0.025$). Moreover, disorder has no detrimental effect on the flattening tendency with increasing J , see Fig. 6(b), allowing us to identify disorder as a truly beneficial mechanism, which significantly reduces quasicontinuum Chern number fluctuations without impeding the formation of flat bands. Note that in Fig. 6(c), we show for simplicity only a small excerpt of quasicontinuous states close to Δ . In the Appendix D we show the full Chern number distribution for the total bandwidth of the quantum dot system (scaling with the large energy $\sim t$), where the reduction of Chern number fluctuations can be appreciated on a much wider range of energy scales.

C. Flattening through scrambling

While the above is a specific example of parameter fine-tuning in multiterminal junctions that are described by an ABS spectrum, we now move on to a more platform independent band-engineering strategy (valid also for other physical junction realizations, such as SIS junctions [88–90]). Both of the techniques discussed below can be summarized as a method to scramble the superconducting phase, such that any ϕ -dependence (be it in the ground state energy ϵ_0 or the corresponding Berry curvatures \mathcal{B} of the generic junction Hamiltonian H_0) is averaged out.

The first idea is similar in spirit to the recent proposal to use higher harmonics in Josephson junctions to engineer arbitrary energy-phase relationships essentially via Fourier transforms [146]. Suppose that a certain three-terminal junction (with two active nodes $\phi_{1,2}$ and one contact to ground) is described by a ground state with energy $\epsilon_0(\phi_1, \phi_2)$ and a Berry curvature $\mathcal{B}(\phi_1, \phi_2) = \mathcal{C}_{12}^{(1)}/2\pi + \delta\mathcal{B}(\phi_1, \phi_2)$ (where we again we separate the constant Chern number contribution from the deviation $\sim \delta\mathcal{B}$, the latter integrating to zero). Any function F that is periodic in all ϕ_z (which is true for $\epsilon_0, \mathcal{B}, \delta\mathcal{B}$) can be written as a discrete Fourier series, $F(\phi_z, \phi_{z'}) = \sum_{m_1, m_2} F_{m_1, m_2} e^{im_1\phi_z} e^{im_2\phi_{z'}}$. The central idea is now that we can attach a certain number of copies of the same element to the same three nodes in a parallel arrangement [see Fig. 8(a), left]. Assuming that these parallel circuit elements can be fabricated with high reproducibility, and only interact weakly (we comment in a moment on the potential impact of imperfections and crosstalk), we can find the new ground state energy and Berry curvature, which need to enter in Eq. (2), as a sum of the individual elements,

$$F(\phi_z, \phi_{z'}) \rightarrow \sum_{k=1}^K \sum_{k'=1}^{K'} F(\phi_z + \delta\phi_k, \phi_{z'} + \delta\phi_{k'}), \quad (38)$$

where $\delta\phi_k, \delta\phi_{k'}$ account for fluxes sent through the extra loops that emerge due to the parallel shunt [see Fig. 8(a), right].

These extra fluxes are used for the flattening procedure, as we can cancel harmonics of a certain order by tuning them to special values. Namely, to exactly cancel all harmonics up to order $|m_1| - 1$ ($|m_2| - 1$) we need $K = |m_1|$ ($K' = |m_2|$) copies with flux shifts $\delta\phi_k = 2\pi k/K$. For generic functions depending on both ϕ_z and $\phi_{z'}$, cancelling all harmonics up to a common order $M - 1$ in both dimensions requires a square grid of $K = K' = M$, and thus in total M^2 parallel copies. There is an important question of convergence, as a generic function F has in general infinitely many Fourier coefficients. But for smooth functions (which is typically true for both ϵ_0 and \mathcal{B}) it is well-known that the Fourier coefficients must decay faster than any polynomial (usually faster than exponential). Hence, we are guaranteed that this procedure converges after a finite number of copies. In fact, this strong (typically exponentially fast) convergence allows us to predict that the main sources of imperfection of flat bands must originate either from deviations in the flux-tuning of $\delta\phi_k, \delta\phi_{k'}$ or limited reproducibility of the elements, such that the sum in Eq. (38), in practice does not go over entirely identical copies of the function F . Because of this, deviations from flat bands are in general only algebraical, but not exponentially suppressed—hence the need for quantum error correction strategies as the previously outlined GKP code.

Two more remarks about the parallelization idea are in order. First, we note that coupling three-terminal junctions in parallel will likely come with cross-talk (an omnipresent issue in any quantum hardware). In this particular case, however, we expect that coherent cross-talk could actually be beneficial, as (depending on the detailed energy structure of the elements) the typical avoided crossing of coherently coupled energy levels is likely to increase flatness. Secondly, if an individual three-terminal element connecting nodes z, z' contributes with a given first Chern number $\mathcal{C}_{zz'}^{(1)}$, K copies in parallel provide the Chern number $K\mathcal{C}_{zz'}^{(1)}$. Consequently, parallelization offers the convenient side-effect of naturally generating large Chern numbers, useful for the GKP code presented above (requiring a minimum Chern number of 18). The only downside of this effect is that if the Chern number of the original element has a certain fluctuation rate (e.g., due to the aforementioned quasiparticle poisoning), then the composite element with K copies has likewise an increase of that fluctuation rate by the factor K . In this regard, we again refer back to Sec. III B, where we explained that Chern number fluctuations are expected to be reasonably slow, such that they can be detected immediately via a discrete change in the Landau level cyclotron frequency.

We now present one final band-engineering strategy. It involves coupling to an environment with a continuous spectrum, and is based on the Schmid-Bulgadaev phase transition [147, 148]. To this end, we pick up on

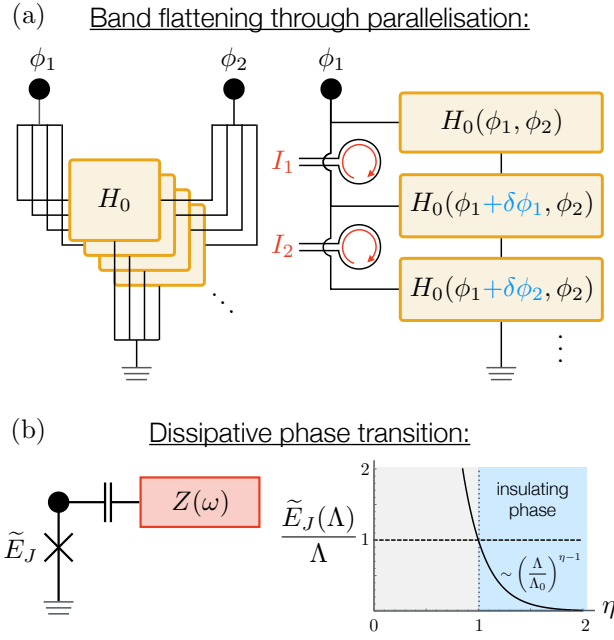


FIG. 8. Flattening topological bands through scrambling of the superconducting phase. (a) Parallelization of identical three-terminal junctions, where external flux lines give rise to phase shifts $\delta\phi_k$. Appropriately choosing the values of $\delta\phi_k$ effectively averages the energy bands and Berry curvatures. (b) Coupling a superconducting node capacitively to an Ohmic bath suppresses the rescaled Josephson energy \tilde{E}_J through quantum fluctuations of the superconducting phase (Schmid-Bulgadaev phase transition).

the coupling of a resonator to a Josephson effect given in Eq. (25), except that we now consider coupling to a continuum of modes, i.e., a resistor [see Fig. 8(b)], $\sum_i g_i (b_i + b_i^\dagger)$ (the bath Hamiltonian being $\sum_i \omega_i b_i^\dagger b_i$). As per standard adiabatic (poor man’s) renormalization group arguments [241], tracing out a window of environment frequencies $\Lambda < \omega < \Lambda_0$ renormalizes the Josephson energy as

$$\tilde{E}_J \rightarrow \tilde{E}_J e^{-\int_{\Lambda}^{\Lambda_0} d\omega \frac{J(\omega)}{\omega^2} \text{Ohmic}} \left(\frac{\Lambda}{\Lambda_0}\right)^\eta \tilde{E}_J, \quad (39)$$

where Λ is the infrared (IR) and Λ_0 the ultraviolet (UV) cutoff. The bath spectral density is $J(\omega) = \frac{1}{2} \sum_i g_i^2 \omega_i^{-2} \delta(\omega - \omega_i)$, which yields $J(\omega) = \eta\omega$ for an Ohmic bath (with the damping coefficient η). We thus obtain the standard suppression of the Josephson effect when driving the system across the dissipative phase transition at $\eta = 1$, as shown in Fig. 8(b). We stress that this result holds for Cooper-pair leakage of *any* kind—i.e., the phase transition suppresses any Josephson effect and finite Berry curvature fluctuations $\delta\mathcal{B}$ (notably including higher harmonics), irrespective of whether the leakage occurs to ground or between nodes.

Particularly a capacitive coupling is of great interest: due to its nonlocal nature via the matrix $q_{zz'}$, see

Eq. (23), driving the coupling across the phase transition could in principle suppress leakage within many nodes at once—using only a single bath as a resistor, coupled to a single node. In relation to that, we note that the Schmid-Bulgadaev phase transition has recently received increased attention regarding its experimental confirmation, especially because of contradictory data [156–166]. It has recently been predicted by some of us [168], that the absence or presence of the phase transition depends on whether or not the environment operator coupling to the qubit has integer eigenvalues. A phase transition was thus excluded in the case of a direct electric contact to a resistor, as it exchanges charge in integer portions. The prerequisites for the phase transition are however met for, e.g., capacitive coupling, where the Ohmic nature of the bath can be connected to a general result of charge counting statistics [242–246], which states that the charge noise always has a logarithmic divergence with respect to the UV cutoff ($\sim \Lambda_0$). We therefore expect that the here proposed engineering of flat bands via dissipation is unaffected by lingering controversies regarding the Schmid-Bulgadaev phase transition.

One potential impediment of the here proposed band engineering via a dissipative phase transition is that the environment provides degrees of freedom at all frequencies, such that it may meddle with a proper functioning of the device as a nearly lossless quantum system at low-energies. We note though, that for our purposes, we do not require the resistor to operate at all frequencies: it only needs to provide quantum fluctuations that renormalize the Josephson amplitudes. That is, the IR cutoff does not necessarily need to be zero. Indeed a finite IR cutoff can in principle be engineered when mediating the interaction between system and resistor via a high-pass filter. A more direct solution consists of a capacitive coupling to a weakly superconducting pseudo-resistor, that is, a material with a low but finite superconducting gap (similar in spirit to gap-engineering ideas for quasiparticle traps [96]). Such a setup would not provide dissipation at low-energies, but still provide finite charge quantum fluctuations that can contribute to renormalization, with Λ remaining finite in Eq. (39).

V. CONCLUSIONS AND OUTLOOK

A. Conclusions

In this work, we demonstrated that geometric (Berry curvature) terms in generic conventional superconducting multiterminal junctions give rise to excitations with anyonic exchange statistics. The fractional exchange phase $\sim q/p$ is linked to the nonzero Chern numbers of the system, and can take in principle any rational value, such that there emerge Majoranas or even more general types of parafermions. The fractional exchange statistics can be measured by a periodicity breaking of the Aharonov-Casher phase, which is associated to a fractional flux car-

ried by the excitations.

Due to the emergent anyonic exchange statistics, the here considered system allows direct implementation of a simulation of fermionic systems with *local* gate operations, relevant for a number of important problems, such as quantum computational chemistry. Errors within the hardware can be corrected by implementing a GKP code, which can be conveniently integrated into the above fermion simulation concept. We note in particular that the hardware overhead (especially for initialization and read-out) does not necessarily scale with the redundancy required for quantum error correction, as the latter scales with the magnitude of the Chern number, and not with the number of circuit nodes.

The magnitude of the coupling between anyon excitations at different nodes depends ultimately on the strength of Cooper pair exchange between the nodes. Precise control of this coupling therefore requires flattening the topological energy bands of the multiterminal junction, which is accomplished in various ways. Via fine-tuning of system parameters of specific junctions (such as multiterminal quantum dot chains), we demonstrate the emergence of chiral scattering at the junction, going hand in hand with a flat topological ground state. We particularly highlight the role of the quasiparticle continuum. On the one hand, it gives rise to detrimental Chern number fluctuations that can be mitigated through disorder. The upshot of the continuum is that it allows circumventing no-go theorems for nontrivial flat bands in systems with few bands. We further show that the circuit hardware offers a number of other band-engineering strategies that rely effectively on averaging out ϕ -dependent fluctuations (which is in a broad sense similar to how quasiperiodic lattice interactions give rise to flat bands). This scrambling in ϕ -space is shown to be possible through repeated parallel shunting of circuit elements or through quantum phase transitions.

Our work also provides a number of insights of fundamental nature. In addition to the obvious analogy with the fractional quantum Hall effect, we particularly highlighted the fact that there naturally occur interactions that break fermion-parity superselection rule (and generalizations thereof for anyons)—an effect that can be related on a circuit level to the breaking of charge conservation with respect to ground. As we have shown, fermion-parity breaking really concerns the emergent excitations in the low-energy sector only, and all states preserve fermion parity in the original electron picture. Moreover, the derivation of the fermion parity breaking theory relies on making a non-relativistic approximation. Nonetheless, the local nature of the fermionic gates allowed us to connect our work to the ongoing endeavour to derive quantum mechanics from an information-theoretic point of view, indicating the importance of relativistic arguments in order to satisfy the no-communication constraint.

Triangular Chern lattice

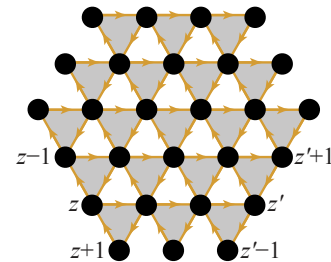


FIG. 9. Triangular arrangement of two-dimensional Chern number network, which implements a scalar version of Chern-Simons theory, for which the no-go theorem derived in Ref. [247] does not apply.

B. Outlook

By including geometric interactions in multiterminal circuits, we lay the groundwork towards a different flavour of quantum information hardware, where the fundamental information unit is an anyonic qudit. The feasibility of this device design will have to be further evaluated in future works, likely involving experimental proofs of concept.

Beyond applications, the here developed theory presents a whole host of important open questions of fundamental nature. For instance, the aforementioned breaking of fermion-parity superselection rules (and anyonic generalizations thereof) stipulates that the understanding of large multiterminal circuit networks involves solving a class of quantum field theories which have so far hardly been examined, as they were not expected to be realized in nature. Take for concreteness the ordinary Hubbard model, which can be realized in circuits with charge-conserving Josephson effects, see Eq. (29). We would for instance deem it highly interesting to investigate if the known phenomenology, such as the phase diagram (for which, incidentally, there still does not exist full consensus [248]), survives the addition of (even weak) fermion-parity breaking processes. Note this is as much a physical question as it is a computational one: the success of many numerical techniques for solving strongly correlated model systems, such as DMRG [249], is connected to entanglement entropy area laws [250], and is known to work best when the ground state is sufficiently close to being a product state [251], which we expect not to be the case for superpositions of states with different fermion parity.

There furthermore exist quite a number of open research directions in relationship to the fractional quantum Hall effect. In this context, we reemphasize that multiterminal junctions can realize a reduced version of Chern-Simons theory, with a number of special properties. Consider a 2D Chern number network with, e.g., a triangular or square lattice structure (see Fig. 9). Near-

est neighbor sites (let us refer to them as z and $z + 1$) contribute to the action a term of the form

$$\sim \frac{\mathcal{C}_{z,z+1}^{(1)}}{4\pi} \left(\phi_z \dot{\phi}_{z+1} - \phi_{z+1} \dot{\phi}_z \right), \quad (40)$$

in accordance with Eqs. (4) and (7). Setting all first Chern numbers to the same value ($\mathcal{C}_{z,z+1}^{(1)} = \mathcal{C}$), and orienting them accordingly, we find in the continuum limit ($\phi_z \rightarrow \phi(x, y)$) the action

$$\mathcal{S} = \iint_{\Sigma} dx dy \left[\frac{c_g}{8\epsilon^2} \dot{\phi}^2 + \frac{\mathcal{C}}{4\pi} \left(\partial_x \phi \partial_y \dot{\phi} - \partial_y \phi \partial_x \dot{\phi} \right) \right], \quad (41)$$

where the first term arises from capacitive coupling to ground, and scales with the capacitive density c_g [252]. The extent of the 2D network is here denoted by the total area manifold Σ on which the theory is defined.

The above term relates to the ordinary Chern-Simons action [181], $\sim \frac{k}{4\pi} \epsilon^{\mu\nu\lambda} \partial_\nu a_\lambda$ (Einstein notation), when setting the vector potential to $a_0 = 0$ and $a_{1,2} = \partial_{x,y} \phi$, and equating the Chern number \mathcal{C} with the level k of the Chern-Simons theory, thus allowing us to draw an even deeper connection with the fractional quantum Hall effect (fQHE) [253–255]. We stress though that this relationship is no mere gauge choice for a , but a *restriction* to a subclass of possible vector field configurations (one first indication of that fact can be obtained by noticing that a is here curl-free by construction). As a consequence, the field theory of Eq. (41) cannot reproduce all properties of Chern-Simons. In particular, via Stokes theorem, it can be shown that the geometric term of the action ($\sim \mathcal{C}$) reduces to

$$\Rightarrow \frac{\mathcal{C}}{4\pi} \oint_{\partial\Sigma} dl \cdot \dot{\phi} \nabla \phi, \quad (42)$$

where $\partial\Sigma$ is the 1D boundary of the 2D manifold Σ , and dl is an infinitesimal tangential vector element on that boundary. We see that the geometric action vanishes in the bulk, such that it cannot couple to charge and current sources in the same ways as the ordinary Chern-Simons term does, and hence fails to mediate anyonic exchange statistics between such sources. As amply demonstrated throughout the main text above, anyons are nonetheless integral part of the circuit's low-energy description in the presence of a capacitive coupling. An important commonality between the original Chern-Simons vector field and the here considered reduced version is that both couple to the boundary (and thus to any kind of geometric defects, including, e.g., holes punctured into Σ), to which one can associate a chiral edge state with finite group velocity (given by the product of the capacitive energy density and the Chern number \mathcal{C}). Consequently, we expect that in spite of the above differences, our theory nonetheless accurately mimics the fQHE edge state transport.

Let us emphasize again that while there exists a considerable body of work on Josephson junction arrays and

circuit cavity networks exhibiting unconventional states of matter (including fQHE) and resulting anyonic excitations [36–38, 256], the models in question require a large real-space array, where the nontrivial physics occur essentially in a very much same way as in correlated solid state systems. In contrast, in our work, the nontrivial physics arise directly from geometric contributions (the Chern numbers) due to intrinsic degrees of freedom of multi-terminal junctions, such that anyonic excitations emerge directly, and already for a very low number of nodes, significantly lowering both theoretical and experimental hurdles for future studies. Moreover, while lattice versions of Chern-Simons theory have likewise been extensively studied already [247, 257–263], the above reduced, scalar version contains a number of features and connections that we believe have not previously been discussed. On the one hand, there exists a no-go theorem to construct a consistent Chern-Simons theory on a triangular lattice [247] (triangular lattice version are possible for a variant called Maxwell-Chern-Simons theory [260]). The here presented reduced version however can exist on the triangular lattice (Fig. 9). Related to that, we notice that the disappearance of the action in the bulk is only exact in the continuum limit, where as for the discrete system, the bulk cancellation is approximate and depends on the lattice structure. For instance, preliminary numerical results indicate a finite width of the edge state, as well as a high sensitivity to the way the edge is cut through the lattice.

A potentially deeper observation concerns the quantization of the Chern-Simons level k , respectively, \mathcal{C} . For ordinary Chern-Simons theory, there exists an elegant argument [264] placing the Chern-Simons theory on a 2+1-dimensional sphere (finite temperature is encoded with a periodic imaginary time) enclosing a Dirac monopole, where quantization of k follows from a generalized notion of gauge invariance. As extensively discussed in our work, the quantization of the Chern numbers follows from compact ϕ . Thus, while the two argumentations are very broadly speaking similar in spirit, the former invokes compactness of the global space-time manifold in which the theory is embedded, whereas the latter assumes locally compact quantum fields—a radically different and completely unrelated notion.

With that in mind, we outline a number of unresolved questions related to the compact nature of ϕ , which are going to be addressed in the future. For an extended field theory (noncompact ϕ), the chiral edge state in Eq. (42) is fully characterized by the first Chern number \mathcal{C} . However, for compact ϕ , we have already shown in the main part of the work, that the naturally occurring higher Chern numbers play an important role to describe the low-energy excitations (in particular the degenerate zero energy modes, which here make up the inert branch of the edge state with zero group velocity). This question is however more difficult to address, since for the triangular lattice (Fig. 9), the total Chern number matrix $g - g^T$ has zero eigenvalues, and, thus, no inverse,

and therefore requires a separate dedicated research effort, starting from the reexamination of Eq. (10). Furthermore, we note that general quantum-Hall-like edge states (that correspond to the zero eigenvalues of $g - g^T$) can be obtained when introducing multiple edge states (Chern-Simons theories) in parallel, and take into account a nonzero coupling. In the very different context of dissipative phase transitions, it has been shown that compact/quantized variables have a significant influence on the renormalization group flow [168]. This leads to the question of what happens to fQHE-like edge states when they couple with each other or with an environment. Finally, we point out some further generalizations. For the specific multiterminal Josephson junction realizations of nonzero Chern numbers, the Chern number can fluctuate, or even be in a coherent quantum superposition. This opens up another door towards analysing networks with dynamical Chern number connections, and explore their emergent behaviour. Moreover, the emergence of second or higher Chern numbers, and of nonabelian Berry curvatures, has been discussed in multiterminal junctions with *degenerate* instead of nondegenerate ground states [94]. If translated to the here developed circuit QED context, such considerations could massively generalize Eq. (11) to a more general class of emergent non-abelian anyons.

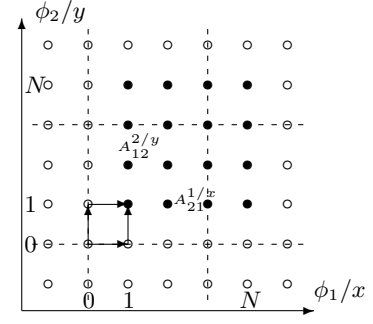
ACKNOWLEDGEMENTS

We warmly thank Fabian Hassler, David DiVincenzo, Maarten R. Wegewijs, Frank Wilhelm-Mauch, Z. Leghtas, P. Campagne-Ibarcq, J.-D. Pillet, L. Bretheau, and Janine Splettstoesser for fruitful discussions. R.M. would like to thank Julia Meyer for her insights and for directing us to relevant literature. This work has been funded by the German Federal Ministry of Education and Research within the funding program Photonic Research Germany under the contract number 13N14891.

Appendix A: Gauges for Uniform Magnetic Field on Torus

As noted in the main text, usual gauge choices for vector potentials in the extended 2D plane are at risk of yielding inconsistent results when embedded on a compact manifold, such as the torus. We here clarify certain gauge aspects for said torus, by means of a numerical investigation. We discretize the torus with a mesh of $N \times N$ points, as shown in Fig. 10. The Hamiltonian resulting from Eq. (4) (under appropriate inclusion of capacitive coupling) can be numerically implemented as the single-particle Hamiltonian hopping between the points on the mesh, and the effective magnetic field can be implemented as the phase acquired along the movement between the neighbour points.

Thus, the Berry connection in this discretized model is described by the values $A_{n,m}^x = \int_{x_n}^{x_{n+1}} A_x(x, y_m) dx$ and



$$H = e^{iA_{nm}^x} |n+1, m\rangle \langle n, m| + e^{iA_{nm}^y} |n, m+1\rangle \langle n, m| + h.c.$$

FIG. 10. Discretizing of the Fock space of two superconducting islands. The mesh is defined on a torus, i.e. index $N \equiv 0$.

same formula for $A_{n,m}^y$ with $x \leftrightarrow y$, and fluxes through the unit cell $\tilde{\mathcal{B}}_{nm} = \int_{x_n}^{x_{n+1}} \int_{y_m}^{y_{m+1}} \tilde{\mathcal{B}}(x, y) dx dy$. Here, to simplify the notation, we denote $x = \phi_1, y = \phi_2$. Periodic boundary conditions are implemented by using cyclic indices n, m , that is, they are set to 0 when they assume the value N . The constant magnetic field \mathcal{B} is implemented through the condition

$$\tilde{\mathcal{B}}_{nm} = A_{n,m}^x + A_{n+1,m}^y - A_{n,m+1}^x - A_{n,m}^y, \quad (\text{A1})$$

$$\exp \left\{ i \tilde{\mathcal{B}}_{nm} \right\} = \exp \left\{ i (2\pi/N)^2 \mathcal{B} \right\}, \quad (\text{A2})$$

where $\tilde{\mathcal{B}}_{nm}$ is basically the flux through the elementary cell. The exponentiation of the phases relates the values up to the 2π , giving us the relation

$$\tilde{\mathcal{B}}_{nm} = (2\pi/N)^2 \mathcal{B} - 2\pi \mathcal{K}_{nm}, \quad \mathcal{K}_{nm} \in \mathbb{Z}. \quad (\text{A3})$$

On the other side, using the definition of $\tilde{\mathcal{B}}_{nm}$ and cyclic indices, we get $\sum_{\forall n,m} \tilde{\mathcal{B}}_{nm} = 0$, which naturally follows from Stokes theorem on the torus. This condition results in the quantization of the magnetic field

$$2\pi \mathcal{B} = \sum_{\forall n,m} \mathcal{K}_{nm} = \mathcal{C} \in \mathbb{Z}, \quad (\text{A4})$$

where \mathcal{C} is the Chern number. Here, the most trivial example is when all ‘‘horns’’ \mathcal{K} (see also main text) are gathered into a single one at (n_0, m_0) , i.e. $\mathcal{K}_{nm} = 0$ everywhere except for $\mathcal{K}_{n_0 m_0} = \mathcal{C}$. Then, for example a linear gauge can be constructed in the following way:

$$\begin{aligned} A_{n_0, m \leq m_0}^x &= -\frac{2\pi \mathcal{C}}{N} m, & A_{n_0, m > m_0}^x &= -\frac{2\pi \mathcal{C}}{N} m + 2\pi \mathcal{C}, \\ A_{n \leq n_0, m}^y &= \frac{2\pi \mathcal{C}}{N^2} n, & A_{n > n_0, m}^y &= \frac{2\pi \mathcal{C}}{N^2} n - \frac{2\pi \mathcal{C}}{N} \end{aligned} \quad (\text{A5})$$

which is also illustrated in Fig. 11.

This discrete gauge in the continuous limit takes the

following form

$$\begin{aligned} A^x(x, y) &= -C\delta(x - x_0)(y - 2\pi\theta(y - y_0)), \\ A^y(x, y) &= \frac{C}{2\pi}(x - 2\pi\theta(x - x_0)), \\ \tilde{B}(x, y) &= \frac{C}{2\pi} - 2\pi C\delta(x - x_0)\delta(y - y_0), \end{aligned} \quad (\text{A6})$$

where $\delta(x) = \theta'(x)$ denotes a 2π periodic Dirac delta function, and the $\theta(x)$ is an extended step function, i.e., not a single step, but a ladder, with steps at $-2\pi, -\pi, 0, 2\pi, 4\pi$, and so on.

Numerical diagonalization of the Hamiltonian given in Fig. 10 for the case $C = 2$ illustrates the predicted C -fold degeneracy of the lowest Landau level on the torus in the main text, see Fig. 11(b), left. On the right-hand side of Fig. 11(b), the probability distribution of the wave function is shown. Here one may notice an important feature. Despite the problem being translational invariant, the physical part of the solution, which is the probability, is not. The wave function has a maximum, and its position is not related to the “horn”, which proves that the “horn” does not affect the measurable part of the solution. But the phase of the wave function is, of course, affected by the gauge. This issue arises from the fact that the gauge invariance means that all fluxes remain the same. In the case of the torus it adds two different types of closed trajectories, for example the loops \mathcal{W}_z and $\mathcal{W}_{z'}$ shown in Fig. 10(b) [in our case $z = 1$ and $z' = 2$]. Thus, we need to fix the values for the fluxes through these loops too. Modifying the gauge, we found the correlation between these fluxes and the solution: the maximum of the wave function coincides with the crossing of the straight trajectories \mathcal{W}_1 and \mathcal{W}_2 , position of which chosen such that the fluxes through these both trajectories are equal to zero (up to 2π addition, of course), see the grey lines in Fig. 11(b), right.

Appendix B: Protocol to probe violation of no-communication theorem

As pointed out in the main text, Ref. [179] introduces a simple protocol which demonstrates how breaking Wigner superselection allows for changing the outcome of a measurement in one subsystem (Alice), by only performing local gates in another, spatially separated subsystem (Bob). We first reiterate the protocol as given in Ref. [179], and then we show how it is implemented within the circuit hardware.

The protocol only requires two fermionic modes, a, a^\dagger for Alice, and b, b^\dagger for Bob, such that $\{a, a^\dagger\}_+ = \{b, b^\dagger\}_+ = 1$, whereas $\{a, b^\dagger\}_+ = 0$ (due to the two modes being spatially separated). Starting from the vacuum state $|0\rangle$ ($a|0\rangle = b|0\rangle = 0$), we first prepare the initial state with a unitary gate performed by Alice, $U_A = (1 - a + a^\dagger)/\sqrt{2}$. This gate is designed to explicitly break Wigner superselection, since the initial state after

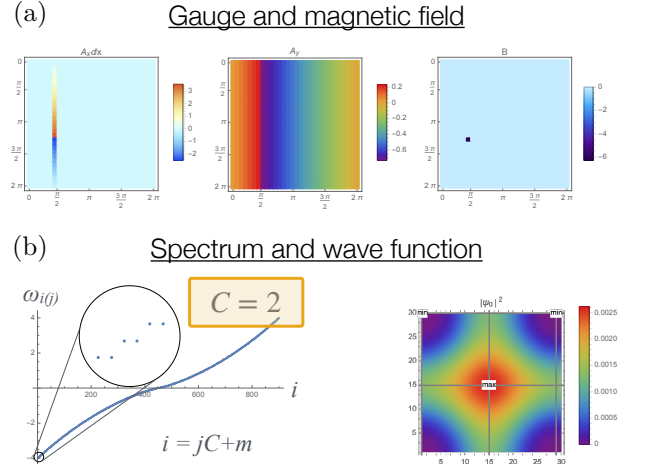


FIG. 11. (a) An example of the linear gauge. In the left plot the phase is scaled by $dx = 2\pi/N$. In the right plot one can clearly see the “horn” in the magnetic field. (b) The numerical solution for the Hamiltonian given in the Fig. 10. On the left is the spectrum with a distinct degeneracy for the Landau level. On the right is the wave function probability. Grey lines correspond to the topologically non-trivial straight loops with zero flux through them.

the gate reads,

$$|\psi_A\rangle = U_A|0\rangle = \frac{|0\rangle + a^\dagger|0\rangle}{\sqrt{2}}. \quad (\text{B1})$$

We now imagine that Alice performs a local measurement with the observable $O_A = a + a^\dagger$, which yields,

$$\langle\psi_A|O_A|\psi_A\rangle = 1. \quad (\text{B2})$$

If, before Alice’s measurement of O_A , we allow Bob to perform a gate of the form $U_B = b + b^\dagger$, yielding the state $|\psi_{AB}\rangle = U_B U_A|0\rangle$, the subsequent measurement on Alice’s side would yield

$$\langle\psi_{AB}|O_A|\psi_{AB}\rangle = -\langle\psi_A|O_A|\psi_A\rangle = -1, \quad (\text{B3})$$

which is manifestly different from the first measurement, demonstrating that here, the local gate applied on Bob’s side immediately influences Alice’s measurement, violating the no-communication theorem.

The above protocol can be significantly generalized to an arbitrary number of fermionic modes, and involving any operator measured on Alice’s side O_A , and any gate U_B applied on Bob’s side, as long as both O_A and U_B are odd in fermion ladder operators. Note that while O_A, U_B being odd means that they change the fermion parity when being applied to a prepared state $|\psi_A\rangle$, they themselves do not violate the parity *superselection* rule: they change the parity of any state they are applied to, but they do not create superpositions of states with different parity. They do however always anticommute, such that we are guaranteed to find $\langle\psi_A|U_B^\dagger O_A U_B|\psi_A\rangle = -\langle\psi_A|O_A|\psi_A\rangle$. Hence, the only

condition for this protocol to violate no-signalling is that $\langle \psi_A | O_A | \psi_A \rangle \neq 0$. Such a nonzero eigenvalue of an odd fermion operator can in turn only emerge if $|\psi_A\rangle$ is in an even-odd superposition.

We now briefly outline, how this protocol is implemented. For this purpose, we consider the Majorana circuit (i.e., all Chern numbers equal 2) in the main text, with four nodes, $Z = 4$. We assign odd nodes 1 and 3 to Alice, and even nodes 2 and 4 to Bob. Choosing the same representation in terms of regular complex fermions as introduced in the main text, we identify $a = c_1 = (\gamma_1 - i\gamma_3)/2$ and $b = c_2 = (\gamma_2 - i\gamma_4)/2$. The preparation of the vacuum state $a|0\rangle = b|0\rangle = 0$ is outlined in Sec. III C of the main text. The gate for the state initialization according to Eq. (B3) is performed straightforwardly. We switch on a Josephson effect between ground and node 3 (on Alice's side), yielding the Hamiltonian

$$H_A = -2\tilde{E}_J\gamma_3 = -2i\tilde{E}_J(a - a^\dagger). \quad (\text{B4})$$

Applying this Hamiltonian for time $\tau = \pi/(8\tilde{E}_J)$ yields exactly the unitary time-evolution U_A as defined above. The measurement of O_A is realized by switching on a Josephson effect between ground and node 1, where the above introduced dispersive readout yields a projective measurement of $O_A = \gamma_1 = a + a^\dagger$. Bob can implement the gate U_B in two equivalent ways. Either, he switches on a Josephson effect between ground and node 2,

$$H_B = -2\tilde{E}_J\gamma_2 = -2\tilde{E}_J(b + b^\dagger), \quad (\text{B5})$$

this time, for double the time duration $\tau = \pi/(4\tilde{E}_J)$, or alternatively, he offsets the charge at node 2, $n_2^{(\text{ext})}$, by ± 1 . As demonstrated above, the expectation value measured on Alice's side swaps sign, depending on whether or not Bob performs gate U_B .

Appendix C: Flat-band scattering matrices in three-terminal junctions

While it has been previously shown [138] that there are non-topological flat bands in multi-terminal Josephson junctions, we argue in the main text that the many-body ground state of the junction is nonetheless topologically nontrivial. We here explain this argument in more detail, and provide explicit calculations.

Starting with a scattering matrix S_N describing the normal metal transport properties of generic multiterminal junctions, we can compute the ABS spectra using the determinant formula [137],

$$\det(I - S_N \cdot R) = 0. \quad (\text{C1})$$

The determinant contains the product of S_N with the Andreev reflection matrix R from the superconducting contacts. For short junctions, S_N can be approximated

to be energy independent. The Andreev reflection process R , on the other hand, explicitly depends on E . Consequently, the above determinant condition serves as an equation to calculate the energy spectrum of Bogoliubov quasiparticles (electron-hole superpositions).

A generic three-terminal device consists of three superconductors connected by a central normal region. Each superconductor is characterized by an order parameter $\Delta_i = \Delta e^{i\phi_i}$, where Δ is the amplitude (same across all reservoirs), and ϕ_i is the phase with $i = 1, 2, 3$. Let us choose a gauge such that $\phi_3 = 0$. The electron and hole degrees of freedom introduces a block structure in the scattering matrices, given by

$$R = \alpha(E) \begin{pmatrix} 0 & e^{i\hat{\phi}} \\ e^{-i\hat{\phi}} & 0 \end{pmatrix}, \quad S_N = \begin{pmatrix} \hat{S} & 0 \\ 0 & \hat{S}^* \end{pmatrix}, \quad (\text{C2})$$

with $\alpha(E) = E/\Delta - i\sqrt{1 - E^2/\Delta^2}$ and the definition of the diagonal matrix $\hat{\phi} = \text{diag}(0, \phi_1, \phi_2)$. Andreev reflection occurs with unit probability for energies $E < \Delta$ and any normal reflection at the normal-superconductor (NS) interface is captured by the matrix S_N . In a three-terminal junction (each with a single conduction channel), $\hat{\phi}$ and \hat{S} are 3×3 matrices. For three-terminal junctions, the Beenakker determinant formula, Eq. (C1), supports the following solutions. There is a pair of subgap energy solutions $\pm E_0(\phi_1, \phi_2)$ (due to particle-hole symmetry), and one spurious, trivial solution pinned to Δ (which always exists when the total number of channels is odd). Discarding the trivial solution (as it does not contribute to transport) the three-terminal device provides a two-band model. The many-body ground state of the device is given by the sum of all negative energy states (bound states plus continuum). Since the continuum spectrum is perfectly flat, we can equate the many-body ground state with the negative energy nontrivial solution of the Beenakker equation, i.e., as $E_g = -E_0(\phi_1, \phi_2) + \text{const.}$, whereas the (even parity) first excited state on the other hand reads $E_e = +E_0(\phi_1, \phi_2) + \text{const.}$, such that it suffices to analyse the single particle energy E_0 .

To create many-body flat bands, the task is therefore to identify scattering matrices yielding constant E_0 . To this end, we first note that the scattering matrix \hat{S} is unitary and belongs to the group $U(3)$, which can be reduced to $SU(3)$ without loss of generality (since a global phase can be eliminated from the scattering matrix, without changing the energy spectrum E). We parameterize \hat{S} using the Gell-Mann matrices λ_j [the generators of $SU(3)$],

$$\hat{S} = e^{i \sum_{j=1}^8 \theta_j \lambda_j / \sqrt{3}} \quad (\text{C3})$$

where θ_j are real parameters. For the sake of completeness, we explicitly provide the Gell-Mann matrices, where for our purposes, it is convenient we distinguish between

the 5 symmetric matrices,

$$\begin{aligned}\lambda_1 &= \begin{pmatrix} 0 & 1 & 0 \\ 1 & 0 & 0 \\ 0 & 0 & 0 \end{pmatrix}, & \lambda_3 &= \begin{pmatrix} 1 & 0 & 0 \\ 0 & -1 & 0 \\ 0 & 0 & 0 \end{pmatrix}, \\ \lambda_4 &= \begin{pmatrix} 0 & 0 & 1 \\ 0 & 0 & 0 \\ 1 & 0 & 0 \end{pmatrix}, & \lambda_6 &= \begin{pmatrix} 0 & 0 & 0 \\ 0 & 0 & 1 \\ 0 & 1 & 0 \end{pmatrix}, \\ \lambda_8 &= \frac{1}{\sqrt{3}} \begin{pmatrix} 1 & 0 & 0 \\ 0 & 1 & 0 \\ 0 & 0 & -2 \end{pmatrix},\end{aligned}\quad (\text{C4})$$

and the 3 skew-symmetric ones

$$\begin{aligned}\lambda_2 &= \begin{pmatrix} 0 & -i & 0 \\ i & 0 & 0 \\ 0 & 0 & 0 \end{pmatrix}, & \lambda_5 &= \begin{pmatrix} 0 & 0 & -i \\ 0 & 0 & 0 \\ i & 0 & 0 \end{pmatrix}, \\ \lambda_7 &= \begin{pmatrix} 0 & 0 & 0 \\ 0 & 0 & -i \\ 0 & i & 0 \end{pmatrix}.\end{aligned}\quad (\text{C5})$$

This distinction is motivated by the fact that any junction can only have a nontrivial topological ground state if the system breaks time-reversal symmetry [62]. For three-terminal junctions, this means that the scattering region itself must not be symmetric [82]. We here first consider the most “extreme” set of asymmetric scattering matrices, where we only use the skew-symmetric generators of the subgroup $SU(3)$,

$$S = e^{i(\theta_2\lambda_2 + \theta_5\lambda_5 + \theta_7\lambda_7)/\sqrt{3}}. \quad (\text{C6})$$

To quantify flatness, we introduce the flatness parameter (f), defined (see also main text) as the ratio of the band gap (δ) between ground and first excited state to the bandwidth (ΔE) of the ground state, i.e.,

$$\frac{1}{f} = \frac{\delta}{\Delta E} \quad (\text{C7})$$

Since the many-body ground and first excited states are straightforwardly related to the only nontrivial solutions of Eq. (C1) ($\pm E_0$), we find the bandwidth to be given as the difference between the minimum and the maximum of E_0 within the 2D space (ϕ_1, ϕ_2), whereas the band gap is given by twice the minimum of E_0 .

We observe that the value of $1/f$ for the non-trivial ABS vanishes (i.e., there is a perfectly flat band) when

$$\theta_2 = -\theta_5 = \theta_7 = \pm 2\pi/3, \pm 4\pi/3, \quad (\text{C8})$$

which is in accordance with Ref. [138]. Furthermore, the corresponding \hat{S} matrices for these θ values indicate chiral scattering behaviour, as discussed in Sec. IV B.

The main objective is to determine the many-body Chern number of the ground state for the above chiral matrix, which would necessitate taking the sum of both bound state and continuum contributions. However, with the here deployed Beenakker formalism, we

only have access to the former. As it turns out, we can nonetheless determine the full many-body Chern number by carefully tracking the topological phase transitions across an appropriately chosen path in θ -space. To this end, we first have to choose a starting point in θ -space, where the many-body Chern number is known. This is the case for $\theta_j = 0$ for all j , where Eq. (C3) returns unity, that is, the junction is fully reflective. This is equivalent to the three superconducting contacts being completely disjoint, such that the many-body ground state is guaranteed to be topologically trivial. Now, we simply have to choose a path from $\theta_j = 0$ to one of the chiral solutions, Eq. (C8), and compute the Chern number of the state belonging to energy E_0 , and check at each change of the Chern number, if the band touches zero energy, or Δ . If E_0 touches zero, then the positive and negative states $\pm E_0$ exchange a Chern number. This means that the many-body ground state (sum over all negative energies) changes its Chern number. If on the other hand E_0 touches Δ , then there is a Chern number exchange between bound state spectrum and continuum. In this case, the Chern number of the many-body ground state stays the same.

To compute the Chern number of state E_0 , we need to compute the wavefunctions of the non-trivial ABS and their associated Berry curvature. This can be done by taking the wavefunction emerging from the scattering eigenvalue equation written as,

$$\begin{aligned}S_N \cdot R |\psi\rangle &= |\psi\rangle \implies \\ \implies S_N \cdot \begin{pmatrix} 0 & e^{i\hat{\phi}} \\ e^{-i\hat{\phi}} & 0 \end{pmatrix} |\psi\rangle &= \alpha^*(E) |\psi\rangle\end{aligned}\quad (\text{C9})$$

Now let us define,

$$M = S_N \cdot \begin{pmatrix} 0 & e^{i\hat{\phi}} \\ e^{-i\hat{\phi}} & 0 \end{pmatrix} \implies M |\psi\rangle = \alpha^*(E) |\psi\rangle \quad (\text{C10})$$

where both $|\psi\rangle$ and E depend on ϕ_1 and ϕ_2 . Note that while the above structure is reminiscent of a Schrödinger equation, M is not Hermitian here, but unitary. Nonetheless, due to unitarity (and $|\alpha(E)|^2 = 1$ for all E), we know that for each eigenvalue of M at a given position ϕ_1, ϕ_2 , we can find a well-defined, real solution for E with $|E| \leq \Delta$. Therefore, we can use the eigenstates $|\psi\rangle$ of M to calculate the Berry curvature (\mathcal{B}) and associated Chern number (\mathcal{C}) as [240],

$$\begin{aligned}\mathcal{B} &= 2\text{Im} \{ \text{tr} [\partial_{\phi_1} P (1 - P) \partial_{\phi_2} P] \}, \\ \mathcal{C} &= \frac{1}{4\pi^2} \int_0^{2\pi} \int_0^{2\pi} d\phi_1 d\phi_2 \mathcal{B},\end{aligned}\quad (\text{C11})$$

where P is the projector operator given by $P = |\psi\rangle \langle \psi|$. We compute the ABS energies from the eigenvalues of the matrix M , resulting in six distinct eigenvalues. These eigenvalues typically appear in conjugate pairs, i.e., $a \pm ib$ and $-a \pm ib$. Due to the nature of the Andreev reflection, where the energy of the incident quasiparticle is

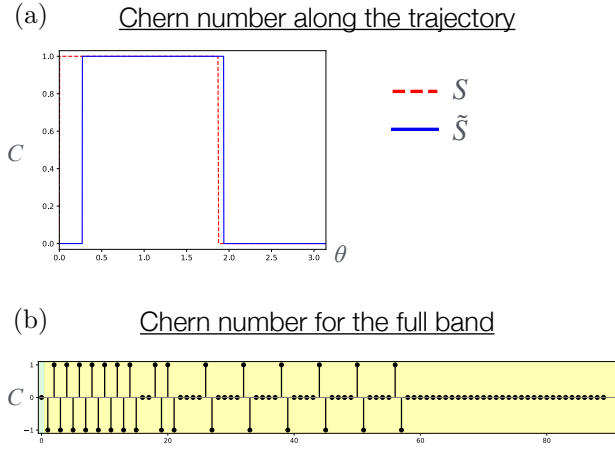


FIG. 12. The Chern number \mathcal{C} as a function of θ for scattering centers S and \tilde{S} . The matrix \tilde{S} is here constructed by fixing $\theta_1 = 0.4$ and $\theta_3 = \theta_4 = \theta_6 = \theta_8 = 0$. (b) The Chern number \mathcal{C} for the individual bands of the quantum dot transistor for $w/\Delta = 0.05$ and $J = 30$. The subgap (supragap) region $E < \Delta$ ($E > \Delta$) is marked with green (yellow) hue.

lower than the superconducting gap Δ , the square root in the expression for the energy yields a positive imaginary part for the physically relevant solutions. Consequently, the eigenvalues with a negative imaginary part, such as $\pm a - ib$, are not physically meaningful and should be discarded. Thus, we retain only the three eigenstates corresponding to the eigenvalues with a positive imaginary component. Next, for the sake of simplicity, we fix $\theta_2 = -\theta_5 = \theta_7 = \theta$ and compute the Chern number as defined above as a function of θ from $\theta = 0$ (where $S = 1$) to $\theta = \pi$. At $\theta = 2\pi/3$, we arrive at the perfectly chiral scattering matrix.

The Chern number as a function of θ is shown in Fig. 12(a) (red dashed line). Notice that the region of nonzero Chern number extends all the way to $\theta \rightarrow 0^+$. This is an artefact. For fully reflecting scattering matrix, all the ABS energies stick to Δ , such that the Chern number, at least as defined above, is not strictly speaking well defined. In order to regularize this result (and make the Chern number well-defined at $\theta = 0$, we include a small, perturbative symmetric component in the scattering matrix,

$$\tilde{S} = \exp \left\{ \frac{i}{\sqrt{3}} \left[(\lambda_2 - \lambda_5 + \lambda_7) \theta + \sum_{i \in \{1,3,4,6,8\}} \theta_i \lambda_i \right] \right\}. \quad (\text{C12})$$

For \tilde{S} , the topological phase transition is shifted, and the region around $\theta = 0$ is trivial, since the bands are no longer pinned to Δ . In Fig. 12(a), the blue solid line shows the Chern number computed with \tilde{S} for $\theta_1 = 0.4$, whereas all other symmetric components remain zero, $\theta_3 = \theta_4 = \theta_6 = \theta_8 = 0$. The graph for S is the one featured in Fig. 6(a) in the main text. Analysing the energy spectrum (computed as detailed here) at the topologi-

cal transitions (where the gap closes), we arrive at the qualitative picture shown in Fig. 6(b).

Appendix D: Chiral scattering matrix for Quantum Dot Transistor

In the main text, we present a transistor composed of chains of quantum dots proximitised by superconductors. In this section, we show that such a setup harbours a nearly chiral scattering matrices, and detail how to compute the many-body Chern number.

The device setup can be seen in Fig 7. The many-body Hamiltonian was given in the main text, either as in Eq. (37) in the absence of pairing, or via $H_{\text{dot}} \rightarrow H_{\text{dot}} + \Delta \sum_{z,j} \left(e^{i\phi_z} d_{z,j,\uparrow}^\dagger d_{z,j,\downarrow}^\dagger + \text{h.c.} \right)$ ($\phi_3 = 0$) to include pairing. We here cast this very same Hamiltonian into the first quantized form,

$$H_{\text{dot}} = \Psi^\dagger h_{\text{dot}} \Psi, \quad (\text{D1})$$

with the field operators

$$\Psi = \sum_{z,j} |z,j\rangle \begin{pmatrix} c_{z,j,\uparrow} \\ c_{z,j,\downarrow}^\dagger \end{pmatrix}. \quad (\text{D2})$$

The single-particle Hamiltonian is of the 2-by-2 form in Nambu space

$$h_{\text{dot}} = \begin{pmatrix} h_0 & \delta \\ \delta^* & -h_0^* \end{pmatrix} \quad (\text{D3})$$

where the normal part of the Hamiltonian is simply

$$\begin{aligned} h_0 = & -t \sum_{z=1}^3 \sum_{j=2}^J (|z,j+1\rangle \langle z,j| + \text{h.c.}) \\ & - t (|2,1\rangle \langle 1,1| + \text{h.c.}) - t (|3,1\rangle \langle 2,1| + \text{h.c.}) \\ & - t (e^{i\phi} |1,1\rangle \langle 3,1| + \text{h.c.}) . \end{aligned} \quad (\text{D4})$$

Note that we chose for convenience a slightly different gauge for the central phase ϕ_0 , which is here fully attached to the link between dot 1 and 3, instead of being distributed equally ($\sim \phi_0/3$) across all three links (as in the main text). The pairing on the other hand is given in first quantization as

$$\delta = \Delta \sum_{z=1}^3 \sum_{j=2}^J e^{i\phi_z} |z,j\rangle \langle z,j|. \quad (\text{D5})$$

Note furthermore, that usually, in any BCS pairing, the chemical potential appears. In the above formulation, we have tacitly set the chemical potential to zero. The reason for this will become clear momentarily.

The first quantization representation conveniently allows us to solve the scattering problem. To this end, we set the pairing to zero, such that we can consider the

electron sector separately, h_0 , and extend the chains to infinity, $J \rightarrow \infty$. We choose the ansatz,

$$|\psi_{\text{in},1}\rangle = \sum_{j=1}^{\infty} \left[(e^{ikj} + r_{11}e^{-ikj}) |1, j\rangle + t_{21}e^{-ikj} |2, j\rangle + t_{31}e^{-ikj} |3, j\rangle \right]. \quad (\text{D6})$$

Let us plug that ansatz into the Schrödinger equation,

$$h_0 |\psi_{\text{in},1}\rangle = -2t \cos(k) |\psi_{\text{in},1}\rangle. \quad (\text{D7})$$

We get nontrivial conditions for,

$$\begin{aligned} \langle 1, 1 | h_0 |\psi_{\text{in},1}\rangle &= -\langle 1, 1 | 2t \cos(k) |\psi_{\text{in},1}\rangle, \\ \langle 2, 1 | h_0 |\psi_{\text{in},1}\rangle &= -\langle 2, 1 | 2t \cos(k) |\psi_{\text{in},1}\rangle, \\ \langle 3, 1 | h_0 |\psi_{\text{in},1}\rangle &= -\langle 3, 1 | 2t \cos(k) |\psi_{\text{in},1}\rangle, \end{aligned} \quad (\text{D8})$$

yielding,

$$\begin{pmatrix} -e^{ik} & 1 & e^{i\phi_0} \\ 1 & -e^{ik} & 1 \\ e^{-i\phi_0} & 1 & -e^{ik} \end{pmatrix} \begin{pmatrix} r_{11} \\ t_{21} \\ t_{31} \end{pmatrix} = \begin{pmatrix} e^{-ik} \\ -1 \\ -e^{-i\phi_0} \end{pmatrix} \quad (\text{D9})$$

Upon inversion, we obtain the coefficients r_{00} , t_{10} and t_{20} .

$$\begin{aligned} r_{11} &= -\frac{2[\cos(\phi_0) + \cos(k)]}{2\cos(\phi_0) + 3e^{ik} - e^{3ik}}, \\ t_{21} &= \frac{e^{-i\phi_0}(e^{-ik} - e^{ik}) + (1 - e^{2ik})}{2\cos(\phi_0) + 3e^{ik} - e^{3ik}}, \\ t_{31} &= \frac{(e^{-ik} - e^{ik}) + e^{-i\phi_0}(1 - e^{2ik})}{2\cos(\phi_0) + 3e^{ik} - e^{3ik}}. \end{aligned} \quad (\text{D10})$$

As it turns out, we can tune the parameters ϕ_0 (the flux threading the central quantum dot triangle) and k (the

incident wave vector, and thus, the chemical potential) to the values $\phi_0 = \frac{\pi}{2}$ and $k = \frac{\pi}{2}$ to arrive at a perfectly chiral scattering matrix [see Eq. (36)]. Namely, by tuning the parameters to these exact values (half flux quantum and half filling factor), we find $r_{00} = t_{10} = 0$, and $t_{20} = 1$. Note that at half-filling, the single-particle energies of the electrons and holes are close to zero, justifying our earlier choice to set the chemical potential to zero.

As already discussed in the main text, the scattering problem is best defined for infinite chains. But for the infinite system, the energy states above the gap form a continuum, whose Chern number contributions are hard to compute. In order to regularize this problem, we consider instead a model with finite chain size J (such that the continuum becomes a quasi-continuum, with level spacing $\sim 1/J$), and explicitly include pairing. We therefore numerically diagonalize the full h_{dot} as given in Eq. (D3), and compute all single-particle eigenvalues and eigenvectors as a function of ϕ_1 and ϕ_2 (we remind that $\phi_3 = 0$). Again, as in Sec. C, the many-body ground state energy is computed as the sum of all negative eigenenergies. For a given single-particle wave function (eigenvector of h_{dot}), we can in addition compute the single-particle contribution to the Berry curvature and Chern number in perfect analogy to Eq. (C11). Thus we calculate the flatness of the energy and Berry curvature, as well as the individual Chern number contributions for bound states and quasi-continuum, see various panels in Fig. 7 in the main text. In Fig. 12(b), we add a plot of the Chern number fluctuations for the entire band width of the device (from energies close to 0, up to energies close to $2t$) for $w/\Delta = 0.05$. The upper right panel of Fig. 7c is a zoomed-in version of Fig. 12(b). The total Chern number (sum of the individual contributions) is nonzero, since the negative and positive bands differ by one. Notice that Chern number fluctuations are more pronounced for states close to Δ , where as higher lying energies (approaching $2t$) have much sparser fluctuations.

-
- [1] V. J. Goldman and B. Su, Resonant tunneling in the quantum hall regime: Measurement of fractional charge, *Science* **267**, 1010 (1995).
- [2] L. Saminadayar, D. C. Glattli, Y. Jin, and B. Etienne, Observation of the $e/3$ fractionally charged Laughlin quasiparticle, *Phys. Rev. Lett.* **79**, 2526 (1997).
- [3] R. de Picciotto, M. Reznikov, M. Heiblum, V. Umansky, G. Bunin, and D. Mahalu, Direct observation of a fractional charge, *Nature* **389**, 162 EP (1997).
- [4] J. Alicea and P. Fendley, Topological phases with parafermions: Theory and blueprints, *Annual Review of Condensed Matter Physics* **7**, 119 (2016).
- [5] C. Castelnovo, R. Moessner, and S. Sondhi, Spin ice, fractionalization, and topological order, *Annual Review of Condensed Matter Physics* **3**, 35 (2012).
- [6] C. Nayak, S. H. Simon, A. Stern, M. Freedman, and S. Das Sarma, Non-abelian anyons and topological quantum computation, *Rev. Mod. Phys.* **80**, 1083 (2008).
- [7] Z. Liu and E. J. Bergholtz, Recent developments in fractional Chern insulators, in *Encyclopedia of Condensed Matter Physics (Second Edition)*, edited by T. Chakraborty (Academic Press, Oxford, 2024) second edition ed., pp. 515–538.
- [8] A. K. Geim and I. V. Grigorieva, Van der Waals heterostructures, *Nature* **499**, 419 (2013).
- [9] Y. Cao, V. Fatemi, S. Fang, K. Watanabe, T. Taniguchi, E. Kaxiras, and P. Jarillo-Herrero, Unconventional superconductivity in magic-angle graphene superlattices, *Nature* **556**, 43 (2018).
- [10] Y. Fu, E. J. König, J. H. Wilson, Y.-Z. Chou, and J. H. Pixley, Magic-angle semimetals, *npj Quantum Materials* **5**, 71 (2020).
- [11] A. González-Tudela and J. I. Cirac, Cold atoms in twisted-bilayer optical potentials, *Phys. Rev. A* **100**, 053604 (2019).

- [12] T. Salamon, A. Celi, R. W. Chhajlany, I. Frérot, M. Lewenstein, L. Tarruell, and D. Rakshit, Simulating twistrionics without a twist, *Phys. Rev. Lett.* **125**, 030504 (2020).
- [13] Y.-Z. Chou, Y. Fu, J. H. Wilson, E. J. König, and J. H. Pixley, Magic-angle semimetals with chiral symmetry, *Phys. Rev. B* **101**, 235121 (2020).
- [14] D. Mao and T. Senthil, Quasiperiodicity, band topology, and moiré graphene, *Phys. Rev. B* **103**, 115110 (2021).
- [15] Z. Meng, L. Wang, W. Han, F. Liu, K. Wen, C. Gao, P. Wang, C. Chin, and J. Zhang, Atomic bose-einstein condensate in a twisted-bilayer optical lattice (2021), arXiv:2110.00149.
- [16] J. Lee and J. H. Pixley, Emulating twisted double bilayer graphene with a multiorbital optical lattice, *SciPost Phys.* **13**, 033 (2022).
- [17] K. Deguchi, S. Matsukawa, N. K. Sato, T. Hattori, K. Ishida, H. Takakura, and T. Ishimasa, Quantum critical state in a magnetic quasicrystal, *Nature Materials* **11**, 1013 (2012).
- [18] J. Ningyuan, C. Owens, A. Sommer, D. Schuster, and J. Simon, Time- and site-resolved dynamics in a topological circuit, *Phys. Rev. X* **5**, 021031 (2015).
- [19] V. V. Albert, L. I. Glazman, and L. Jiang, Topological properties of linear circuit lattices, *Phys. Rev. Lett.* **114**, 173902 (2015).
- [20] S. Imhof, C. Berger, F. Bayer, J. Brehm, L. W. Molenkamp, T. Kiessling, F. Schindler, C. H. Lee, M. Greiter, T. Neupert, and R. Thomale, Topoelectrical-circuit realization of topological corner modes, *Nature Physics* **14**, 925 (2018).
- [21] E. Zhao, Topological circuits of inductors and capacitors, *Annals of Physics* **399**, 289 (2018).
- [22] Y. Lu, N. Jia, L. Su, C. Owens, G. Juzeliūnas, D. I. Schuster, and J. Simon, Probing the berry curvature and fermi arcs of a weyl circuit, *Physical Review B* **99**, 020302 (2019).
- [23] S. M. Rafi-Ul-Islam, Z. Bin Siu, and M. B. A. Jalil, Topoelectrical circuit realization of a weyl semimetal heterojunction, *Communications Physics* **3**, 72 (2020).
- [24] Y. Wang, H. M. Price, B. Zhang, and Y. D. Chong, Circuit implementation of a four-dimensional topological insulator, *Nature Communications* **11**, 2356 (2020).
- [25] R. Yu, Y. X. Zhao, and A. P. Schnyder, 4D spinless topological insulator in a periodic electric circuit, *National Science Review* **7**, 1288 (2020).
- [26] C. H. Lee, S. Imhof, C. Berger, F. Bayer, J. Brehm, L. W. Molenkamp, T. Kiessling, and R. Thomale, Topoelectrical circuits, *Communications Physics* **1**, 39 (2018).
- [27] M. Ezawa, Higher-order topological electric circuits and topological corner resonance on the breathing kagome and pyrochlore lattices, *Physical Review B* **98**, 201402 (2018).
- [28] Y. Li, Y. Sun, W. Zhu, Z. Guo, J. Jiang, T. Kariyado, H. Chen, and X. Hu, Topological lc-circuits based on microstrips and observation of electromagnetic modes with orbital angular momentum, *Nature Communications* **9**, 4598 (2018).
- [29] J. Lantz, M. Wallquist, V. S. Shumeiko, and G. Wendin, Josephson junction qubit network with current-controlled interaction, *Phys. Rev. B* **70**, 140507 (2004).
- [30] M. Wallquist, J. Lantz, V. S. Shumeiko, and G. Wendin, Superconducting qubit network with controllable nearest-neighbour coupling, *New Journal of Physics* **7**, 178 (2005).
- [31] S. Gladchenko, D. Olaya, E. Dupont-Ferrier, B. Douçot, L. B. Ioffe, and M. E. Gershenson, Superconducting nanocircuits for topologically protected qubits, *Nature Physics* **5**, 48 (2009).
- [32] B. M. Terhal, F. Hassler, and D. P. DiVincenzo, From majorana fermions to topological order, *Phys. Rev. Lett.* **108**, 260504 (2012).
- [33] A. A. Houck, H. E. Türeci, and J. Koch, On-chip quantum simulation with superconducting circuits, *Nature Physics* **8**, 292 (2012).
- [34] N. A. Olekhno, A. D. Rozenblit, A. A. Stepanenko, A. A. Dmitriev, D. A. Bobylev, and M. A. Gorlach, Topological transitions driven by quantum statistics and their electrical circuit emulation, *Phys. Rev. B* **105**, 205113 (2022).
- [35] A. A. Odintsov and Y. V. Nazarov, Incompressible quantum hall states in josephson-junction arrays, *Phys. Rev. B* **51**, 1133 (1995).
- [36] J. Cho, D. G. Angelakis, and S. Bose, Fractional quantum hall state in coupled cavities, *Phys. Rev. Lett.* **101**, 246809 (2008).
- [37] B. Douçot, M. V. Feigel'man, and L. B. Ioffe, Topological order in the insulating josephson junction array, *Phys. Rev. Lett.* **90**, 107003 (2003).
- [38] B. Douçot, L. B. Ioffe, and J. Vidal, Discrete non-abelian gauge theories in josephson-junction arrays and quantum computation, *Physical Review B* **69**, 214501 (2004).
- [39] B. Douçot, M. V. Feigel'man, L. B. Ioffe, and A. S. Ioselevich, Protected qubits and chern-simons theories in josephson junction arrays, *Phys. Rev. B* **71**, 024505 (2005).
- [40] Y. S. Kivshar and B. A. Malomed, Dynamics of solitons in nearly integrable systems, *Rev. Mod. Phys.* **61**, 763 (1989).
- [41] A. Ustinov, Solitons in josephson junctions, *Physica D: Nonlinear Phenomena* **123**, 315 (1998), annual International Conference of the Center for Nonlinear Studies.
- [42] A. Wallraff, A. V. Ustinov, V. V. Kurin, I. A. Shereshevsky, and N. K. Vdovicheva, Whispering vortices, *Phys. Rev. Lett.* **84**, 151 (2000).
- [43] K. A. Matveev, A. I. Larkin, and L. I. Glazman, Persistent current in superconducting nanorings, *Phys. Rev. Lett.* **89**, 096802 (2002).
- [44] V. Gurarie and A. M. Tsvelik, A superconductor-insulator transition in a one-dimensional array of josephson junctions, *Journal of Low Temperature Physics* **135**, 245 (2004).
- [45] M. Houzet and L. I. Glazman, Microwave spectroscopy of a weakly pinned charge density wave in a superinductor, *Phys. Rev. Lett.* **122**, 237701 (2019).
- [46] S. Teitel and C. Jayaprakash, Josephson-junction arrays in transverse magnetic fields, *Phys. Rev. Lett.* **51**, 1999 (1983).
- [47] B. Pannetier, J. Chaussy, R. Rammal, and J. C. Villegier, Experimental fine tuning of frustration: Two-dimensional superconducting network in a magnetic field, *Phys. Rev. Lett.* **53**, 1845 (1984).
- [48] B. J. van Wees, H. S. J. van der Zant, and J. E. Mooij, Phase transitions of josephson-tunnel-junction arrays at zero and full frustration, *Phys. Rev. B* **35**, 7291 (1987).

- [49] L. N. Vu, M. S. Wistrom, and D. J. Van Harlingen, Imaging of magnetic vortices in superconducting networks and clusters by scanning SQUID microscopy, *Applied Physics Letters* **63**, 1693 (1993).
- [50] J. C. Ciria and C. Giovannella, Vortex dynamics in classical josephson junction arrays: models and recent experimental developments, *Journal of Physics: Condensed Matter* **10**, 1453 (1998).
- [51] R. Fazio and H. van der Zant, Quantum phase transitions and vortex dynamics in superconducting networks, *Physics Reports* **355**, 235 (2001).
- [52] A.-G. Penner, K. Flensberg, L. I. Glazman, and F. von Oppen, Resistivity tensor of vortex-lattice states in josephson junction arrays, *Phys. Rev. Lett.* **131**, 206001 (2023).
- [53] P. D. Nation, M. P. Blencowe, A. J. Rimberg, and E. Buks, Analogue hawking radiation in a dc-squid array transmission line, *Phys. Rev. Lett.* **103**, 087004 (2009).
- [54] X.-G. Lan, Measuring hawking radiation of a kerr-newman black hole in a superconducting transmission line, *International Journal of Theoretical Physics* **54**, 116 (2015).
- [55] Z. Tian and J. Du, Analogue hawking radiation and quantum soliton evaporation in a superconducting circuit, *Eur. Phys. J. C.* **79**, 994 (2019).
- [56] H. Katayama, N. Hatakenaka, and T. Fujii, Analogue hawking radiation from black hole solitons in quantum josephson transmission lines, *Phys. Rev. D* **102**, 086018 (2020).
- [57] H. Katayama, S. Ishizaka, N. Hatakenaka, and T. Fujii, Solitonic black holes induced by magnetic solitons in a dc-squid array transmission line coupled with a magnetic chain, *Phys. Rev. D* **103**, 066025 (2021).
- [58] H. Katayama, N. Hatakenaka, T. Fujii, and M. P. Blencowe, Analog black-white hole solitons in traveling wave parametric amplifiers with superconducting nonlinear asymmetric inductive elements, *Phys. Rev. Res.* **5**, L022055 (2023).
- [59] M. A. Javed, D. Kruti, A. Kenawy, T. Herrig, C. Koliotofoti, O. Kashuba, and R. P. Riwar, [Utilizing and extending superconducting circuit toolbox to simulate analog quantum gravity](#) (2024), arXiv:2406.01261 [cond-mat.mes-hall].
- [60] F. Arute, K. Arya, R. Babbush, D. Bacon, J. C. Bardin, R. Barends, R. Biswas, S. Boixo, F. G. S. L. Brandao, D. A. Buell, B. Burkett, Y. Chen, Z. Chen, B. Chiaro, R. Collins, W. Courtney, A. Dunsworth, E. Farhi, B. Foxen, A. Fowler, C. Gidney, M. Giustina, R. Graff, K. Guerin, S. Habegger, M. P. Harrigan, M. J. Hartmann, A. Ho, M. Hoffmann, T. Huang, T. S. Humble, S. V. Isakov, E. Jeffrey, Z. Jiang, D. Kafri, K. Kechedzhi, J. Kelly, P. V. Klimov, S. Knysh, A. Korotkov, F. Kostritsa, D. Landhuis, M. Lindmark, E. Lucero, D. Lyakh, S. Mandrà, J. R. McClean, M. McEwen, A. Megrant, X. Mi, K. Michielsen, M. Mohseni, J. Mutus, O. Naaman, M. Neeley, C. Neill, M. Y. Niu, E. Ostby, A. Petukhov, J. C. Platt, C. Quintana, E. G. Rieffel, P. Roushan, N. C. Rubin, D. Sank, K. J. Satzinger, V. Smelyanskiy, K. J. Sung, M. D. Trevithick, A. Vainsencher, B. Villalonga, T. White, Z. J. Yao, P. Yeh, A. Zalcman, H. Neven, and J. M. Martinis, Quantum supremacy using a programmable superconducting processor, *Nature* **574**, 505 (2019).
- [61] See <https://www.ibm.com/blogs/research/2020/09/ibm-quantum-roadmap/> (2020).
- [62] R.-P. Riwar, M. Houzet, J. S. Meyer, and Y. V. Nazarov, Multi-terminal josephson junctions as topological matter, *Nature Communications* **7**, 11167 (2016).
- [63] M. Rymarz, S. Bosco, A. Ciani, and D. P. DiVincenzo, Hardware-encoding grid states in a nonreciprocal superconducting circuit, *Phys. Rev. X* **11**, 011032 (2021).
- [64] B. Yurke and J. S. Denker, Quantum network theory, *Phys. Rev. A* **29**, 1419 (1984).
- [65] D. Loss and K. Mullen, Effect of dissipation on phase periodicity and the quantum dynamics of josephson junctions, *Phys. Rev. A* **43**, 2129 (1991).
- [66] K. Mullen, D. Loss, and H. T. C. Stoof, Resonant phenomena in compact and extended systems, *Phys. Rev. B* **47**, 2689 (1993).
- [67] C. Koliotofoti and R.-P. Riwar, Compact description of quantum phase slip junctions, *npj Quantum Information* **9**, 125 (2023).
- [68] Whether or not ϕ is compact (or more precisely, closed) depends on the existence a mechanism to entangle with the number turns a given circuit performs in ϕ -space, see Refs. [65–67].
- [69] G. Viola and D. P. DiVincenzo, Hall effect gyrators and circulators, *Phys. Rev. X* **4**, 021019 (2014).
- [70] S. Barzanjeh, M. Wulf, M. Peruzzo, M. Kalaee, P. Dieterle, O. Painter, and J. M. Fink, Mechanical on-chip microwave circulator, *Nature communications* **8**, 953 (2017).
- [71] F. Lecocq, L. Ranzani, G. Peterson, K. Cicak, R. Simmonds, J. Teufel, and J. Aumentado, Nonreciprocal microwave signal processing with a field-programmable josephson amplifier, *Physical Review Applied* **7**, 024028 (2017).
- [72] B. J. Chapman, E. I. Rosenthal, J. Kerckhoff, B. A. Moores, L. R. Vale, J. Mates, G. C. Hilton, K. Lalumiere, A. Blais, and K. Lehnert, Widely tunable on-chip microwave circulator for superconducting quantum circuits, *Physical Review X* **7**, 041043 (2017).
- [73] E. I. Rosenthal, B. J. Chapman, A. P. Higginbotham, J. Kerckhoff, and K. Lehnert, Breaking lorentz reciprocity with frequency conversion and delay, *Physical Review Letters* **119**, 147703 (2017).
- [74] A. Mahoney, J. Colless, S. Pauka, J. Hornibrook, J. Watson, G. Gardner, M. Manfra, A. Doherty, and D. Reilly, On-chip microwave quantum hall circulator, *Physical Review X* **7**, 011007 (2017).
- [75] A. C. Mahoney, J. I. Colless, L. Peeters, S. J. Pauka, E. J. Fox, X. Kou, L. Pan, K. L. Wang, D. Goldhaber-Gordon, and D. J. Reilly, Zero-field edge plasmons in a magnetic topological insulator, *Nature communications* **8**, 1836 (2017).
- [76] A. Parra-Rodriguez, I. L. Egusquiza, D. P. DiVincenzo, and E. Solano, Canonical circuit quantization with linear nonreciprocal devices, *Phys. Rev. B* **99**, 014514 (2019).
- [77] C. Leroux, A. Parra-Rodriguez, R. Shillito, A. D. Paolo, W. D. Oliver, C. M. Marcus, M. Kjaergaard, A. Gyenis, and A. Blais, [Nonreciprocal devices based on voltage-tunable junctions](#) (2022), arXiv:2209.06194 [quant-ph].
- [78] L.-A. Sellem, A. Sarlette, Z. Leghtas, M. Mirrahimi, P. Rouchon, and P. Campagne-Ibarcq, A gkp qubit protected by dissipation in a high-impedance superconducting circuit driven by a microwave frequency comb (2023), arXiv:2304.01425 [quant-ph].

- [79] K. Flensberg, F. von Oppen, and A. Stern, Engineered platforms for topological superconductivity and majorana zero modes, *Nature Reviews Materials* **6**, 944 (2021).
- [80] T. Yokoyama and Y. V. Nazarov, Singularities in the andreev spectrum of a multiterminal josephson junction, *Physical Review B* **92**, 155437 (2015).
- [81] E. Eriksson, R.-P. Riwar, M. Houzet, J. S. Meyer, and Y. V. Nazarov, Topological transconductance quantization in a four-terminal josephson junction, *Physical Review B* **95**, 075417 (2017).
- [82] J. S. Meyer and M. Houzet, Nontrivial chern numbers in three-terminal josephson junctions, *Physical Review Letters* **119**, 136807 (2017).
- [83] H.-Y. Xie, M. G. Vavilov, and A. Levchenko, Topological andreev bands in three-terminal josephson junctions, *Physical Review B* **96**, 161406 (2017).
- [84] H.-Y. Xie, M. G. Vavilov, and A. Levchenko, Weyl nodes in andreev spectra of multiterminal josephson junctions: Chern numbers, conductances, and supercurrents, *Physical Review B* **97**, 035443 (2018).
- [85] O. Deb, K. Sengupta, and D. Sen, Josephson junctions of multiple superconducting wires, *Phys. Rev. B* **97**, 174518 (2018).
- [86] E. V. Repin, Y. Chen, and Y. V. Nazarov, Topological properties of multiterminal superconducting nanostructures: Effect of a continuous spectrum, *Physical Review B* **99**, 165414 (2019).
- [87] W. Belzig, Quantum geometry of topological josephson matter, in *NANO-2019: Limits of Nanoscience and Nanotechnologies* (2019) pp. 107–107.
- [88] V. Fatemi, A. R. Akhmerov, and L. Bretheau, Weyl josephson circuits, *Physical Review Research* **3**, 013288 (2021).
- [89] L. Peyruchat, J. Griesmar, J. D. Pillet, and c. O. Girit, Transconductance quantization in a topological josephson tunnel junction circuit, *Physical Review Research* **3**, 013289 (2021).
- [90] T. Herrig and R.-P. Riwar, Cooper-pair transistor as a minimal topological quantum circuit, *Phys. Rev. Research* **4**, 013038 (2022).
- [91] R. L. Klees, J. C. Cuevas, W. Belzig, and G. Rastelli, Many-body quantum geometry in superconductor-quantum dot chains (2020), [arXiv:2009.11768 \[cond-mat.mes-hall\]](https://arxiv.org/abs/2009.11768).
- [92] R. L. Klees, J. C. Cuevas, W. Belzig, and G. Rastelli, Ground-state quantum geometry in superconductor-quantum dot chains, *Phys. Rev. B* **103**, 014516 (2021).
- [93] L. Teshler, H. Weisbrich, J. Sturm, R. L. Klees, G. Rastelli, and W. Belzig, Ground state topology of a four-terminal superconducting double quantum dot, *SciPost Phys.* **15**, 214 (2023).
- [94] H. Weisbrich, R. L. Klees, G. Rastelli, and W. Belzig, Second chern number and non-abelian berry phase in topological superconducting systems, *PRX Quantum* **2**, 010310 (2021).
- [95] H. Weisbrich, M. Bestler, and W. Belzig, Tensor monopoles in superconducting systems, *Quantum* **5**, 601 (2021).
- [96] R.-P. Riwar and G. Catelani, Efficient quasiparticle traps with low dissipation through gap engineering, *Phys. Rev. B* **100**, 144514 (2019).
- [97] M. A. Javed, J. Schwibbert, and R.-P. Riwar, Fractional josephson effect versus fractional charge in superconducting-normal metal hybrid circuits, *Phys. Rev. B* **107**, 035408 (2023).
- [98] D. C. Ohnmacht, V. Wilhelm, H. Weisbrich, and W. Belzig, Non-hermitian topology in multiterminal superconducting junctions (2024), [arXiv:2408.01289 \[cond-mat.mes-hall\]](https://arxiv.org/abs/2408.01289).
- [99] J. Cayao and M. Sato, Non-hermitian multiterminal phase-biased josephson junctions (2024), [arXiv:2408.17260 \[cond-mat.mes-hall\]](https://arxiv.org/abs/2408.17260).
- [100] T. Herrig, J. H. Pixley, E. J. König, and R. P. Riwar, Quasiperiodic circuit quantum electrodynamics, *npj Quantum Information* **9**, 116 (2023).
- [101] E. Strambini, S. D’Ambrosio, F. Vischi, F. S. Bergeret, Y. V. Nazarov, and F. Giazotto, The ω -squist as a tool to phase-engineer josephson topological materials, *Nature Nanotechnology* **11**, 1055 (2016).
- [102] F. Vischi, M. Carrega, E. Strambini, S. D’Ambrosio, F. S. Bergeret, Y. V. Nazarov, and F. Giazotto, Coherent transport properties of a three-terminal hybrid superconducting interferometer, *Phys. Rev. B* **95**, 054504 (2017).
- [103] N. Pankratova, H. Lee, R. Kuzmin, K. Wickramasinghe, W. Mayer, J. Yuan, M. G. Vavilov, J. Shabani, and V. E. Manucharyan, Multiterminal josephson effect, *Physical Review X* **10**, 10.1103/physrevx.10.031051 (2020).
- [104] E. G. Arnault, T. F. Q. Larson, A. Seredinski, L. Zhao, S. Idris, A. McConnell, K. Watanabe, T. Taniguchi, I. Borzenets, F. Amet, and G. Finkelstein, Multiterminal inverse ac josephson effect, *Nano Letters* **21**, 9668 (2021).
- [105] K.-F. Huang, Y. Ronen, R. Mélin, D. Feinberg, K. Watanabe, T. Taniguchi, and P. Kim, Evidence for 4e charge of cooper quartets in a biased multi-terminal graphene-based josephson junction, *Nature Communications* **13**, 3032 (2022).
- [106] G. V. Graziano, M. Gupta, M. Pendharkar, J. T. Dong, C. P. Dempsey, C. Palmstrøm, and V. S. Pribiag, Selective control of conductance modes in multi-terminal josephson junctions, *Nature Communications* **13**, 5933 (2022).
- [107] S. Matsuo, T. Imoto, T. Yokoyama, Y. Sato, T. Lindemann, S. Gronin, G. C. Gardner, S. Nakosai, Y. Tanaka, M. J. Manfra, and S. Tarucha, Phase-dependent andreev molecules and superconducting gap closing in coherently-coupled josephson junctions, *Nature Communications* **14**, 8271 (2023).
- [108] M. Coraiola, D. Z. Haxell, D. Sabonis, H. Weisbrich, A. E. Svetogorov, M. Hinderling, S. C. ten Kate, E. Cheah, F. Krizek, R. Schott, W. Wegscheider, J. C. Cuevas, W. Belzig, and F. Nichele, Phase-engineering the andreev band structure of a three-terminal josephson junction, *Nature Communications* **14**, 6784 (2023).
- [109] M. Kedves, T. Pápai, G. m. H. Fülöp, K. Watanabe, T. Taniguchi, P. Makk, and S. Csonka, Self-heating effects and switching dynamics in graphene multiterminal josephson junctions, *Phys. Rev. Res.* **6**, 033143 (2024).
- [110] L. Peyruchat, R. H. Rodriguez, J. L. Smirr, R. Leone, and Ç. Girit, Spectral signatures of non-trivial topology in a superconducting circuit (2024), [arXiv:2401.10876 \[cond-mat.mes-hall\]](https://arxiv.org/abs/2401.10876).
- [111] W. Jung, S. Jin, S. Park, S.-H. Shin, K. Watanabe, T. Taniguchi, G. Y. Cho, and G.-H. Lee, Full tomography of topological andreev bands in graphene josephson junctions (2024), [arXiv:2411.01170 \[cond-mat.mes-hall\]](https://arxiv.org/abs/2411.01170).

- [112] P. Virtanen and T. T. Heikkilä, Nonreciprocal josephson linear response, *Phys. Rev. Lett.* **132**, 046002 (2024).
- [113] G. Romero, I. Lizuain, V. S. Shumeiko, E. Solano, and F. S. Bergeret, Circuit quantum electrodynamics with a superconducting quantum point contact, *Phys. Rev. B* **85**, 180506 (2012).
- [114] R. P. Riwar, Discrete control of capacitance in quantum circuits (2023), [arXiv:2306.00587 \[cond-mat.supr-con\]](https://arxiv.org/abs/2306.00587).
- [115] F. Matute-Cañadas, L. Tosi, and A. L. Yeyati, Quantum circuits with multiterminal josephson-andreev junctions, *PRX Quantum* **5**, 020340 (2024).
- [116] F. D. M. Haldane and E. H. Rezayi, Periodic Laughlin-Jastrow wave functions for the fractional quantized Hall effect, *Phys. Rev. B* **31**, 2529 (1985).
- [117] A. Fayyazuddin and D. Li, Haldane's fractional statistics and the lowest Landau level on a torus, *Phys. Rev. Lett.* **76**, 1707 (1996).
- [118] E. Onofri, Landau levels on a torus, *International Journal of Theoretical Physics* **40**, 537 (2001).
- [119] D. Simms and N. Woodhouse, *Lectures on Geometric Quantization*, Lecture Notes in Physics (Springer Berlin Heidelberg, 1976).
- [120] I. M. Pop, B. Douçot, L. Ioffe, I. Protopopov, F. Lecocq, I. Matei, O. Buisson, and W. Guichard, Experimental demonstration of Aharonov-Casher interference in a Josephson junction circuit, *Phys. Rev. B* **85**, 094503 (2012).
- [121] V. E. Manucharyan, N. A. Masluk, A. Kamal, J. Koch, L. I. Glazman, and M. H. Devoret, Evidence for coherent quantum phase slips across a Josephson junction array, *Phys. Rev. B* **85**, 024521 (2012).
- [122] J. Ulrich and F. Hassler, Dual approach to circuit quantization using loop charges, *Phys. Rev. B* **94**, 094505 (2016).
- [123] S. E. de Graaf, S. T. Skacel, T. Hönlgl-Decrinis, R. Shaikhaidarov, H. Rotzinger, S. Linzen, M. Ziegler, U. Hübner, H. G. Meyer, V. Antonov, E. Il'ichev, A. V. Ustinov, A. Y. Tzalenchuk, and O. V. Astafiev, Charge quantum interference device, *Nature Physics* **14**, 590 (2018).
- [124] A. Cottet, *Implementation of a quantum bit in a superconducting circuit*, Ph.D. thesis, Université Paris VI (2002).
- [125] D. M. Pozar, *Microwave Engineering* (Wiley, Hoboken, NJ, 2012).
- [126] Y. Cao, J. Romero, J. P. Olson, M. Degroote, P. D. Johnson, M. Kieferová, I. D. Kivlichan, T. Menke, B. Peropadre, N. P. D. Sawaya, S. Sim, L. Veis, and A. Aspuru-Guzik, Quantum chemistry in the age of quantum computing, *Chemical Reviews* **119**, 10856 (2019).
- [127] S. McArdle, S. Endo, A. Aspuru-Guzik, S. C. Benjamin, and X. Yuan, Quantum computational chemistry, *Rev. Mod. Phys.* **92**, 015003 (2020).
- [128] R. Barends, L. Lamata, J. Kelly, L. García-Álvarez, A. G. Fowler, A. Megrant, E. Jeffrey, T. C. White, D. Sank, J. Y. Mutus, B. Campbell, Y. Chen, Z. Chen, B. Chiaro, A. Dunsworth, I. C. Hoi, C. Neill, P. J. J. O'Malley, C. Quintana, P. Roushan, A. Vainsencher, J. Wenner, E. Solano, and J. M. Martinis, Digital quantum simulation of fermionic models with a superconducting circuit, *Nature Communications* **6**, 7654 (2015).
- [129] M. P. Kaicher, S. B. Jäger, P.-L. Dallaire-Demers, and F. K. Wilhelm, Roadmap for quantum simulation of the fractional quantum Hall effect, *Phys. Rev. A* **102**, 022607 (2020).
- [130] U. E. Khodaeva, D. L. Kovrizhin, and J. Knolle, Quantum simulation of the one-dimensional fermi-hubbard model as a z_2 lattice-gauge theory, *Phys. Rev. Res.* **6**, 013032 (2024).
- [131] V. Rosenhaus, An introduction to the syk model, *Journal of Physics A: Mathematical and Theoretical* **52**, 323001 (2019).
- [132] S. Sachdev and J. Ye, Gapless spin-fluid ground state in a random quantum Heisenberg magnet, *Phys. Rev. Lett.* **70**, 3339 (1993).
- [133] A. Kitaev, A simple model of quantum holography (part 1), <http://online.kitp.ucsb.edu/online/entangled15/kitaev/> (2015), talk at KITP, University of California, Santa Barbara, CA, U.S.A., 7 April 2015.
- [134] S. Lloyd, Universal quantum simulators, *Science* **273**, 1073 (1996).
- [135] J. B. James D. Whitfield and A. Aspuru-Guzik, Simulation of electronic structure Hamiltonians using quantum computers, *Molecular Physics* **109**, 735 (2011).
- [136] D. Gottesman, A. Kitaev, and J. Preskill, Encoding a qubit in an oscillator, *Phys. Rev. A* **64**, 012310 (2001).
- [137] C. W. J. Beenakker, Universal limit of critical-current fluctuations in mesoscopic Josephson junctions, *Phys. Rev. Lett.* **67**, 3836 (1991).
- [138] A. Mukhopadhyay, U. Khanna, and S. Das, *Anomalous topology and synthetic flat band in multi-terminal Josephson junctions* (2023), [arXiv:2309.15159 \[cond-mat.mes-hall\]](https://arxiv.org/abs/2309.15159).
- [139] L. Chen, T. Mazaheri, A. Seidel, and X. Tang, The impossibility of exactly flat non-trivial Chern bands in strictly local periodic tight binding models, *Journal of Physics A: Mathematical and Theoretical* **47**, 152001 (2014).
- [140] N. Read, Compactly supported Wannier functions and algebraic k -theory, *Phys. Rev. B* **95**, 115309 (2017).
- [141] R. Bezrukavnikov and A. Kapustin, Localization properties of Chern insulators, *Arnold Mathematical Journal* **5**, 15 (2019).
- [142] A. Kapustin and L. Fidkowski, Local commuting projector Hamiltonians and the quantum Hall effect, *Communications in Mathematical Physics* **373**, 763 (2020).
- [143] D. Varjas, A. Abouelkomsan, K. Yang, and E. J. Bergholtz, Topological lattice models with constant Berry curvature, *SciPost Phys.* **12**, 118 (2022).
- [144] P. Sathe and R. Roy, Topological triviality of flat Hamiltonians, [arXiv:2309.06487](https://arxiv.org/abs/2309.06487) (2023), preprint.
- [145] We incidentally believe that such Chern number fluctuations could be a likely reason why dc measurements have so far not had the desired success in detecting a quantized transconductance.
- [146] A. M. Bozkurt, J. Brookman, V. Fatemi, and A. R. Akhmerov, Double-Fourier engineering of Josephson energy-phase relationships applied to diodes, *SciPost Phys.* **15**, 204 (2023).
- [147] A. Schmid, Diffusion and localization in a dissipative quantum system, *Phys. Rev. Lett.* **51**, 1506 (1983).
- [148] S. A. Bulgadaev, Phase diagram of a dissipative quantum system, *JETP Letters* **39**, 315 (1984).
- [149] C. Aslangul, N. Pottier, and D. Saint-James, Quantum ohmic dissipation: Particle on a one-dimensional periodic lattice, *Physics Letters A* **111**, 175 (1985).

- [150] F. Guinea, V. Hakim, and A. Muramatsu, Diffusion and localization of a particle in a periodic potential coupled to a dissipative environment, *Phys. Rev. Lett.* **54**, 263 (1985).
- [151] G. Schön and A. Zaikin, Quantum coherent effects, phase transitions, and the dissipative dynamics of ultra small tunnel junctions, *Physics Reports* **198**, 237 (1990).
- [152] C. P. Herrero and A. D. Zaikin, Superconductor-insulator quantum phase transition in a single josephson junction, *Phys. Rev. B* **65**, 104516 (2002).
- [153] N. Kimura and T. Kato, Temperature dependence of zero-bias resistances of a single resistance-shunted josephson junction, *Phys. Rev. B* **69**, 012504 (2004).
- [154] P. Werner and M. Troyer, Efficient simulation of resistively shunted josephson junctions, *Phys. Rev. Lett.* **95**, 060201 (2005).
- [155] S. L. Lukyanov and P. Werner, Resistively shunted josephson junctions: quantum field theory predictions versus monte carlo results, *Journal of Statistical Mechanics: Theory and Experiment* **2007**, P06002 (2007).
- [156] A. Murani, N. Bourlet, H. le Sueur, F. Portier, C. Altimiras, D. Esteve, H. Grabert, J. Stockburger, J. Ankerhold, and P. Joyez, Absence of a dissipative quantum phase transition in josephson junctions, *Phys. Rev. X* **10**, 021003 (2020).
- [157] P. J. Hakonen and E. B. Sonin, Comment on “absence of a dissipative quantum phase transition in josephson junctions”, *Phys. Rev. X* **11**, 018001 (2021).
- [158] A. Murani, N. Bourlet, H. le Sueur, F. Portier, C. Altimiras, D. Esteve, H. Grabert, J. Stockburger, J. Ankerhold, and P. Joyez, Reply to “comment on ‘absence of a dissipative quantum phase transition in josephson junctions’”, *Phys. Rev. X* **11**, 018002 (2021).
- [159] R. Kuzmin, N. Mehta, N. Grabon, R. A. Mencia, A. Burshtein, M. Goldstein, and V. E. Manucharyan, Observation of the schmid-bulgadaev dissipative quantum phase transition (2023), [arXiv:2304.05806](https://arxiv.org/abs/2304.05806) [quant-ph].
- [160] M. Houzet, T. Yamamoto, and L. I. Glazman, Microwave spectroscopy of schmid transition (2023), [arXiv:2308.16072](https://arxiv.org/abs/2308.16072) [cond-mat.supr-con].
- [161] A. Burshtein and M. Goldstein, Inelastic decay from integrability (2023), [arXiv:2308.15542](https://arxiv.org/abs/2308.15542) [quant-ph].
- [162] K. Masuki, H. Sudo, M. Oshikawa, and Y. Ashida, Absence versus presence of dissipative quantum phase transition in josephson junctions, *Phys. Rev. Lett.* **129**, 087001 (2022).
- [163] T. Sépulcre, S. Florens, and I. Snyman, Comment on “absence versus presence of dissipative quantum phase transition in josephson junctions”, *Phys. Rev. Lett.* **131**, 199701 (2023).
- [164] K. Masuki, H. Sudo, M. Oshikawa, and Y. Ashida, Masuki et al. reply:, *Phys. Rev. Lett.* **131**, 199702 (2023).
- [165] L. Giacomelli and C. Ciuti, Emergent quantum phase transition of a josephson junction coupled to a high-impedance multimode resonator (2023), [arXiv:2307.06383](https://arxiv.org/abs/2307.06383) [quant-ph].
- [166] C. Altimiras, D. Esteve, Ç. Girit, H. le Sueur, and P. Joyez, Absence of a dissipative quantum phase transition in josephson junctions: Theory (2023), [arXiv:2312.14754](https://arxiv.org/abs/2312.14754) [cond-mat.supr-con].
- [167] D. Subero, O. Maillet, D. S. Golubev, G. Thomas, J. T. Peltonen, B. Karimi, M. Marín-Suárez, A. L. Yeyati, R. Sánchez, S. Park, and J. P. Pekola, Bolometric detection of josephson inductance in a highly resistive environment (2023), [arXiv:2210.14953](https://arxiv.org/abs/2210.14953) [cond-mat.mes-hall].
- [168] O. Kashuba and R. P. Riwar, Phase transitions and compact observables (2024), [arXiv:2312.15951](https://arxiv.org/abs/2312.15951) [cond-mat.mes-hall].
- [169] G. C. Wick, A. S. Wightman, and E. P. Wigner, The intrinsic parity of elementary particles, *Phys. Rev.* **88**, 101 (1952).
- [170] G. M. D’Ariano, F. Manessi, P. Perinotti, and A. Tosini, The feynman problem and fermionic entanglement: Fermionic theory versus qubit theory, *International Journal of Modern Physics A* **29**, 1430025 (2014).
- [171] D. Deutsch and P. Hayden, Information flow in entangled quantum systems, *Proceedings of the Royal Society of London. Series A: Mathematical, Physical and Engineering Sciences* **456**, 1759 (2000).
- [172] R. Clifton, J. Bub, and H. Halvorson, Characterizing quantum theory in terms of information-theoretic constraints, *Foundations of Physics* **33**, 1561 (2003).
- [173] A. Peres and D. R. Terno, Quantum information and relativity theory, *Rev. Mod. Phys.* **76**, 93 (2004).
- [174] J. Bub, Quantum mechanics is about quantum information, *Foundations of Physics* **35**, 541 (2005).
- [175] G. Chiribella, G. M. D’Ariano, and P. Perinotti, Informational derivation of quantum theory, *Phys. Rev. A* **84**, 012311 (2011).
- [176] P. Raymond-Robichaud, A local-realistic model for quantum theory, *Proceedings of the Royal Society A: Mathematical, Physical and Engineering Sciences* **477**, 20200897 (2021).
- [177] N. Friis, A. R. Lee, and D. E. Bruschi, Fermionic-mode entanglement in quantum information, *Phys. Rev. A* **87**, 022338 (2013).
- [178] N. Friis, Reasonable fermionic quantum information theories require relativity, *New Journal of Physics* **18**, 033014 (2016).
- [179] M. Johansson, Comment on ‘reasonable fermionic quantum information theories require relativity’ (2016), [arXiv:1610.00539](https://arxiv.org/abs/1610.00539) [quant-ph].
- [180] N. Tibau Vidal, V. Vedral, and C. Marletto, A local-realistic theory for fermions, *AVS Quantum Science* **4**, 013802 (2022).
- [181] A. Zee, Quantum hall fluids, in *Field Theory, Topology and Condensed Matter Physics*, edited by H. B. Geyer (Springer Berlin Heidelberg, Berlin, Heidelberg, 1995) pp. 99–153.
- [182] G. Burkard, R. H. Koch, and D. P. DiVincenzo, Multi-level quantum description of decoherence in superconducting qubits, *Phys. Rev. B* **69**, 064503 (2004).
- [183] U. Vool and M. Devoret, Introduction to quantum electromagnetic circuits, *International Journal of Circuit Theory and Applications* **45**, 897 (2017).
- [184] C. A. Mead and D. G. Truhlar, On the determination of Born–Oppenheimer nuclear motion wave functions including complications due to conical intersections and identical nuclei, *The Journal of Chemical Physics* **70**, 2284 (1979).
- [185] A. Metelmann and A. A. Clerk, Nonreciprocal photon transmission and amplification via reservoir engineering, *Phys. Rev. X* **5**, 021025 (2015).
- [186] Energy levels on a periodic but extended system and a compact system are related by a Bloch theorem. Therefore, the Landau levels must persist in exactly the same

form for both choices.

- [187] F. Gantmacher, *Theory of matrices* (Moscow: State Publishing House of technical and theoretical literature, 1953).
- [188] N. Bourbaki, *Elements of mathematics, 2. Linear and multilinear algebra* (Addison-Wesley, 1973).
- [189] W. Burnside, *Theory of groups of finite order* (Cambridge, The University Press, 1897).
- [190] I. R. Charles W. Curtis, *Representation Theory of Finite Groups and Associative Algebras* (John Wiley & Sons, New York, London, 1962).
- [191] W. Fulton and J. Harris, *Representation Theory: A First Course*, 1st ed., Graduate Texts in Mathematics (Springer New York, NY, 1991) pp. XV, 551.
- [192] Wikipedia, [Wiki](#) (2024), accessed: 2024-07-24.
- [193] J. K. Jain, Incompressible quantum hall states, *Phys. Rev. B* **40**, 8079 (1989).
- [194] M. Greiter and F. Wilczek, Heuristic principle for quantized hall states, *Modern Physics Letters B* **04**, 1063 (1990).
- [195] With topologically trivial we mean a contribution that does not change the Chern numbers $C_{zz'}^{(1)}$.
- [196] W. J. Elion, J. J. Wachtors, L. L. Sohn, and J. E. Mooij, Observation of the aharonov-casher effect for vortices in josephson-junction arrays, *Phys. Rev. Lett.* **71**, 2311 (1993).
- [197] J. E. Mooij and Y. V. Nazarov, Superconducting nanowires as quantum phase-slip junctions, *Nature Physics* **2**, 169 (2006).
- [198] O. V. Astafiev, L. B. Ioffe, S. Kafanov, Y. A. Pashkin, K. Y. Arutyunov, D. Shahar, O. Cohen, and J. S. Tsai, Coherent quantum phase slip, *Nature* **484**, 355 (2012).
- [199] R. P. Riwar and D. P. DiVincenzo, Circuit quantization with time-dependent magnetic fields for realistic geometries, *npj Quantum Information* **8**, 36 (2022).
- [200] K. Serniak, M. Hays, G. de Lange, S. Diamond, S. Shankar, L. D. Burkhardt, L. Frunzio, M. Houzet, and M. H. Devoret, Hot nonequilibrium quasiparticles in transmon qubits, *Physical Review Letters* **121**, 157701 (2018).
- [201] K. Serniak, S. Diamond, M. Hays, V. Fatemi, S. Shankar, L. Frunzio, R. J. Schoelkopf, and M. H. Devoret, Direct dispersive monitoring of charge parity in offset-charge-sensitive transmons, *Physical Review Applied* **12**, 014052 (2019).
- [202] D. Willsch, D. Rieger, P. Winkel, M. Willsch, C. Dickel, J. Krause, Y. Ando, R. Lescanne, Z. Leghtas, N. T. Bronn, P. Deb, O. Lanes, Z. K. Mineev, B. Denny, S. Geisert, S. Günzler, S. Ihssen, P. Paluch, T. Reisinger, R. Hanna, J. H. Bae, P. Schüffelgen, D. Grützmaker, L. Buimaga-Iarinca, C. Morari, W. Wernsdorfer, D. P. DiVincenzo, K. Michielsen, G. Catelani, and I. M. Pop, Observation of josephson harmonics in tunnel junctions, *Nature Physics* **20**, 815 (2024).
- [203] M. A. Rampp and J. Schmalian, Integer and fractionalized vortex lattices and off-diagonal long-range order, *Journal of Physics Communications* **6**, 055013 (2022).
- [204] V. B. Geshkenbein, A. I. Larkin, and A. Barone, Vortices with half magnetic flux quanta in “heavy-fermion” superconductors, *Phys. Rev. B* **36**, 235 (1987).
- [205] H.-Y. Kee, Y. B. Kim, and K. Maki, Half-quantum vortex and d-soliton in Sr_2RuO_4 , *Phys. Rev. B* **62**, R9275 (2000).
- [206] D. A. Ivanov, Non-abelian statistics of half-quantum vortices in p -wave superconductors, *Phys. Rev. Lett.* **86**, 268 (2001).
- [207] J. Ge, P. Wang, Y. Xing, Q. Yin, A. Wang, J. Shen, H. Lei, Z. Wang, and J. Wang, Charge- $4e$ and charge- $6e$ flux quantization and higher charge superconductivity in kagome superconductor ring devices, *Phys. Rev. X* **14**, 021025 (2024).
- [208] P. Krantz, M. Kjaergaard, F. Yan, T. P. Orlando, S. Gustavsson, and W. D. Oliver, A quantum engineer’s guide to superconducting qubits, *Applied Physics Reviews* **6**, 021318 (2019).
- [209] Note that for capacitive coupling, the coupling prefactor gets effectively reduced by a q/p prefactor, and the coupling is in general nonlocal between different nodes, see also Eq. (23).
- [210] Note that we here distinguish between offset charge noise within the device part that realizes the black box H_0 , and offset charge noise on the external nodes z , as discussed in the subsequent item. The former changes the parameters within H_0 and is therefore treated differently.
- [211] A. Zazunov, A. Brunetti, A. L. Yeyati, and R. Egger, Quasiparticle trapping, andreev level population dynamics, and charge imbalance in superconducting weak links, *Phys. Rev. B* **90**, 104508 (2014).
- [212] R.-P. Riwar, M. Houzet, J. S. Meyer, and Y. V. Nazarov, Strong effects of weak ac driving in short superconducting junctions, *Phys. Rev. B* **91**, 104522 (2015).
- [213] C. Janvier, L. Tosi, L. Bretheau, Ç. Girit, M. Stern, P. Bertet, P. Joyez, D. Vion, D. Esteve, M. Goffman, *et al.*, Coherent manipulation of andreev states in superconducting atomic contacts, *Science* **349**, 1199 (2015).
- [214] E. T. Mannila, P. Samuelsson, S. Simbierowicz, J. T. Peltonen, V. Vesterinen, L. Grönberg, J. Hassel, V. F. Maisi, and J. P. Pekola, A superconductor free of quasiparticles for seconds, *Nature Physics* **18**, 145 (2022).
- [215] B. Douçot and J. Vidal, Pairing of cooper pairs in a fully frustrated josephson-junction chain, *Phys. Rev. Lett.* **88**, 227005 (2002).
- [216] W. C. Smith, A. Kou, X. Xiao, U. Vool, and M. H. Devoret, Superconducting circuit protected by two-cooper-pair tunneling, *npj Quantum Information* **6**, 8 (2020).
- [217] W. C. Smith, M. Villiers, A. Marquet, J. Palomo, M. R. Delbecq, T. Kontos, P. Campagne-Ibarcq, B. Douçot, and Z. Leghtas, Magnifying quantum phase fluctuations with cooper-pair pairing, *Phys. Rev. X* **12**, 021002 (2022).
- [218] S. Sachdev and J. Ye, Gapless spin-fluid ground state in a random quantum heisenberg magnet, *Physical review letters* **70**, 3339 (1993).
- [219] Y. You and F. von Oppen, Building fracton phases by majorana manipulation, *Phys. Rev. Res.* **1**, 013011 (2019).
- [220] M. Pretko, X. Chen, and Y. You, Fracton phases of matter, *International Journal of Modern Physics A* **35**, 2030003 (2020).
- [221] D. S. Abrams and S. Lloyd, Quantum algorithm providing exponential speed increase for finding eigenvalues and eigenvectors, *Phys. Rev. Lett.* **83**, 5162 (1999).
- [222] M. Troyer and U.-J. Wiese, Computational complexity and fundamental limitations to fermionic quantum monte carlo simulations, *Phys. Rev. Lett.* **94**, 170201 (2005).

- (2005).
- [223] J. Preskill, Quantum Computing in the NISQ era and beyond, *Quantum* **2**, 79 (2018).
- [224] S. B. Bravyi and A. Y. Kitaev, Fermionic quantum computation, *Annals of Physics* **298**, 210 (2002).
- [225] V. c. v. Havlíček, M. Troyer, and J. D. Whitfield, Operator locality in the quantum simulation of fermionic models, *Phys. Rev. A* **95**, 032332 (2017).
- [226] M. Christandl, N. Datta, A. Ekert, and A. J. Landahl, Perfect state transfer in quantum spin networks, *Phys. Rev. Lett.* **92**, 187902 (2004).
- [227] M.-H. Yung, Quantum speed limit for perfect state transfer in one dimension, *Phys. Rev. A* **74**, 030303 (2006).
- [228] L. Vinet and A. Zhedanov, How to construct spin chains with perfect state transfer, *Phys. Rev. A* **85**, 012323 (2012).
- [229] R. J. Chapman, M. Santandrea, Z. Huang, G. Corrielli, A. Crespi, M.-H. Yung, R. Osellame, and A. Peruzzo, Experimental perfect state transfer of an entangled photonic qubit, *Nature Communications* **7**, 11339 (2016).
- [230] M. Nägele, C. Schweizer, F. Roy, and S. Filipp, Effective nonlocal parity-dependent couplings in qubit chains, *Phys. Rev. Res.* **4**, 033166 (2022).
- [231] K. Vilkelis, A. Manesco, J. D. T. Luna, S. Miles, M. Wimmer, and A. Akhmerov, Fermionic quantum computation with Cooper pair splitters, *SciPost Phys.* **16**, 135 (2024).
- [232] A. R. H. Smith and M. Ahmadi, Quantum clocks observe classical and quantum time dilation, *Nature Communications* **11**, 5360 (2020).
- [233] L. Chirulli and J. E. Moore, Enhanced coherence in superconducting circuits via band engineering, *Physical Review Letters* **126**, 187701 (2021).
- [234] K. Kaur, T. Sépulcre, N. Roch, I. Snyman, S. Florens, and S. Bera, Spin-boson quantum phase transition in multilevel superconducting qubits, *Phys. Rev. Lett.* **127**, 237702 (2021).
- [235] Y. V. Nazarov and Y. M. Blanter, *Quantum Transport: Introduction to Nanoscience* (Cambridge University Press, 2009).
- [236] There is strictly speaking a third band, as the Beenakker equation for three-terminals always allows for a solution at energy equal to the gap Δ . But this solution is spurious since it has no particle-hole partner, and its proper treatment requires including the continuum.
- [237] H. Georgi, *Lie algebras in particle physics*, 2nd ed., Vol. 54 (Perseus Books, Reading, MA, 1999).
- [238] H. Vignaud, D. Perconte, W. Yang, B. Kousar, E. Wagner, F. Gay, K. Watanabe, T. Taniguchi, H. Courtois, Z. Han, H. Sellier, and B. Sacépé, Evidence for chiral supercurrent in quantum hall josephson junctions, *Nature* **624**, 545 (2023).
- [239] Note that the $z - 1$ subscript in Eq. (37) is used in a cyclic fashion, that is, for $z = 1$, $z - 1 = 0 \rightarrow 3$.
- [240] B. A. Bernevig, *Topological Insulators and Topological Superconductors* (Princeton University Press, Princeton, 2013) pp. 24–29.
- [241] A. J. Leggett, S. Chakravarty, A. T. Dorsey, M. P. A. Fisher, A. Garg, and W. Zwerger, Dynamics of the dissipative two-state system, *Rev. Mod. Phys.* **59**, 1 (1987).
- [242] D. N. Aristov, Bosonization for a wigner-jordan-like transformation: Backscattering and umklapp processes on a fictitious lattice, *Phys. Rev. B* **57**, 12825 (1998).
- [243] D. B. Gutman, Y. Gefen, and A. D. Mirlin, Full counting statistics of a luttinger liquid conductor, *Phys. Rev. Lett.* **105**, 256802 (2010).
- [244] D. A. Ivanov, A. G. Abanov, and V. V. Cheianov, Counting free fermions on a line: a fisher–hartwig asymptotic expansion for the toeplitz determinant in the double-scaling limit, *Journal of Physics A: Mathematical and Theoretical* **46**, 085003 (2013).
- [245] D. A. Ivanov and I. P. Levkivskiy, Fermionic full counting statistics with smooth boundaries: From discrete particles to bosonization, *Europhysics Letters* **113**, 17009 (2016).
- [246] O. Kashuba, T. L. Schmidt, F. Hassler, A. Haller, and R.-P. Riwar, Counting interacting electrons in one dimension, *Phys. Rev. B* **108**, 235133 (2023).
- [247] K. Sun, K. Kumar, and E. Fradkin, Discretized abelian chern-simons gauge theory on arbitrary graphs, *Phys. Rev. B* **92**, 115148 (2015).
- [248] D. P. Arovas, E. Berg, S. A. Kivelson, and S. Raghu, The hubbard model, *Annual Review of Condensed Matter Physics* **13**, 239 (2022).
- [249] U. Schollwöck, The density-matrix renormalization group, *Rev. Mod. Phys.* **77**, 259 (2005).
- [250] J. Eisert, M. Cramer, and M. B. Plenio, Colloquium: Area laws for the entanglement entropy, *Rev. Mod. Phys.* **82**, 277 (2010).
- [251] F. Verstraete and J. I. Cirac, Matrix product states represent ground states faithfully, *Phys. Rev. B* **73**, 094423 (2006).
- [252] The capacitive density follows from the lattice capacitance C_g through appropriate rescaling with the lattice spacing.
- [253] S. C. Zhang, T. H. Hansson, and S. Kivelson, Effective-field-theory model for the fractional quantum hall effect, *Phys. Rev. Lett.* **62**, 82 (1989).
- [254] A. Lopez and E. Fradkin, Fractional quantum hall effect and chern-simons gauge theories, *Phys. Rev. B* **44**, 5246 (1991).
- [255] X.-G. Wen, Topological orders and edge excitations in fractional quantum hall states, *Advances in Physics* **44**, 405 (1995).
- [256] B. Douçot, M. Feigel’Man, L. Ioffe, and A. Ioselevich, Protected qubits and chern-simons theories in josephson junction arrays, *Physical Review B* **71**, 024505 (2005).
- [257] E. Fradkin, Jordan-wigner transformation for quantum-spin systems in two dimensions and fractional statistics, *Phys. Rev. Lett.* **63**, 322 (1989).
- [258] D. Eliezer and G. Semenoff, Intersection forms and the geometry of lattice chern-simons theory, *Physics Letters B* **286**, 118 (1992).
- [259] A. Lopez, A. G. Rojo, and E. Fradkin, Chern-simons theory of the anisotropic quantum heisenberg antiferromagnet on a square lattice, *Phys. Rev. B* **49**, 15139 (1994).
- [260] B. Douçot and L. B. Ioffe, Exact solution of the Z_2 chern-simons model on a triangular lattice, *Phys. Rev. A* **72**, 032303 (2005).
- [261] B. Douçot and L. B. Ioffe, Non-abelian chern-simons models with discrete gauge groups on a lattice, *New Journal of Physics* **7**, 187 (2005).
- [262] B. Zhang, Abelian chern-simons gauge theory on the lattice, *Phys. Rev. D* **105**, 014507 (2022).
- [263] J. Das, A. Kumar, A. Maity, and V. Tripathi, Jordan-wigner fermionization of quantum spin systems on arbi-

trary two-dimensional lattices: A mutual chern-simons approach, *Phys. Rev. B* **108**, 085110 (2023).

[264] D. Tong, [Lectures on the quantum hall effect](#) (2016), [arXiv:1606.06687 \[hep-th\]](#).